The impact of myeloperoxidase on LCMV-induced immunopathology

Inaugural-Dissertation

zur

Erlangung des Doktorgrades

der Mathematisch-Naturwissenschaftlichen Fakultät

der Universität zu Köln

vorgelegt von

Michelle Arlette Paillard

aus Neuwied

Köln 2019

Berichterstatter: PD Dr. Thomas Wunderlich

Prof. Dr. Peter Kloppenburg

Tag der mündlichen Prüfung: 29.11.2019

Table of contents

Abbreviations

ALT	alanin aminotransferase (GPT)
APC	allophycocyanin
AST	aspartat aminotransferase (GOT)
^{51}Cr	chromium-51
CD	cluster of differentiation
CNS	central nervous system
cpm	counts per minute
CTL	cytotoxic T lymphocyte
DC	dendritic cell
DMEM	Dulbecco´s minimal essential medium
DMSO	Dimethyl sulfoxide
DNA	Deoxyribonucleic acid
DTH	delayed-type hypersensitivity reaction
E:T	effector : target
ELISA	enzyme linked immunosorbent assay
FACS	fluorescence activated cell sorting
FasL	Fas Ligand
FCS	fetal calf serum
Fig.	Figure
FITC	fluorescein isothiocyanate
GP	glycoprotein
Gzm	granzyme
H&E	Hematoxylin and eosin
HOCl	hypochlorous acid
IgG	Immunoglobulin G
IFNγ	Interferon-gamma
IU	infectious units
i.c.	intracranial
i.p.	intraperitoneal
i.v.	intravenous
KC	Kupffer cell

LCMV	Lymphocytic choriomeningitis virus
mAb	monoclonal antibody
MHC	Major Histocompatibility Complex
MIU	mouse infectious unit
MOI	multiplicity of infection
MPO	Myeloperoxidase
MPO$^{-/-}$	Myeloperoxidase-deficient
MEF	mouse embryonic fibroblasts
NETs	neutrophil extracellular traps
NOX	NADPH oxidase
NP	nucleoprotein
n. s.	not significant
pAb	polyclonal antibody
PBS	phosphate buffered saline
PE	phycoerythrin
PFA	paraformaldehyde
PFU	plaque forming unit
pH	pH value; negative decadic logarithm of the H^+ concentration
P/S	Penicillin/Streptomycin
p.i.	post infection
ROS	reactive oxygen species
RPMI	Roswell Park Memorial Institute
SEM	standard error of mean
SV	Simian virus
s.c.	subcutaneous
TCR	T cell receptor
TGFβ	Transforming growth factor beta
TNF	tumor necrosis factor
U/L	units per liter
WB	western blot
wt	wild type

1 Introduction

1.1 Myeloperoxidase

Myeloperoxidase (MPO, EC 1.11.2.2) is a ~150 kDa, cationic, heme-containing enzyme, first described in 1941 by Agner *et al*. [1, 2] (reviewed in [3]). Expression of MPO in humans is restricted to phagocytes, where it is stored particularly in primary granules of neutrophils and to a lesser extent in granules of monocytes and tissue macrophage subsets (reviewed in [4]). In rodents, MPO is assumed to be exclusively expressed in neutrophils [5].

MPO catalyzes the generation of highly microbicidal oxidants (reviewed in [6, 7]). This process is dependent on the presence of hydrogen peroxide (H_2O_2). For the generation of hydrogen peroxide, superoxide anions ($O_2^{-\cdot}$) are reduced in an either spontaneous or enzymatically-mediated dismutation reaction. Throughout the body, there are various sources providing reactive oxygen species (ROS). In phagocytes, ROS are predominantly produced by NADPH oxidase 2 (NOX2). In addition to this, other members of the NOX family and the mitochondrial respiratory chain may provide ROS for the MPO-H_2O_2 system (reviewed in [8, 9]) [10]. MPO oxidizes halides, predominantly chloride, but also bromide and pseudohalides. Thereby, it generates extremely reactive hypohalous acids (reviewed in [11]).

For a long time, the major function of MPO was considered to be the generation of reactive oxidants for the inactivation of internalized pathogens. Following phagocytosis, MPO is released from primary granules into the phagosome, where it mainly generates hypochlorous acid (HOCl) (reviewed in [12]) [13]. Intraphagosomal inactivation of pathogens by MPO is predominantly dependent on ROS generated by the NOX2 complex, which assembles in the phagosomal membrane upon pathogen uptake (reviewed in [14]). However, the function of MPO is more complex than killing ingested pathogens by generation of ROS. Beyond that, MPO can be released to the extracellular environment (reviewed in [15]) [16, 17]. Secretion can occur either directly from primary granules or by formation of neutrophil extracellular traps (NETs) [18]. In the extracellular environment, hypochlorous acid can attack any chemical group of proteins, nucleic acids, carbohydrates and lipids that can be oxidized and thereby disturb the integrity of microorganisms, but also of host tissues (reviewed in [4, 19]) [20-25]. MPO-derived oxidants critically impact cellular homeostasis and the

initiation and progression of various diseases. MPO was reported to promote various sterile inflammatory processes, *e.g*. cardiovascular and neurodegenerative diseases, as well as liver fibrosis in steatosis (reviewed in [3, 7, 26]) [27-30]. *In vitro* studies showed that hypochlorous acid increases cell permeability by chlorination of lipids and induces direct cell lysis or apoptotic and necrotic pathways in various cell types *e.g.* epithelial cells, fibroblasts and hepatocytes [31-34].

1.2 Neutrophils

MPO is the most abundant granule protein in neutrophils (reviewed in [7]). In human neutrophils its mass was reported to be higher than 5 % of the dry weight of cells [35, 36]. MPO levels in murine neutrophils only reach about 10 % of that of human neutrophils (reviewed in [7]). Additionally, neutrophils comprise the largest number of leukocytes in the human circulation (~ 70-80 %), while in mice only 20-30 % of white blood cells are neutrophils [35, 36].

Beyond MPO, neutrophils carry a variety of antimicrobial molecules within intracellular granules *e.g.* neutrophil elastase, lysozyme and α-defensin [37-39]. Together, these molecules are involved in different defense mechanisms of neutrophils in various infections, predominantly by bacteria and fungi (reviewed in [40, 41]). Neutrophils are professional phagocytes and combat pathogens in the circulation and in tissues either by phagocytosis or by release of granule contents to the extracellular environment (**Fig. 1**). Effective inactivation of pathogens is dependent on synergistic action of an array of antimicrobial molecules. During phagocytosis, release of contents from primary granules to phagosomal compartments potently inactivates pathogens (**Fig. 1A**) (reviewed in [41]).

By degranulation and NETosis, neutrophils release antimicrobial molecules, including MPO to the extracellular environment (**Fig. 1B, C**) (reviewed in [15, 38, 42, 43]) [44, 45]. NETs are web-like chromatin structures mainly composed of DNA. These structures contain proteins from neutrophil granules and the cytosol (reviewed in [46]). Bacteria, fungi and some viruses are trapped and disarmed or killed by exposure to antimicrobial molecules [18, 47, 48].

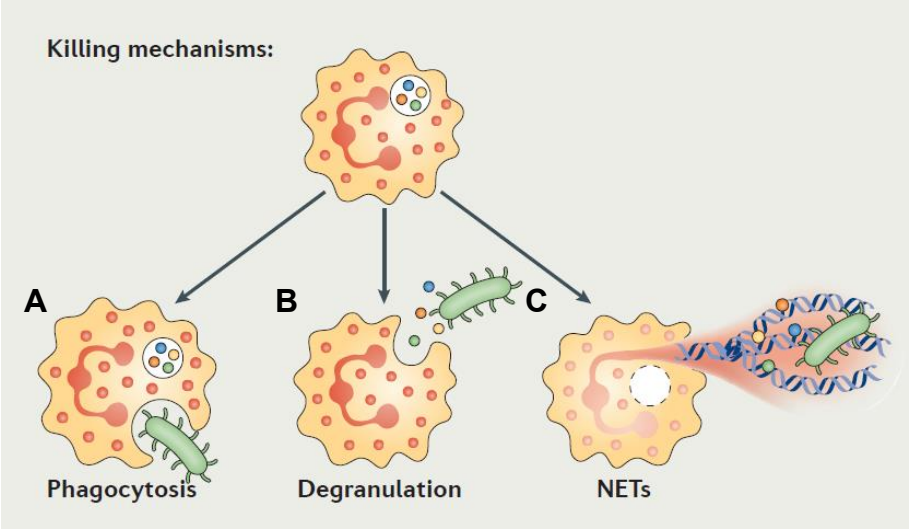

Fig. 1 Major mechanisms of pathogen inactivation by neutrophils [41].
Neutrophils can inactivate pathogens by three major mechanisms: (**A**) Following phagocytosis, microorganisms are rendered harmless by ROS or antimicrobial granule proteins. Inactivation of extracellular pathogens is achieved by (**B**) degranulation and (**C**) NETosis via release of granule proteins.

1.3 Neutrophils and MPO in anti-viral immunity

As part of the innate immune system, neutrophils belong to the host´s first line of defense against invading pathogens. The role of neutrophils in the clearance of bacterial and fungal infections is well characterized. However, their contribution to antiviral immunity is less clear (reviewed in [49]).

Indeed, the few studies about the role of neutrophils and MPO during viral infections are rather controversial. On the one hand, in mouse models for influenza A virus (IAV) infection, neutrophils had a protective role for the host (reviewed in [50]) [51]. Furthermore, neutrophil-derived NETs were reported to capture and immobilize human immunodeficiency virus (HIV)-1 virions and this mechanism was dependent on MPO and α-defensin [48]. On the other hand, massive infiltration of neutrophils in infected tissues can result in acute inflammation and damage of non-infected bystander cells [52]. In patients with hepatitis B virus (HBV) or hepatitis C virus (HCV) infection, MPO plasma levels and infiltration of neutrophils were shown to correlate with liver damage [53, 54].

Thus, depending on the virus, neutrophils and MPO have the potential to ease or aggravate the course of an infection. Because of that, it is indispensable that the antiviral response of neutrophils is tightly regulated to hold the balance between immunoprotection and immunopathology.

1.4 Lymphocytic Choriomeningitis Virus (LCMV)

To study the role of neutrophils and MPO during an antiviral immune response, we used the model of acute infection of mice with LCMV, strain WE. LCMV belongs to the genus of Arenaviruses and was first isolated by Charles Armstrong in 1933 [55].

LCMV is a rodent-borne pathogen with the common house mouse, *Mus musculus*, as primary host. However, exposure to excretions or secretions from persistently infected rodents is contagious for humans. Infection of pregnant women can be transmitted vertically to the fetus and may result in fetal death or the development of severe birth defects [56-58]. In adults, if at all, symptoms of LCMV infection occur approximately 8 days after infection and are similar to those of influenza *e.g.* fever, headache, muscle aches and nausea [59]. Invasion of the CNS is very rare and mortality in this case is less than 1 % [60].

Since its discovery, LCMV has been used to study virological and immunological questions [61-63]. By means of LCMV as model pathogen important immunological mechanisms *i.e.* MHC restriction, T cell memory, persistent infections, T cell exhaustion and immunopathology have been unraveled (reviewed in [64]) [65-78].

LCMV infects cells by attatching to cell surfaces via binding of glycoprotein GP-1 to α-Dystroglycan (α-DG) on the cell [79]. The latter has a broad tropism and is expressed in various tissues of *e.g.* the liver, kidney and small intestine [80].

LCMV is a non-cytopathic virus. Meaning, the infected cell is not visibly affected during viral replication or shedding (reviewed in [81]) [82, 83]. Instead, the virus induces a vigorous immune response, mediated by cytotoxic T lymphocytes (CTLs), which lyse infected cells in a major histocompatibility complex (MHC) class I-restricted manner.

1.4.1 The LCMV-specific immune response

Immunopathology during acute hepatitis is mediated consecutively by NK cells, $CD8^+$ T cells and $CD4^+$ T cells (reviewed in [84]) [85]. However, the most severe destruction is mediated by $CD8^+$ T cells, since cytotoxic T lymphocytes (CTLs) play the key role in virus elimination after acute infection of mice with LCMV [86]. Upon acute systemic infection, LCMV epitope-specific $CD8^+$ T cells become fully activated cytotoxic T lymphocytes (CTLs), they massively expand (about 16.000-fold) and eliminate the virus within approximately 10-14 days [87, 88].

CTLs with an LCMV-specific T cell receptor (TCR_{LCMV}) recognize viral peptides loaded on major histocompatibility complex (MHC) class I on the surface of infected host cells. After antigen encounter, CTLs mediate cytotoxicity by several effector pathways (reviewed in [89]). Upon TCR-mediated signaling, the CTL releases its effector molecules *i.e.* perforin and serine proteases, namely granzymes by degranulation towards the infected target cell (reviewed in [90]). Perforin-deficient mice were reported to have defective ability to clear LCMV infection [91]. When perforin is released into the immunological synapse, the intercellular space between the CTL and the target cell, it contributes to pore formation in the target cell membrane (reviewed in [92]). Granzymes can now enter the pore and induce apoptosis of the target cell mainly by induction of the caspase cascade.

Beyond target cell killing in a perforin-dependent manner apoptosis can be induced by receptor-mediated pathways. Engagement of FAS receptor (CD95) on a target cell with FAS ligand (CD95L) expressed by a CTL results in apoptotic death of the target cell by activation of caspase pathways [93]. These two strategies are responsible for most of contact-dependent target cell killing.

CTLs also secrete pro-inflammatory cytokines, such as tumor-necrosis factor alpha (TNFα) and interferon gamma (IFNγ) that can be cytolytic to the target cell. Upon infections with intracellular pathogens, IFNγ induces the upregulation of MHC class I molecules on the surface of target cells, which increases the chance for cytolysis by CTLs (reviewed [94]). Via TNF receptor engagement, TNFα can induce signaling pathways that lead to caspase activation and subsequent apoptosis of the infected cell (reviewed in [95]) [96].

During choriomeningitis upon intracerebral infection of the mouse central nervous system (CNS) with the Lymphocytic choriomeningitis virus (LCMV), neutrophils were reported to be recruited by T cells and to cause vascular leakage and acute lethality [97]. Depending on the route of virus inoculation, LCMV can induce further immunopathological syndromes. Subcutaneous (s.c.), intraplantar inoculation of LCMV into the footpad induces a delayed-type hypersensitivity (DTH) reaction and intraperitoneal (i.p.) injection leads to acute hepatitis [98-100]. Little is known about the impact of neutrophils on the induction of these immunopathological syndromes during infection of mice with LCMV and the contribution of MPO in these models is so far unresolved.

1.5 Aim of this work

The function of MPO during viral infections is double-edged, since MPO may contribute to virus clearance, but also to host tissue damage. So far, the role of MPO during LCMV-induced immunopathology remained completely unknown.
The aim of this study is to elucidate how MPO influences the course of disease during acute infection of mice with LCMV.

2 Materials and Methods

2.1 Materials

2.1.1 Mice

Breeding pairs of MPO-deficient ($MPO^{-/-}$) mice [101] of the C57BL/6 strain were kindly provided by Stefan Baldus (Department of Internal Medicine and Cardiology, University Clinics Cologne). The mice were heterozygously mated to generate wt littermates as controls.

Mice of the C57BL/6 strain in which the promoter region and first two exons of the NOX2 gene ($NOX2^{fl/fl}$) are flanked by loxP sites [102] were kindly provided by Ralf Brandes (Vascular Research Center, University Frankfurt).

To obtain mice with cell type-specific deletion of NOX2 in myeloid cells $NOX2^{flox/flox}$ mice were mated with transgenic mice expressing the Cre recombinase under control of the M lysozyme (LysM)-promotor (LysM Cre^{pos} [103]), which were donated by Jens Brüning (CECAD, MPI for Metabolism Research, University of Cologne, Germany).

All strains of mice were back-crossed at least 10 times to the C57BL/6J background. Genotyping was performed by PCR analysis of tail- or ear-biopsies as published for the above listed mouse strains. The mice were bred and maintained under specific pathogen-free (SPF) conditions in the Center for Molecular Medicine Cologne (CMMC) and were used at an age of 8 to 12 weeks. Experiments were performed in accordance with the Animal Protection Law of Germany in compliance with the Ethics Committee at the University of Cologne.

2.1.2 Virus

The Lymphocytic Choriomeningitis Virus (LCMV), strain WE, was propagated and titrated as plaque forming units (PFU) on murine L929 cells, clone L13 as described previously [104].

2.1.3 Cell lines

Simian virus 40 [105] transformed mouse embryonic fibroblasts (MEF) derived from C57BL/6 mice (C57/SV) were used as target cells or controls. C57/SV and L929 cells, clone L13 were propagated in Dulbecco´s minimal essential medium (DMEM) supplemented with 5% heat-inactivated fetal calf serum (FCS) at 37 °C and 5% CO_2.

2.1.4 Cell culture media, chemicals, buffers and solutions

All cell culture media, chemicals, buffers and solutions were of research grade and purchased from Biochrom AG, MERCK, ROTH or Sigma-Aldrich, if not specified otherwise. All buffers and solutions were prepared using deionised or bidestilled water ($_{dd}H_2O$) from an EASYpure® UV/UF water purification unit (Werner Reinstwassersysteme), sterilized by autoclaving or sterile-filtered with a 0.2 µm filter, if necessary and stored at room temperature (RT) unless specified otherwise.

Denotation	Composition/Manufacturer
4-Aminobenzoic acid hydrazide (4-ABAH)	14 mg/mL in DMSO, stored at -20 °C, Cayman Chemicals
Acrylamide 4K-Solution (40%) Mix	stored at 4 °C, AppliChem
Amersham ELC Detection reagents	stored at 4 °C, GE Healthcare
Benzonase	stored at 4 °C, Novagen
Blocking solution (BSA)	PBS with 3 % BSA and 0.1 % Triton-X-100, stored at 4 °C
Blocking solution (milk)	TBS-T with 5 % powdered milk, stored at 4 °C
ß-mercaptoethanol (ß-ME)	0.02 M in $_{dd}H_2O$, stored at 4 °C
Bovine Serum Albumin (BSA)	stored at 4 °C, Sigma-Aldrich

Denotation	Composition/Manufacturer
Buffer for mouse infection	PBS with 1 % FCS and 5 % P/S, stored at 4 °C
Buffer for virus dilutions for virus titration	PBS with 2 % FCS and 1% P/S, stored at 4 °C
Buffer for organ homogenization for virus titration	PBS with 1 % FCS and 2 % P/S, stored at 4 °
Buffer for FACS staining	PBS with 0.5 % BSA and 2 mM EDTA, stored at 4 °C
Buffer for cell sorting	PBS with 2 % FCS and 1mM EDTA, stored at 4 °C
Collagenase type IV	40 mg/mL in HBSS, stored at -20 °C, Merck
Crystal violet	$_{dd}H_20$, supplemented with 0.2 % crystal violet, 2 % ethanol, 11 % formaldehyde
Cultivation medium for cell culture and target cells	1 x DMEM supplemented with 5 or 10 % FCS, stored at 4 °C
Cultivation medium for T cells	1 x VLE RPMI 1640, supplemented with 10 % FCS, 1 % P/S and 50 µM ß-ME, stored at 4 °C
Dimethylsulfoxid (DMSO)	Merck
Ethylenediaminetetraacetic acid (EDTA)	Carl Roth GmbH & Co. KG
FCS	heat-inactivated at 56 °C for 30 min, stored at 4 °C, Biowest
Formaldehyde, 16 %, methanol-free	Polysciences, Inc.
Freezing medium	FCS containing 10 % DMSO, stored at 4 °C
Glucose oxidase	Sigma-Aldrich, stored at -20 °C
Growth medium L929 cells for virus titration	DMEM, supplemented with 5 % FCS, 1 % P/S, stored at 4 °C

Denotation	Composition/Manufacturer
HBSS, no calcium, no magnesium, no phenol red	Gibco™
Hoechst 33342	ThermoFisher Scientific
Laemmli buffer (5x)	60 mM Tris/HCl, 25 % Glycerol 10 % β-ME, 2 % SDS 0.2 % bromphenol blue in H_2O Stored at -20 °C
Liver digestion medium	DMEM supplemented with 5 % FCS, 1 % P/S, 1 mg/mL collagenase (type IV)
Lysis buffer for ^{51}Cr-release	1.6 % Triton-X-100 (v/v) in $_{dd}H_2O$, stored at 4 °C
Methyl cellulose medium for virus titration	20 % 10 x DMEM 220 mg/L Sodium-Pyruvate 7.4 g/L NaHCO3 1.16 g/L L-Glutamine 2 % P/S 10 % FCS 54 % $_{dd}H_2O$ 0.9 % methyl cellulose
Myeloperoxidase, human	Lee Biosolutions, stored at 4 °C
Natrium Chloride (NaCl)	AppliChem
PageRuler Prestained Protein Ladder	stored at -20 °C, ThermoScientific
Paraformaldehyde (PFA) solution	4 % PFA in PBS, stored at -20 °C
PBS	1 x Dulbecco´s phosphate buffered salt solution, pH 7.4, stored at 4 °C
peqGOLD TriFast™	stored in the dark at 4 °C, Peqlab
P/S	penicillin (10000 U/mL) and streptomycin (10 ng/mL) in $_{dd}H_2O$, stored at -20 °C

Denotation	Composition/Manufacturer
Phorbol 12-myristate 13-acetate (PMA)	1 mg in 1 mL ethanol, stored in the dark at -20 °C, Sigma-Aldrich
Phosphatase inhibitors	stored at 4 °C, Roche
Powdered milk	Carl Roth GmbH & Co. KG
ProLong™ Gold Antifade Mountant	ThermoFisher Scientific
Propidium Iodide	BD Pharmingen™, stored at 4°C
Protease inhibitors	Roche
RIPA buffer	150 mM NaCl, 50 mM TrisHCl, 1 % SDS, 0.5 % Nonidet P40, 0.1 % deoxicolic acid
RNase A	stored at -20 °C, ThermoFisher Scientific
RNaseZAP™	Sigma-Aldrich
Roti-Blot A anode buffer (10x)	Carl Roth GmbH & Co. KG
Roti-Blot K cathode buffer (10x)	Carl Roth GmbH & Co. KG
Sodium chromate [^{51}Cr]	400 µL sodium chromate (Na_2CrO_4), 2 mCi/ml, Hartmann Analytics
Sytox Green 5 mM	stored at -20 °C, ThermoFisher Scientific
TBS	150 mM NaCl, 10 mM TrisHCl in $_{dd}H_2O$
TBS-T	0.1 % Tween 20 in TBS
TEMED	stored at 4 °C, AppliChem
TrisHCl buffer	Bio-Rad Laboratories, Inc.
Triton X-100	Sigma-Aldrich
Trypanblue solution	1 x ready to use solution
Trypsin-EDTA solution	10 x trypsin-EDTA solution, diluted to 1 x using sterile $_{dd}H_2O$
Tween 20	AppliChem

2.1.5 Antibodies

Antigen	Specification	Provider
primary		
β-actin	mouse anti-mouse, unconjugated mAb (clone AC-74) 1:10000 for Western Blot	Sigma-Aldrich
CD4 (L3T4)	rat anti-mouse APC-, PE- or FITC-conjugated mAb (clone GK1.5); 1:200 for FACS	eBioscience
CD8a	rat anti-mouse APC-conjugated mAb (clone GK1.5); 1:200 for FACS	BD Biosciences
CD11b	rat anti-mouse APC-conjugated mAb (clone M1/70); 1:200 for FACS	BD Biosciences
cl. caspase 3	rabbit anti-mouse, unconjugated mAb (clone RM250) 1:1000 for Western Blot	Sigma
F4/80	rat anti-mouse, PE-conjugated mAb (clone BM8); 1:200 for FACS	eBioscience
IFNγ	rat anti-mouse, FITC-conjugated mAb (clone XMG1.2) 1:100 for FACS	BD Biosciences
Ly6C	rat anti-mouse, APC-conjugated mAb (clone AL-21); 1:200 for FACS	BD Biosciences

Antigen	Specification	Provider
primary		
Ly6G	rat anti-mouse, unconjugated mAb (clone 1A8); 400 µg for *in vivo* neutrophil depletion	BioXCell
	rat anti-mouse, PE-conjugated mAb (clone 1A8); 1:200 for FACS	BioLegend
MPO	mouse anti-mouse, FITC-conjugated mAb (clone 8F4); 1:50 for FACS 1:50 for immunofluorescence	Hycult Biotech
<u>Major Histocompatibility Complex (MHC) dextramers</u>		
H-2 D^b-dextramers	H-2D^b-restricted immunodominant epitope loaded with GP_{33-41} of LCMV (KAVYNFATC), $GP_{276-286}$ of LCMV (FQPQNGQFI) and $NP_{396-404}$ of LCMV (SGVENPGGYCL); PE-conjugated MHC dextramer; 1:100 for FACS	Immudex (Denmark)

Antigen	Specification	Provider
Secondary		
IgG	goat anti-mouse, HRP-conjugated polyclonal Ab 1:6000 for Western Blot	Sigma-Aldrich

IgG	goat anti-rabbit, HRP-conjugated polyclonal Ab 1:5000 for Western Blot	Sigma-Aldrich
IgG	goat anti-mouse, Alexa Fluor 488-conjugated polyclonal Ab 1:500 for immunofluorescence	

Antigen	**Specification**	**Provider**
isotype control		
IgG1	mouse anti-mouse, FITC-conjugated mAb (clone MOPC-21); 1:50 for FACS	Hycult Biotech
IgG1κ	rat anti-mouse, FITC-conjugated mAb (clone R3-34) 1:100 for FACS	BD Biosciences

2.1.6 Kits

Denotation	**Composition/Manufacturer**
BCA Protein Assay	ThermoFisher Scientific
Click-iT™ Plus TUNEL Assay	ThermoFisher Scientific
Cytofix/Cytoperm™ Fixation/Permeabilization	BD
DNase I	Sigma-Aldrich
DyNAmo Flash SYBR Green qPCR	ThermoFisher Scientific
EasySep™ Mouse CD8a Positive Selection	STEMCELL Technologies
EasySep™ Mouse Neutrophil Enrichment	STEMCELL Technologies
ELISA mouse MPO	Hycult Biotech
RevertAid First Strand cDNA Synthesis	ThermoFisher Scientific

2.1.7 Technical equipment

Device	Specification	Company
Centrifuge	5417 R	Eppendorf
Cell counting chamber	Neubauer Improved	LO Laboroptik
EasySep™ Magnet	EasyEights™	STEMCELLTechnologies
Electrophoresis cell	Criterion Cell	Bio-Rad Laboratories, Inc.
Flow cytometer	FACSCalibur	Becton Dickinson
Fluorescence microscope	IX81	Olympus
γ-counter	COBRA II	Canberra Packard
GentleMACS	Octo Dissociator	Miltenyi Biotech
Imaging system	MF-ChemiBIS 3.2	DNR Bio Imaging Systems
Incubator	Heracell	Heraeus
LightCycler® 480	Instrument II	Roche
Magnetic mixer	RET	IKA
Megafuge	1.0 R	Heraeus
Microtiterplate-reader	Tecan infinite M1000	Tecan Group Ltd.
Microscope	DMi1	Leica
Multimode reader	TrisStar LB941	Berthold
NanoDrop™	One/One^{W}	ThermoFisher Scientific
Protein blotting system	Trans-Blot Turbo	Bio-Rad Laboratories, Inc.
Reflotron	Reflotron® Plus System	Roche
Spring caliper	Oditest	H. C. Kroplin GmbH
Thermomixer	Comfort	Eppendorf
TissueLyser	LT	Qiagen
Vortex	Genie 2	Scientific Industries
Working Bench	Herasafe	Heraeus

2.1.8 Consumables

Denotation	Composition/Manufacturer
Bottle-Top-Filter, 0.45 µm	Nalgene
Cell Culture Plastic	TPP
Cell strainer 40 or 70 µm	Falcon
Cover glass (13 mm)	VWR International
FACS tubes	BD Biosciences
Falcon tubes (15 and 50 mL)	Greiner Bio-One
gentleMACS M tubes	Miltenyi Biotec
Microscope slides	Engelbrecht
Reflotron® GOT	Roche
Reflotron® GPT	Roche
Syringes and needles	Braun
Whatman 3 mm (filter paper)	GE Healthcare
Whatman Nitrocellulose membrane	GE Healthcare

2.1.9 Software

Denotation	Composition/Manufacturer
Cell Quest Pro	Becton Dickinson
Fluoview FV1000 Ver. 1.7a	Olympus Corporation
GraphPad Prism 7	GraphPad Software, Inc.
ImageJ 1.46h software	Wayne Rasband
Office Professional Plus 2010	Microsoft
Photo Shop CS3	Adobe
Sigma Plot 13.0	Systat Software, Inc.

2.2 Methods

2.2.1 Cell culture

Cells were cultured under sterile conditions at 37 °C in a humid atmosphere containing 5 % CO_2. Cells were grown and maintained in tissue culture flasks and passaged in a ratio of one to five every 2-3 days after treatment with trypsin-EDTA. For long-term storage at -150 °C, cells were suspended in FCS containing 10 % DMSO.

2.2.2 Induction of immunopathological syndromes

2.2.2.1 Infection of mice with LCMV

For infection of adult mice (6 to 8 weeks of age) with LCMV, strain WE, plaque-forming units (PFU) were converted into infectious units (IU) by multiplying the PFU with a factor of 10 as previously described [106]. To induce LCMV-mediated hepatitis, mice were infected by intraperitoneal (i.p.) inoculation of 1 x 10^6 IU of LCMV in PBS with 1 % FCS and 5 %. For delayed-type hypersensitivity (DTH) reaction LCMV was subcutaneously (s.c.) inoculated at a dose of 1 x 10^5 IU into the right hind footpad. To induce choriomeningitis mice were infected by intracranial (i.c.) injection of 10^3 IU of LCMV.

2.2.2.2 LCMV-induced choriomeningitis

Following i.c. injection of 10^3 IU of LCMV, mice were monitored for their clinical symptoms. Initially, mice were inspected and weighed daily. After first appearance of symptoms, mice were observed at 6 h intervals.

2.2.2.3 Delayed-type hypersensitivity (DTH) reaction

To induce DTH reaction, 10^5 IU of LCMV were subcutaneously (s.c.) inoculated into the right hind foot pad. From day 5 onwards, footpad swelling was measured daily with a spring caliper (Oditest, especially equipped with a soft spring, H. C. Kroplin GmbH, Schluchtern. Germany). The swelling was expressed as the factor of the thickness of the inoculated foot to the thickness of the contralateral non-inoculated foot [107, 108].

2.2.2.4 LCMV-induced hepatitis

Mice were infected i.p. with 10^6 IU of LCMV. At the indicated days, serum samples were prepared to measure activity of the hepatic enzymes alanine aminotransferase (ALT) and aspartate aminotransferase (AST) with the appropriate test strips using the Reflotron Plus System according to the instructions of the manufacturer (Roche).
Additionally, liver sections were prepared for histopathological analysis in cooperation with Dr. Katharina Pütz, Institute for Pathology, University Hospital Cologne and Dr. Sonja Djudjaj, Institute of Pathology, University hospital RWTH Aachen. After 24 h of fixation in 4 % buffered formalin, liver specimens were embedded into paraffin. Histological quantitative examination of liver fibrosis was performed after hematoxylin and eosin (H&E) staining. Inflammatory activity (i.e. periportal or periseptal interface hepatitis, confluent necrosis, focal (spotty) lytic necrosis, apoptosis and focal inflammation as well as portal inflammation) was assessed according to the Ishak score [109].

2.2.3 Virus titration

The WE strain of LCMV was propagated and titrated as plaque-forming units (PFU) on L929 cells as previously described [110]. Viral loads in spleen or liver

samples were titrated as PFU per gram. At the indicated days post infection (p.i.), organs of LCMV-infected mice were collected. The weight of organ pieces was determined and organ samples were homogenized in homogenization buffer supplemented with 1 % FCS and 2 % P/S by use of M-tubes in the gentleMACS Octo Dissociator (program protein_01). The samples were centrifuged for 10 min, at 4 °C and 300 x g, aliquoted and stored at -80 °C. 18 h prior to virus titration, 2 mL of L929 cell suspension at a density of 1.215 x 10^5 cells/mL were seeded into 6-well plates and incubated at 37 °C and 5 % CO_2. On the following day, the homogenized spleen and liver samples were thawed and diluted in 10-fold steps in PBS supplemented with 2 % FCS and 1 % P/S. For homogenized organ samples from days 6, 8 and 10 p.i., a serial dilution of 10^{-1}, 10^{-2} and 10^{-3}, for days 2 and 4 p.i. 10^{-3}, 10^{-4} and 10^{-5} for the spleen and for the liver 10^{-1}, 10^{-2} and 10^{-3} was used. Medium from the 6-well plates was aspirated carefully and 100 µL of the dilution of each sample was applied per well. Each dilution was analyzed in duplicates. After 30 min incubation at 37 °C and 5 % CO_2, cells were covered with 2 mL methyl cellulose medium. After 3 days of incubation at 37 °C and 5 % CO_2, 1.5 mL growth medium for virus titration was added per well. On the next day, medium was removed and 1 mL crystal violet was added per well and cells were fixed and stained. After 15 min of incubation, plates were rinsed with VE-water and dried for analysis.

2.2.4 Preparation of single cell suspensions

2.2.4.1 Single cell suspension from the spleen

At the experimental day, animals were sacrificed and their spleens were removed under sterile conditions. Single cell suspensions were obtained by gently squeezing the spleen and passing cell suspensions through a 70 µm nylon mesh with the plunger of a 3 mL syringe. Cells were centrifuged at 300 x g, for 10 min at 4 °C and cell pellets were resuspended in 5 mL T cell cultivation medium or buffer for FACS staining and passed through a 70 µm nylon mesh again. Viable cells were counted by Trypanblue exclusion in a Neubauer chamber.

2.2.4.2 Single cell suspension from the liver

At the experimental day, animals were sacrificed and their livers were perfused with 10 mL ice cold 0.9 % NaCl in a syringe by puncturing the portal vein and cutting the inferior vena cava to allow the fluid to flow freely through the liver until the liver turned brighter. The liver was removed and cut into small pieces. Liver digestion was performed with 5 mL pre-warmed liver digestion medium on a magnetic stirrer at 37 °C for 30 min. After digestion, the cell suspension was taken up in 20 mL ice cold PBS to stop the enzymatic activity and passed through a 70 µm nylon mesh. Cells were centrifuged at 50 x g, for 10 min at 4 °C. After centrifugation, hepatocytes made up the cell pellet and leukocytes were in the supernatant. For continued use of leukocytes, cells were centrifuged twice at 300 x g, for 10 min at 4 °C to get rid of remaining collagenase. For continued use of hepatocytes, cells were centrifuged twice at 50 x g, for 10 min at 4°C. Afterwards both cell types were resuspended in 5 mL cultivation medium or buffer for FACS staining. Viable cells were counted by Trypanblue exclusion in a Neubauer chamber.

2.2.5 Immunomagnetic enrichment of $CD8^+$ T cells from the spleen or the liver

For positive selection, $CD8^+$ T cells were immunomagnetically enriched from splenic or hepatic cell suspensions (2.2.4.1 and 2.2.4.2), using a combination of CD8α-specific Abs following the manufacturer's instructions (STEMCELL Technologies). After 3 min of incubation at room temperature (RT), cells were magnetically labelled with dextran beads for 3 min at RT. Samples were placed in either 15 mL Falcons or FACS tubes into the EasySep™ "EasyEights™" magnet for 10 min at RT. Magnetically labelled cells were retained in the tube, while unlabeled cells were aspirated. This step was repeated twice. After removal from the magnetic field, cells were resuspended in buffer or medium, centrifuged and counted by Trypanblue exclusion in a Neubauer chamber. The frequencies of enriched $CD8^+$ T cells were assessed by flow cytometry to be between 95–98 %.

2.2.6 Immunomagnetic enrichment of neutrophils from the bone marrow

Mice were sacrificed by cervical dislocation and the skin and muscles were removed from the hind legs. Afterwards, the legs were detached from the mouse and the ends of the femur and shin were opened. The opened bones were rinsed with 5 mL VLE RPMI 1640 medium, using a syringe with a thin needle (0.6 x 30 mm). The released bone marrow was resuspended and collected in a 50 mL falcon tube.
For negative selection of neutrophils, other cell types in the cell suspension were immunomagnetically removed, using a combination of specific Abs following the manufacturer's instructions (STEMCELL Technologies). After incubation for 15 min at 4 °C, cells were washed and a biotin selection cocktail was added, followed by incubation for 15 min at 4 °C. Afterwards, magnetic particles were added and cells were incubated for another 10 min at 4 °C. The tubes were placed in the magnetic field and labelled cells were kept in the tube, while enriched neutrophils remained unbound in the supernatant. The frequencies of enriched neutrophils were assessed by flow cytometry to be between 80–90 %.

2.2.7 Assay for virus-specific cytotoxicity of $CD8^+$ T cells

The virus-specific cytotoxic activity of $CD8^+$ T cells from the spleen or the liver was measured in ^{51}Chromium ([^{51}Cr])-release assays according to Brunner et al. [111] with modifications [112].

Effector cells

Total splenocytes, enriched splenic or enriched hepatic $CD8^+$ T cells were used as effector cells. $CD8^+$ T cells were immunomagnetically enriched from splenic or hepatic single cell suspensions of mice acutely infected with LCMV on days 7 and 8 p.i., as described under 2.2.4.1 and 2.2.4.2. Effector cells were adjusted to 3 x 10^6 cells/mL in RPMI medium supplemented with 10 % FCS, 1 % P/S and 50 µM ß-ME.

Target cells

C57/SV target cells were plated at a density of 5 x 10^5 or 1 x 10^6, respectively, into 10 cm cell culture dishes two days before the experiment. After attachment, target cells were infected with LCMV at an MOI of 0.01. As negative control, non-infected fibroblasts were used. 1 x 10^6 target cells were incubated with approximately 50 µCi of [^{51}Cr] sodium chromate (Hartmann Analytics) for 60 min at 37 °C, washed three times and adjusted to a density of 3 x 10^4 cells per mL.

Procedure

In three replicates, 200 µL of the effector cell suspension was dispensed in 96-U bottom plate and diluted 1:2 three times, to get effector to target ratios of 100:1, 50:1, 25:1 and 12.5:1. Afterwards, 100 µL of the target cell suspension was added to each well with effector cells. The spontaneous release of [^{51}Cr] by [^{51}Cr]-labelled target cells was determined in 6 wells without effector cells to be less than 9 % of the maximum release. The maximal [^{51}Cr]-release was determined by target cell lysis in 100 µL 1.6 % Triton X-100. The virus-specific cytotoxic activity of $CD8^+$ T cells was determined after 4 h incubation at 37 °C and 5 % CO_2. Cells were spun down and 100 µL of cell-free supernatants was harvested. Supernatants from each well were measured in a γ-counter to detect the amount of [^{51}Cr] released by target cells as counts per minute (cpm). The mean of the 4 replicates was calculated before the virus-specific lysis of target cells was calculated with correction for spontaneous lysis, as following for each effector to target ratio:

$$\% \text{ specific lysis} = (cpm_{sample} - cpm_{spontan}) / (cpm_{maximal} - cpm_{spontan}) \times 100$$

2.2.8 Stimulation of LCMV-specific $CD8^+$ T cells

To investigate the role of MPO on IFNγ production by $CD8^+$ T cells, the intracellular accumulation of IFNγ was analyzed. To this end, enriched $CD8^+$ T cells were co-incubated with LCMV-infected fibroblasts (MHC class I restriction to CD8).

2.2.8.1 Preparation of target cells for CD8$^+$ T cell stimulation

For antigen-specific stimulation of enriched CD8$^+$ T cells, LCMV-infected C57/SV target cells were prepared as described under 2.2.7.

2.2.8.2 Antigen-specific stimulation of CD8$^+$ T cells

For measurement of intracellular accumulation of IFNγ, 1 x 10^5 enriched splenic or hepatic CD8$^+$ T cells were incubated for 4 h with either LCMV-infected or non-infected C57/SV fibroblasts. To prevent secretion of IFNγ, cells were treated with 1 µL BD GolgiStopTM (BD Biosciences) 1h prior to stimulation until fixation.

2.2.9 Flow cytometry

2.2.9.1 Staining of surface molecules

The frequencies of cells or expression intensities of surface molecules (indicated as mean fluorescence intensity (MFI)) were determined by flow cytometry. Cells were washed with PBS supplemented with 0.5 % BSA and 2 mM EDTA. To avoid unspecific Ab binding and staining of cells, 1x10^6 cells were incubated with 1 µL FcR Block™ for 10 min at 4 °C. Staining was performed for 15 min with 0.5 µg of fluorochrome-conjugated mAb specific for CD4, CD8α, CD11b, F4/80, Ly6-C or Ly6-G at 4 °C in the dark. After incubation, cells were washed twice with cold PBS supplemented with 0.5 % BSA and 2 mM EDTA and analyzed by flow cytometry using a FACSCalibur (BD).

LCMV-specific CD8$^+$ T cells were detected among spleen or liver cells of C57BL/6 mice by using PE-conjugated H-2Db-dextramers loaded with either of the three H-2D^b-restricted immunodominant epitopes of LCMV (GP_{33-41}, $GP_{276-286}$, and $NP_{396-404}$) (Immudex, Copenhagen, Denmark). Dot plots of total splenocytes or liver leukocytes from C57BL/6 mice displayed co-staining for H-2D^b-restricted immunodominant epitopes GP_{33-41}, $GP_{276-286}$, and $NP_{396-404}$ with CD8.

The frequencies of LCMV-specific $CD8^+$ T cells were calculated as follows:

% TCR_{LCMV}^+ $CD8^+$ cells / % $CD8^+$ spleen cells x 100

Bar charts show the percentage of $CD8^+$ spleen cells from C57BL/6 mice expressing TCR in sum for the three major immunodominant H-$2D^b$-restricted epitopes GP_{33-41}, $GP_{276-286}$, and $NP_{396-404}$.

2.2.9.2 Staining of intracellular molecules

For analysis of intracellular IFNγ and MPO, 1 x 10^6 splenocytes or liver leukocytes were washed twice with PBS and fixed with 100 µL Fixation/Permeabilization solution (BD Biosciences) in a 96-U bottom plate for 20 min at 4 °C. Afterwards, cells were washed twice with 1 x Perm/Wash™ (BD Biosciences) with 250 µL/wash total volume to remove all traces of Fixation/Permeabilization solution. Primary mAbs were diluted in 50 µL 1 x Perm/Wash™ and added to fixed cells for 30 min at 4 °C. After two times washing with Perm/Wash™ in 250 µL/wash total volume, cells were analyzed for intracellular IFNγ and MPO expression by flow cytometry.

2.2.9.3 MPO cytotoxicity assay with murine primary hepatocytes

Hepatocytes were isolated according to procedure under 2.2.4.2. Hepatocytes were seeded at a density of 2 x 10^5 / mL in DMEM with 1 % P/S without FCS in a 24-well plate. Cells were incubated with either 0.1 U/mL Glucose oxidase (GOX), 0.1 U/mL MPO or 1.0 U/mL MPO alone or in combination with GOX and 0.1 U/mL or 1.0 U/mL MPO. Control cells were left untreated. After incubation for 4 h at 37°C, specific cell death was assessed by flow cytometry via Propidium iodide staining. Hepatocytes were analyzed according to appearance in the FSC and SSC and spontaneous cell death of untreated cells was substracted from data obtained from treated cells.

2.2.9.4 SYTOX Green NETosis assay

Inactive neutrophils were enriched from the bone marrow of naive mice according to the procedure described under 2.2.6. Neutrophils were adjusted to a density of 1 x 10^6 cells/mL and 5 x 10^5 cells were seeded in a 48-well microtiterplate. Cells were stimulated with either 25 nM PMA, or LCMV at MOI 10 and MOI 100 for 4 h at 37 °C and 5 % CO_2. Controls remained untreated. After incubation, cells were washed twice with HBSS and adjusted to a density of 1 x 10^6 cells/mL, 100 µl of cell suspension was used for flow cytometry. Extracellular DNA was stained with 100 nM of cell impermeable dye SYTOX Green for 15 min at 4 °C, followed by two washing steps with HBSS. Extracellular DNA released by neutrophils was analyzed by flow cytometry.

2.2.9.5 Cell cycle analysis of hepatocytes using propidium iodide

Cell cycle analysis of hepatocytes was performed by quantification of DNA content with propidium iodide by flow cytometry. Primary hepatocytes were isolated as described in 2.2.4.2. Cells were fixed in cold 70 % ethanol for 30 min at 4 °C. Afterwards, cells were washed twice in PBS and centrifuged at 850 x g for 5 min. The cell pellet was taken up in 1 mL PBS. As propidium iodide also stains RNA, cells were treated with 1 µg RNase A for 15 min at 37 °C. For FACS analysis 150 µL of the cell suspension was taken up in 350 µL FACS buffer and DNA was stained by addition of 0.5 µg propidium iodide and analyzed immediately.
Cells that are in the S phase will have more DNA than in the G1 phase and cells in the G2 phase will be approximately twice as bright.

2.2.10 Western Blot analysis of cleaved caspase 3

2.2.10.1 Homogenization of liver tissue

Freshly isolated liver tissue (~10 mg) was taken up into m-tubes (Miltenyi Biotec) in 500 µL RIPA buffer with benzonase and protease/phosphatase inhibitors. Tissue was homogenized using GentleMACS^{TM} Octo Dissociator (Miltenyi Biotec) at program protein_01. Homogenates were centrifuged at 836 x g, for 10 min at 4 °C, the pellet was discarded. Lysates were transferred into 1.5 mL Eppendorf tubes followed by incubation at 95 °C for 5 min. After short condensation on ice, the samples were briefly centrifuged. Protein concentration was determined using BCA Protein Assay Kit in accordance with the protocol of the supplier (Pierce, Thermo Scientific). Finally, protein concentration was adjusted to 35 µg in 5 x Laemmli buffer and H_2O.

2.2.10.2 SDS-PAGE and Western Blot

Prior to SDS PAGE, the lysates were incubated at 95° C for 10 min. SDS PAGE was performed according to the manufacturer´s protocol (Bio-Rad Laboratories, Inc.), using a Criterion Cell filled with (1 x) TGS running buffer and Criterion Cassettes containing a 14 % Tris/HCl gel for cleaved caspase 3 blot. After SDS-PAGE, proteins were transferred onto a nitrocellulose membrane according to the manufacturer´s protocol (Bio-Rad Laboratories, Inc.) using a Trans-Blot Turbo system.

In order to block unspecific binding sites, the membranes were incubated in milk blocking solution for 30 min at RT. Afterwards the membranes were incubated with primary Ab in blocking solution overnight at 4 °C. Monoclonal Abs against cleaved caspase 3 and β-actin (diluted in milk blocking solution) were from Sigma-Aldrich. Unbound Abs were removed by triple washing of the membrane with TBST. Thereafter, membranes were incubated with HRP-conjugated secondary Abs in blocking solution for 60 min at RT. Again, unbound Abs were removed by washing two times with TBST and once with TBS. The immune complex was visualized using

Amersham ELC Detection reagents (GE Healthcare) and detected using the MF-ChemiBIS 3.2 imaging system (DNR Bio Imaging Systems). PageRuler Prestained Protein Ladder (Thermo Scientific) was used for identification of protein size. Specific bands on immunoblots were quantified by densitometry using ImageJ 1.46h software (Wayne Rasband, NIH, USA).

2.2.11 Quantification of MPO in the plasma and liver tissue homogenates

At the experimental days, blood was collected from the superficial temporal vein of mice. Plasma was prepared by use of Mircovette 500 LH according to the manufacturer´s protocol (Sarstedt). After incubation for 5 min, blood samples were centrifuged for 5 min at 2000 x g and plasma was aliquoted and stored at -80 °C. For liver tissue homogenization, snap-frozen tissue was prepared as described under 2.2.10.1. Protein concentration was determined using BCA Protein Assay Kit in accordance with the protocol of the supplier (Pierce, Thermo Scientific).
Systemic levels of extracellular MPO in the plasma of mice and total protein levels in liver tissue homogenates were analyzed with the MPO mouse ELISA kit (HycultBiotech) according to the manufacturer´s instructions.

2.2.12 Quantitative real-time PCR

2.2.12.1 RNA isolation and cDNA synthesis

To obtain total RNA from liver tissue, peqGOLD TriFast™ was used according to manufacturer's instructions (peqlab).
The RNA yield was quantified by NanoDrop™ Spectrophotometer (ThermoFisher Scientific). The quality of RNA was determined through the ratio of A260/A280 (ratio of ~2.0 is accepted). DNA digestion was performed using the DNase I kit according to the manufacturer´s instructions (Sigma-Aldrich). For cDNA synthesis a total amount of 1 µg of RNA was used. Synthesis of cDNA was performed with the RevertAid First Strand cDNA Synthesis kit (ThermoFisher Scientific) according to the manufacturer´s protocol.

2.2.12.2 Quantitative real-time PCR (qRT-PCR)

Quantitative real-time PCR was performed with the DyNAmo Flash SYBR Green qPCR kit (ThermoFisher Scientific). The qRT-PCR was performed in the LightCyler480 (Roche). Gene expression of β-actin, Nox4, p21, p53 and TGFβ was analyzed by use of specific primer pairs for each gene, respectively. Primers were purchased by Sigma-Aldrich.

The composition of each PCR reaction sample was as follows:

2 µL cDNA
10 µL 2 x qPCR master mix
1 µM forward primer
1 µM reverse primer
6 µL DEPC-treated $_{dd}H_2O$
Total volume: 20 µL per reaction

PCR program:

1. Initial denaturation 95 °C 10 min

45 cycles

2. Denaturation 95 °C 10 sec
3. Annealing/Extension 60 °C 10 sec

Gene expression for each gene was determined by calculation of the threshold cycle- (Ct-) value. The value obtained for each gene was normalized to that of the housekeeping gene encoding β-actin. Then the fold change was calculated.

2.2.12.3 Primers

β-actin

Forward

5´-AGACCTGTACGCCAACACAG-3´

Reverse

5´-AGGAGGAGCAATGATCTTG-3´

Nox4

Forward

5´-AGAGCATCTGCATCTGTCCTGAACC-3´

Reverse

5´-AACAATCTTCTTGTTCTCCTGCTAGGGAC-3´

p21 [113]

Forward

5´-AGATCCACAG CGATATCCAGAC-3´

Reverse

5´-ACCGAAGAGACAACGGCACACT-3´

p53 [114]

Forward

5´- CTCCGAAGACTGGATGACTGC-3´

Reverse

5´- CAACAGATCGTCCATGCAGTG-3´

TGFβ [115]

Forward

5'-GGAGAGCCCTGGATACCAAC-3'

Reverse

5'-CAACCCAGGTCCTTCCTAAA-3'

2.2.13 Immunofluorescence microscopy

Cryo sections (5 µm) of liver tissue were kindly generated by Gülsah Schwab (Heartcenter, University Hospital Cologne).

2.2.13.1 TUNEL staining

DNA double-strand breaks were stained using the Click-iT™ Plus TUNEL Assay (ThermoFisher Scientific). Sections were fixed and stained according to the manufacturer´s protocol (ThermoFisher Scientific).

2.2.13.2 MPO and Hoechst staining

Cryo sections were fixed with 4 % methanol-free formaldehyde for 15 min at room temperature (RT), followed by three washing steps with PBS for 5 min at RT. Cells were permeabilized with PBS containing 0.1 % Trition X-100 for 20 min at RT. Unspecific binding sites were blocked with PBS containing 3 % BSA and 0.1 % Triton X-100 for 1 h at RT. Afterwards, MPO was stained using mouse anti-mouse FITC-conjugated MPO mAb for 1 h at RT. Thereafter, sections were washed thrice with PBS in the dark. Nuclei were stained with 1:2000 of 10 mg/mL solution Hoechst 33342 (ThermoFisher Scientific) for 10 min at RT in the dark. Finally, slides were washed three times with PBS in the dark and coverslips were mounted on the microscope slides with ProLong™ Gold Antifade Mountant. Sections of the preparations were analyzed by confocal laser scanning microscopy.

2.2.14 *In vivo* neutrophil depletion

For neutrophil depletion, mice were intraperitoneally injected with 400 µg anti-Ly6-G (clone 1A8) Ab in PBS twice, one day prior to LCMV-infection an on day 4 p.i.. Control mice did not receive Ab-treatment. Neutrophil depletion was proven by flow cytometry via CD11b and Gr-1 staining. Populations of $CD11b^{+}/Gr\text{-}1^{hi}$ cells were characterized as neutrophils.

2.2.15 *In vivo* MPO inhibition

For MPO inhibition mice were intraperitoneally injected with 25 µg/g body weight 4-Aminobenzoic acid hydrazide (4-ABAH) in PBS on the day of LCMV-infection and every second day until the experimental end. 4-ABAH was diluted to a stock concentration of 14 mg/mL in DMSO. Control mice were treated with DMSO in PBS alone at the indicated days.

2.2.16 Statistical analysis

Data on continuous variables were summarized by mean and standard error of the mean (SEM). Groups were compared using independent two-tailed student´s t-test. The p-values of $p < 0.05$, $p < 0.01$ or $p < 0.001$ are indicated by *, ** or ***, respectively. The numbers of mice per group are indicated in the respective figure legends.

3 Results

3.1 Effects of MPO-deficiency on LCMV-specific immunopathological responses

LCMV is a non-cytopathic virus. However, it induces robust immunopathological reactions depending on the route of infection [116]. During acute infection of mice with LCMV, immunopathology is primarily mediated by virus-specific $CD8^+$ T cells [117].

To assess whether MPO has an influence on immunopathology upon infection with LCMV, MPO-deficient ($MPO^{-/-}$) mice and wt littermates were infected via different routes of virus inoculation to analyze the resulting immunopathological syndromes.

3.1.1 Influence of MPO on LCMV-induced choriomeningitis

Upon inoculation of LCMV by intracerebral (i.c.) injection, the resulting fatal disease is mediated by immune cells, which infiltrate into the brain [118]. The immunopathological reaction of wt mice induced by i.c. inoculation of 10^3 IU of LCMV, strain WE, was lethal for 100 % of mice by day 8 p.i. (**Fig. 1A**). For $MPO^{-/-}$ mice, i.c. infection was lethal for all individuals by day 9 p.i.. Over the course of infection, $MPO^{-/-}$ and wt mice dramatically lost weight from day 5 p.i. on. However, weight loss was also comparable in wt and $MPO^{-/-}$ mice (**Fig. 1B**).

These data indicate that $MPO^{-/-}$ activity is not involved in the lethal outcome of immunopathology after i.c. infection of mice with LCMV.

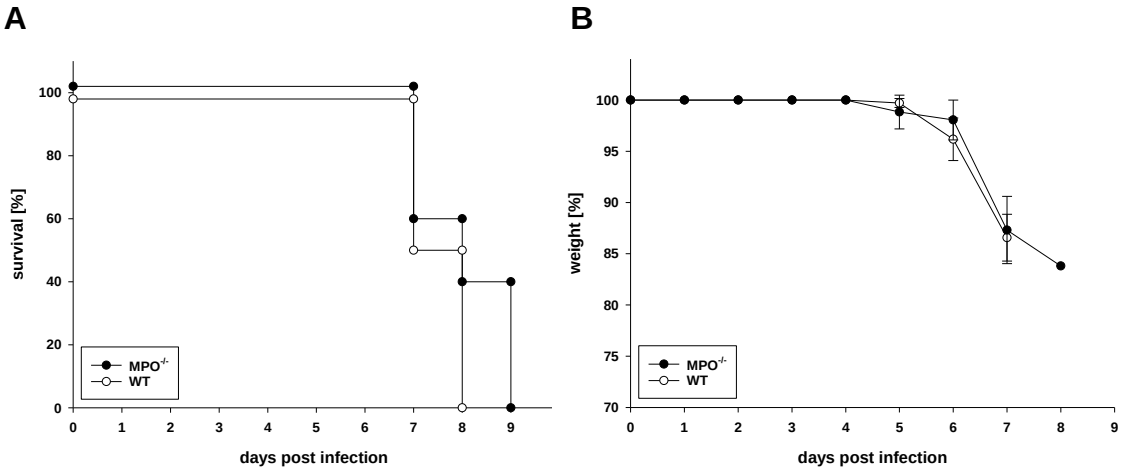

Fig. 1 Clinical course of meningitis after i.c. infection with LCMV

Groups MPO$^{-/-}$ and wt mice were infected by i.c. injection of 10^3 IU of LCMV, strain WE. (**A**) Survival and (**B**) body weight of the mice were observed daily. Shown are data from 1 experiment with n = 5 MPO$^{-/-}$ mice and n = 6 wt mice. Survival p.i. is shown as Kaplan-Meier plot.

3.1.2 Influence of MPO on LCMV-induced DTH reaction

Subcutaneous (s.c.) intraplantar inoculation of LCMV into the hind footpad of mice induces a delayed-type hypersensitivity (DTH) reaction. The immune reaction occurs in two distinct phases [98]. CD8$^+$ T cells mediate a first swelling phase, which peaks around day 8 p.i.. A second minor swelling phase (days 10 to 16 p.i.) is mediated by CD4$^+$ T cells [86]. The LCMV-induced DTH reaction was similar in both MPO$^{-/-}$ and wt mice. In both, footpad swelling peaked to a similar extent on day 8 p.i. and slowly declined within the following days (**Fig. 2**).

These data show that the lack of MPO has no influence on the intensity of the LCMV-induced DTH reaction. This indicates that MPO does not impact the T cell response after s.c. intraplantar infection of mice with LCMV.

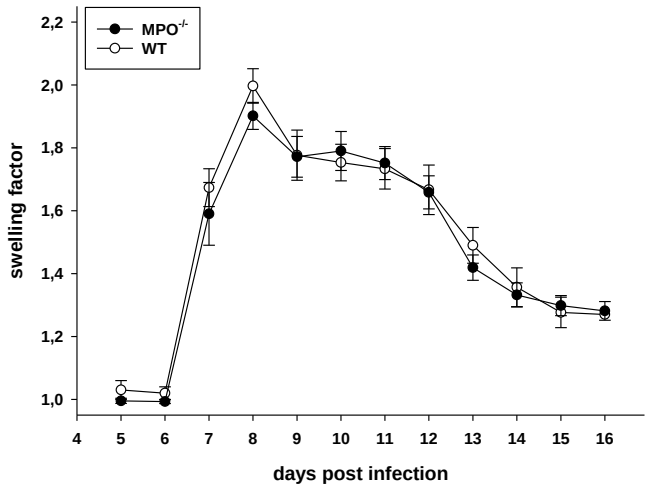

Fig. 2 Influence of MPO on LCMV-specific delayed-type hypersensitivity (DTH) reaction

Groups of $MPO^{-/-}$ and wt mice were infected by s.c. injection with 10^5 IU LCMV, strain WE, into the right hind footpad. On the indicated days p.i., the swelling factor (ratio of the dorso-ventral thickness of the inoculated foot over that of the non-inoculated foot) was determined. Shown are cumulative data as means ±SEM from 2 experiments with n = 13 $MPO^{-/-}$ mice and n = 3 wt mice.

3.1.3 Course of hepatitis during acute infection of mice with LCMV

Acute hepatitis following intraperitoneal (i.p.) injection of LCMV was investigated by determining serum transaminase activity of aspartate aminotransferase (AST) and alanine aminotransferase (ALT) (**Fig. 3**).

In naïve $MPO^{-/-}$ and wt mice, background AST activity was at about 90 U/L. Until day 4 p.i. background levels were not exceeded in neither $MPO^{-/-}$ nor wt mice. On day 6 p.i., AST activity increased to about 300 U/L in $MPO^{-/-}$ mice and to 500 U/L in wt mice. In wt mice, maximum AST activity was observed at about 2100 U/L on day 8 p.i., while there was a significant reduction in $MPO^{-/-}$ mice at about 1400 U/L. Between days 8 and 10 p.i., AST activity decreased to ranges of about 500 U/L until it returned to background levels in both $MPO^{-/-}$ and wt mice by day 14 p.i. (**Fig. 3A**). Similar to AST, ALT activity peaked on day 8 p.i. in $MPO^{-/-}$ and wt mice. In serums of $MPO^{-/-}$ mice, ALT activity was about 30 % lower on day 8 p.i. with 500 U/L. In wt

mice, the peak reached about 850 U/L. By day 14 p.i., ALT activity decreased to background levels of about 40 U/L in both $MPO^{-/-}$ and wt mice (**Fig. 3B**).

Hepatic lesions were investigated with hematoxylin and eosin (H&E) staining of liver sections on day 8 p.i.. In $MPO^{-/-}$ mice, portal inflammation and interface hepatitis were less pronounced than in wt mice (**Fig. 4A, B**). In addition, necrotic lesions were less dense $MPO^{-/-}$ mice (**Fig. 4C, D**). Fibrosis, *i.e*. the accumulation of collagen was monitored by van Gieson staining, which revealed that fibrosis was absent in both $MPO^{-/-}$ and wt mice (**Fig. 4E, F**). Quantitative histological grading of hepatitis according to the Ishak score showed that liver inflammation and damage were significantly reduced in $MPO^{-/-}$ mice on day 8 p.i.. In wt mice the Ishak score indicated a moderate stage of hepatitis scoring of about 8, while $MPO^{-/-}$ mice had only mild signs of hepatitis with a scoring of about 3.5 (**Fig. 5**).

$CD8^+$ T cells lyse infected hepatocytes by a perforin- and granzyme B-dependent mechanism [90]. This induces a signaling cascade involving cleavage of caspase 3, which leads to apoptosis. On day 8 p.i., cleaved caspase 3 was detectable in liver homogenates of $MPO^{-/-}$ and wt mice. Similar to the above described observations, levels of cleaved caspase 3 in the liver of $MPO^{-/-}$ mice were significantly reduced (**Fig. 6**).

After acute infection of mice with LCMV, the virus is cleared within 10 to 14 days. Virus elimination from the liver and the spleen was analyzed over the course of infection. Although liver damage was significantly lower in $MPO^{-/-}$ mice, virus elimination from the liver and the spleen was similar in $MPO^{-/-}$ and wt mice over the whole course of infection (**Fig. 7**).

Together, these data indicate that MPO-deficiency ameliorates the course of hepatitis, while virus elimination is not affected.

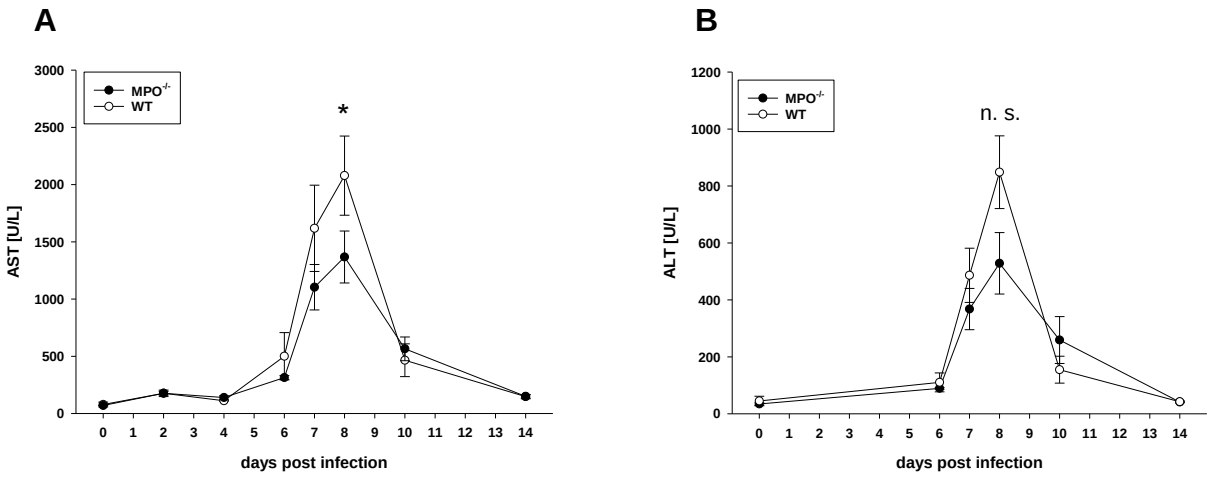

Fig. 3 Course of LCMV-induced hepatitis in MPO$^{-/-}$ and wt mice: serum transaminase activity

Groups of MPO$^{-/-}$ and wt mice were infected by i.p. injection of 10^6 IU of LCMV, strain WE. Activity of the serum transaminases AST (**A**) and ALT (**B**) was measured. Serum samples were prepared on the indicated days p.i.. Shown are cumulative data as means ±SEM from 1 (days 0, 2, 4 and 14), 3 (days 6, 7 and 10) and 9 (day 8) experiments with n = 3 (day 0), n = 2 (days 2 and 4), n = 7 (day 6), n = 18 (day 7), n = 31 (day 8), n = 12 (day 10) and n = 4 (day 14) MPO$^{-/-}$ mice and from 1 (days 0, 2, 4 and 14), 2 (days 6 and 10), 3 (day 7) and 7 (day 8) experiments with n = 2 (day 0), n = 5 (day 6), n = 14 (day 7), n = 24 (day 8), n = 6 (day 10) and n = 3 (day 14) for wt mice. Statistical significance was assessed by Student´s t-test and is indicated by * for p≤0.05

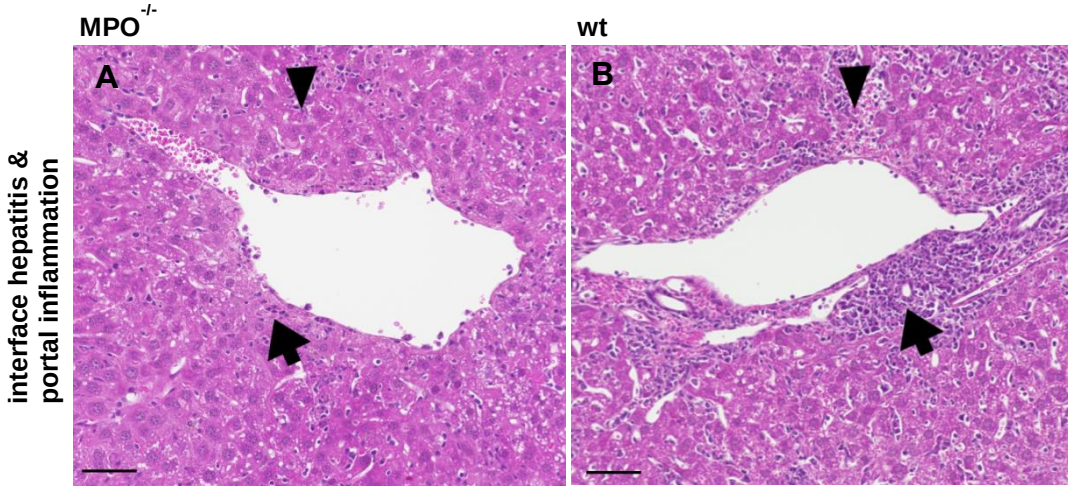

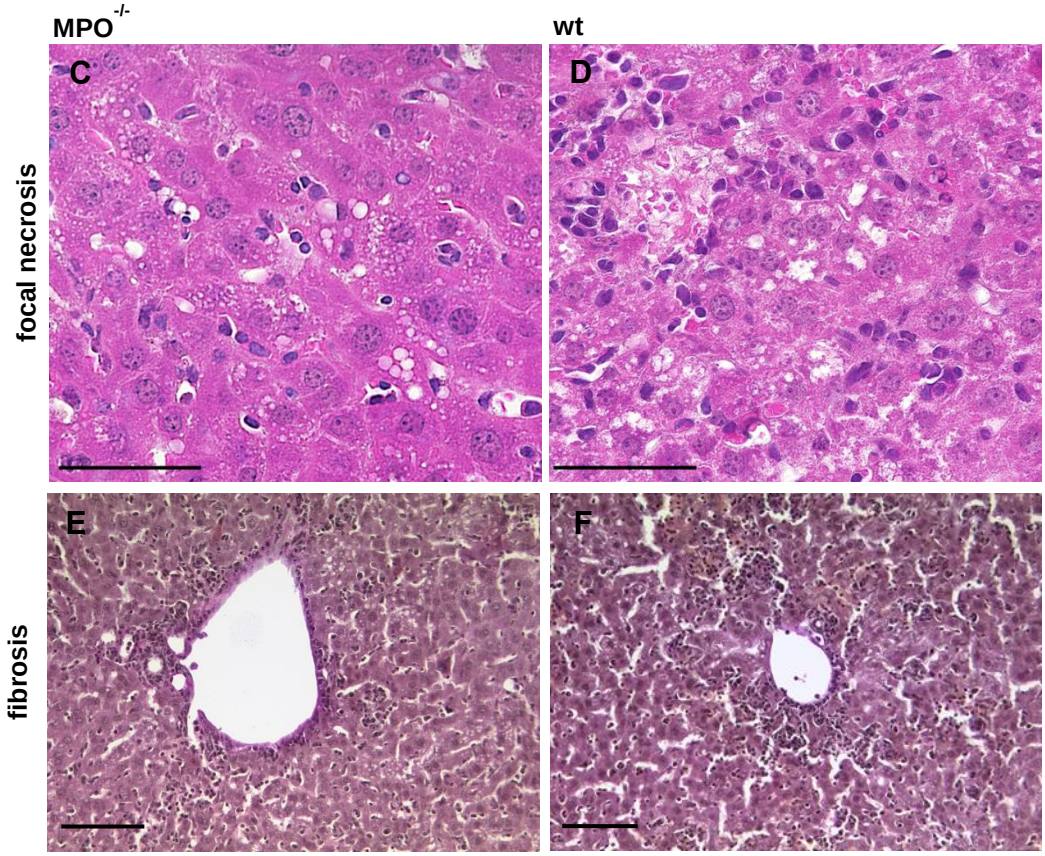

Fig. 4 H&E and van Gieson staining of liver sections on day 8 p.i.

(**A, C, E**) MPO$^{-/-}$ and (**B, D, F**) wt mice were infected by i.p. injection of 10^6 IU of LCMV, strain WE. On day 8 p.i., liver samples were prepared and fixed in 4 % PFA. Sections of the liver were subjected to standard hematoxylin and eosin (H&E) staining (**A, B**) arrow heads indicate portal inflammation, triangles indicate interface hepatitis. (**C, D**) focal necrosis. (**E, F**) van Gieson staining. Scale bars: 50 µm (**A, B, C, D**) or 100 µm (**E, F**).

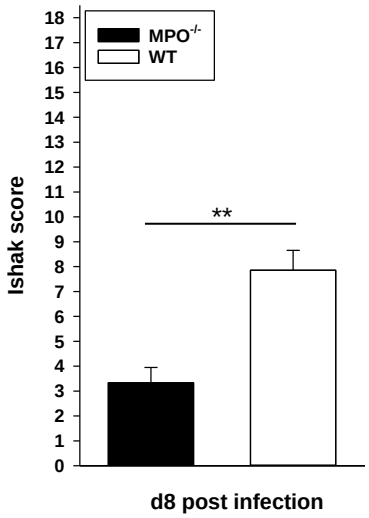

Fig. 5 Quantification of hepatitis activity according to the Ishak score

Groups of MPO$^{-/-}$ and wt mice were infected by i.p. injection of 10^6 IU of LCMV, strain WE. On day 8 p.i. liver samples were prepared. Liver inflammation was assessed according to the Ishak score on micrographs of H&E-stained liver sections. Shown are cumulative data as means ±SEM from 2 experiments with n = 6 MPO$^{-/-}$ mice and n = 7 wt mice. Statistical significance is indicated by ** for p≤0.01.

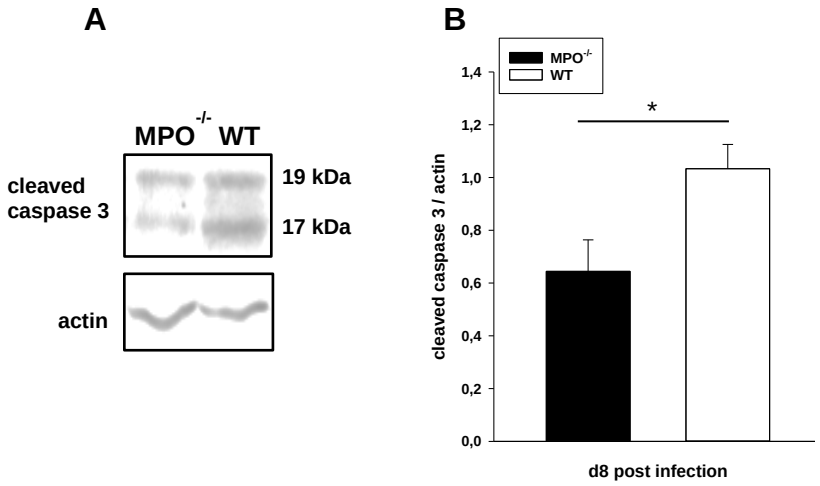

Fig. 6 Cleaved caspase 3 in the liver of MPO$^{-/-}$ and wt mice on day 8 p.i.

Groups of MPO$^{-/-}$ and wt mice were infected by i.p. injection of 10^6 IU of LCMV, strain WE. Cleaved caspase 3 was detected in liver homogenates using specific antibodies by (**A**) Western blot and quantified by (**B**) densitometry. Shown are cumulative data as means ±SEM from 2 experiments with n = 3 MPO$^{-/-}$ mice and n = 4 wt mice. Statistical significance is indicated by * for p≤0.05

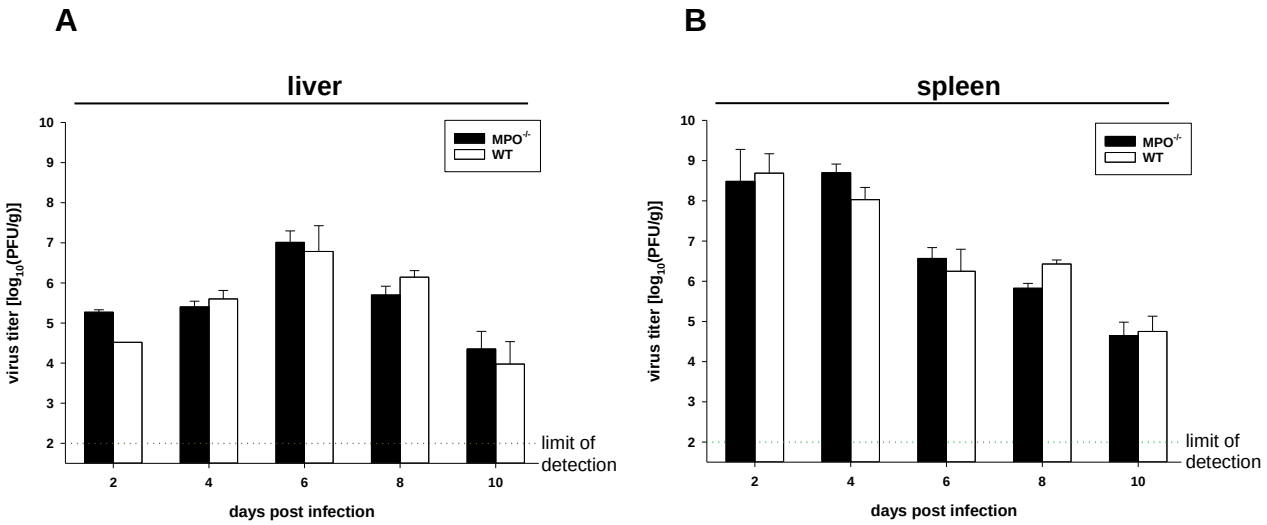

Fig. 7 Course of LCMV-induced hepatitis: viral loads in the liver and the spleen
Groups of $MPO^{-/-}$ and wt mice were infected by i.p. injection of 10^6 IU of LCMV, strain WE. Viral loads in (**A**) liver and (**B**) spleen as [$\log_{10}$ (PFU/g)] were determined at the indicated days p.i.. Shown are cumulative data as means ±SEM from 1 (day 2), 3 (day 4), 3 (day 6), 7 (day 8) and 3 (day 10) experiments with n = 2 (day 2), n = 6 (days 4, 6), n = 21 (day 8) and n = 7 (day 10) for $MPO^{-/-}$ mice and 1 (day 2), 3 (days 4, 6), 6 (day 8) and 2 (day 10) experiments with n = 1 (day 2), n = 6 (days 4, 6), n = 17 (day 8) and n = 4 (day 10) for wt mice.

3.2 The impact of MPO on the $CD8^+$ T cell response during acute LCMV-induced hepatitis

During acute infection of mice with LCMV, $CD8^+$ T cells are essential for virus elimination, however thereby they mediate immunopathology [86, 119]. Thus, the ameliorated course of hepatitis in $MPO^{-/-}$ mice suggested that MPO contributes to liver damage by influencing the effector functions of $CD8^+$ T cells.

3.2.1 Influence of MPO on T cell expansion in the spleen

In wt mice infected with LCMV, antigen-specific $CD8^+$ T cells massively expand in lymphoid organs until day 8 p.i. [84, 87, 120]. Over the course of infection

(days 0 to 10 p.i.), T cell expansion in the spleen was analyzed by flow cytometry. Among the lymphatic cells in the spleen of naïve mice, about 10 % were $CD8^+$ T cells (**Fig. 8A**). These percentages did not change until day 6 p.i.. On day 8 p.i., percentages of about 25 % were reached, in both $MPO^{-/-}$ and wt mice. By day 10 p.i., the percentages dropped to about 15 % in $MPO^{-/-}$ and wt mice. Over the whole course of infection, $CD8^+$ T cell frequencies were similar in $MPO^{-/-}$ and wt mice.
During acute infection with LCMV, $CD4^+$ T cells also proliferate and contribute to the anti-viral immune response [117]. Over the whole course of infection, the frequencies of $CD4^+$ T cells among the lymphatic cells in the spleen were similar in both, $MPO^{-/-}$ and wt mice (**Fig. 8B**).

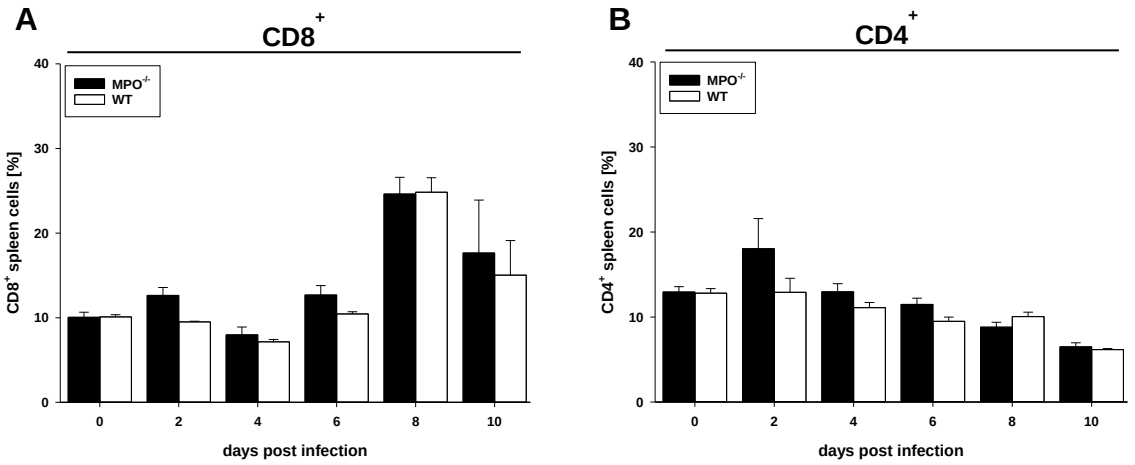

Fig. 8 Kinetics of splenic $CD8^+$ and $CD4^+$ T cells during acute LCMV-induced hepatitis
Groups of $MPO^{-/-}$ and wt mice were infected by i.p. injection with 10^6 IU of LCMV, strain WE. Percentages of (**A**) $CD8^+$ and (**B**) $CD4^+$ T cells among lymphatic spleen cells were determined by flow cytometry. Shown are cumulative data as means ±SEM from 2 (day 0), 1 (day 2), 3 (day 4, 6), 6 (day 8) and 1 (day 10) experiments with n = 4 (day 0), n = 2 (days 2, 10), n = 6 (day 4, 6) and n = 16 (day 8) $MPO^{-/-}$ mice and from 2 (day 0), 1 (day 2), 3 (day 4), 2 (day 6), 6 (day 8) and 1 (day 10) experiments with n = 4 (day 0), n = 2 (days 2, 6, 10) and n = 15 (day 8) wt mice.

3.2.2 The impact of MPO on the effector functions of T cells in the spleen

To investigate, whether MPO has an influence on the effector functions of $CD8^+$ T cells, the virus-specific cytotoxic activity of these cells was analyzed *ex vivo*. In wt mice, the cytotoxic activity of $CD8^+$ T cells usually peaks on day 8 p.i. [121]. Specific lysis by total splenocytes as effector cells from both $MPO^{-/-}$ and wt mice was about 20 % at an effector:target ratio of 100:1, on day 8 p.i. (**Fig. 9A**). To assess the cytotoxic activity of $CD8^+$ spleen cells without any possible interference of other spleen cells, $CD8^+$ T cells were immunomagnetically enriched to purities of >95 %. Specific lysis of LCMV-infected target cells by these enriched $CD8^+$ T cells reached about 40 % at an effector:target ratio of 100:1, for both $MPO^{-/-}$ and wt mice on day 8 p.i. (**Fig. 9B**).

Antigen-specific target cell killing *in vitro* depends on the frequency of LCMV-specific $CD8^+$ T cells among $CD8^+$ splenocytes. The frequencies of LCMV-specific $CD8^+$ T cells were assessed by flow cytometry using dextramers loaded with either of the three H-$2D^b$-restricted immunodominant epitopes of LCMV, GP_{33-41}, $GP_{276-286}$ and $NP_{396-404}$. On day 8 p.i., about 20 % of $CD8^+$ spleen cells expressed LCMV-specific T cell receptors (TCRs) for these three epitopes (TCR_{LCMV}^+) in both, $MPO^{-/-}$ and wt mice (**Fig. 9C**).

Mature LCMV-specific $CD8^+$ T cells secrete IFNγ upon antigen recognition. Following 4 h *in vitro* stimulation with non-infected or LCMV-infected fibroblasts, splenic $CD8^+$ T cells were analyzed for intracellular accumulation of IFNγ by flow cytometry on day 8 p.i.. Upon stimulation with non-infected fibroblasts, about 1 % of $CD8^+$ T cells expressed IFNγ in both $MPO^{-/-}$ and wt mice (**Fig. 10**).

After stimulation with LCMV-infected fibroblasts, the frequencies of $CD8^+$ T cells expressing IFNγ reached about 2 % in $MPO^{-/-}$ and wt mice.

Altogether, the percentages of $CD4^+$ and $CD8^+$ T cells, the cytotoxic activity, as well as the frequencies of virus-specific $CD8^+$ T cells and intracellular accumulation of IFNγ were similar in $MPO^{-/-}$ and wt mice. This is surprising, because in $MPO^{-/-}$ mice significantly lower serum levels of transaminases were detected over the course of LCMV infection. It is well established that this hepatic destruction is mainly mediated by $CD8^+$ T cells. This raised the question about the MPO-dependent mechanism

mediating immunopathology, which does not affect the generation of a virus-specific $CD8^+$ T cell response.

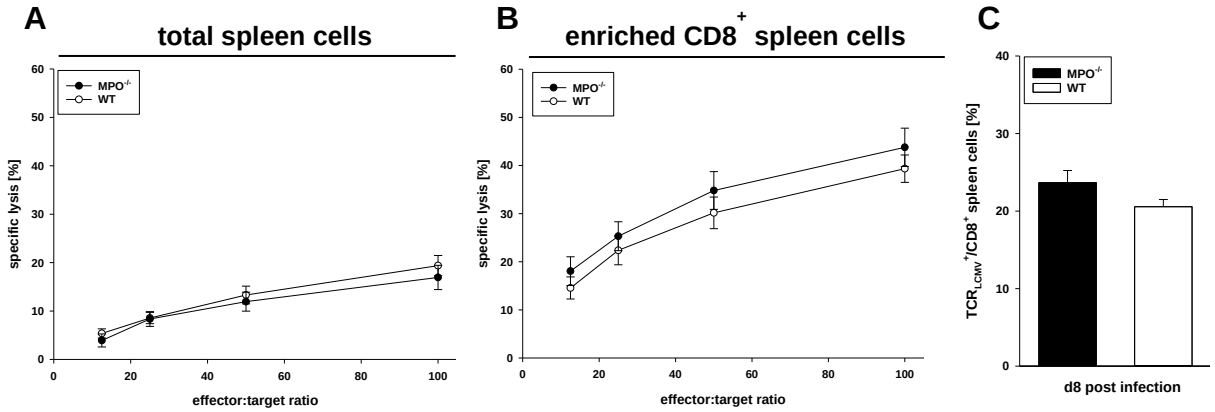

Fig. 9 Cytotoxic activity of splenic $CD8^+$ T cells on day 8 p.i..

Groups of $MPO^{-/-}$ and wt mice were infected by i.p. injection with 10^6 IU of LCMV, strain WE. At day 8 p.i. LCMV-specific cytotoxic activity of (**A**) total spleen cells or (**B**) immunomagnetically enriched $CD8^+$ effector cells (purity >95 %) against LCMV-infected syngeneic fibroblasts was determined by 4 h [51Cr]-release assay. Cytotoxic activity is shown as mean ±SEM from 3 experiments with n = 7 $MPO^{-/-}$ and n = 8 wt mice. (**C**) Percentages of LCMV-specific $CD8^+$ T cells were determined by flow cytometry using MHC dextramers loaded with LCMV-specific epitopes (MHC I alleles and epitopes: H-$2D^b$-restricted immunodominant epitopes GP_{33-41}, $GP_{276-286}$, and $NP_{396-404}$). From these data, the frequencies of LCMV-specific $CD8^+$ T cells were calculated as follows: % $TCR_{LCMV}{}^+$ $CD8^+$ cells / % $CD8^+$ spleen cells x 100 %. Columns show cumulative data of the frequencies of LCMV-specific $CD8^+$ spleen cells as means ±SEM from 8 experiments with n = 24 $MPO^{-/-}$ mice and n = 24 wt mice.

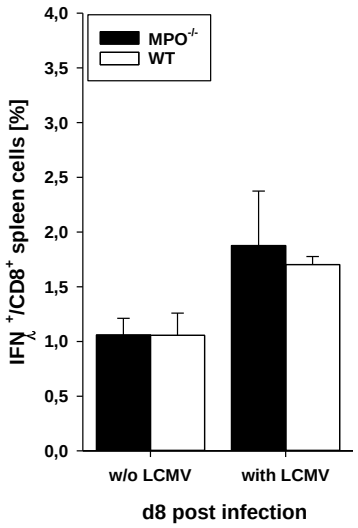

Fig. 10 IFNγ accumulation in splenic CD8$^+$ T cells after stimulation with LCMV-infected fibroblasts

Groups of MPO$^{-/-}$ and wt mice were infected by i.p. injection with 10^6 IU of LCMV, strain WE. On day 8 p.i., accumulation of intracellular IFNγ in immunomagnetically enriched CD8$^+$ effector cells upon 4 h co-culture with non-infected or LCMV-infected syngeneic fibroblasts was determined by flow cytometry. Frequencies of IFNγ$^+$/CD8$^+$ T cells are shown as mean ±SEM from 1 experiment with n = 3 MPO$^{-/-}$ and n = 3 wt mice.

3.2.3 Influence of MPO on T cell infiltration in the liver during acute LCMV-induced hepatitis

The immune response of splenic CD8$^+$ T cells was not altered in MPO$^{-/-}$ mice. However, deficiency in MPO has a strong impact on LCMV-induced liver-specific immunopathology. Therefore, the presence and activity of LCMV-induced T cells in the liver was characterized.

After virus-specific induction and expansion, T cells infiltrate in the liver during acute LCMV-mediated hepatitis [99, 122]. To investigate, whether the milder course of hepatitis in MPO$^{-/-}$ mice was due to reduced T cell infiltration, frequencies of CD8$^+$ and CD4$^+$ T cells in the liver were analyzed by flow cytometry (**Fig.11**).

Low percentages of about 2 % CD8$^+$ T cells were detectable among leukocytes in the liver of naïve mice (**Fig 11A**). In both, MPO$^{-/-}$ and wt mice, percentages increased by

day 6 p.i. to about 40 % $CD8^+$ T cells among lymphatic leukocytes. On day 8 p.i., $CD8^+$ T cell frequencies in the liver peaked at about 50 % in $MPO^{-/-}$ and wt mice. Over the whole course of infection (days 0 to 10 p.i.) the frequencies of $CD8^+$ T cells were similar in both, $MPO^{-/-}$ and wt mice.

In naïve $MPO^{-/-}$ and wt mice, about 4 % of leukocytes in the liver were $CD4^+$ T cells. Over the course of infection, the frequencies of $CD4^+$ T cells in the liver stayed in a range of 4-6 % in both, $MPO^{-/-}$ and wt mice (**Fig 11B**).

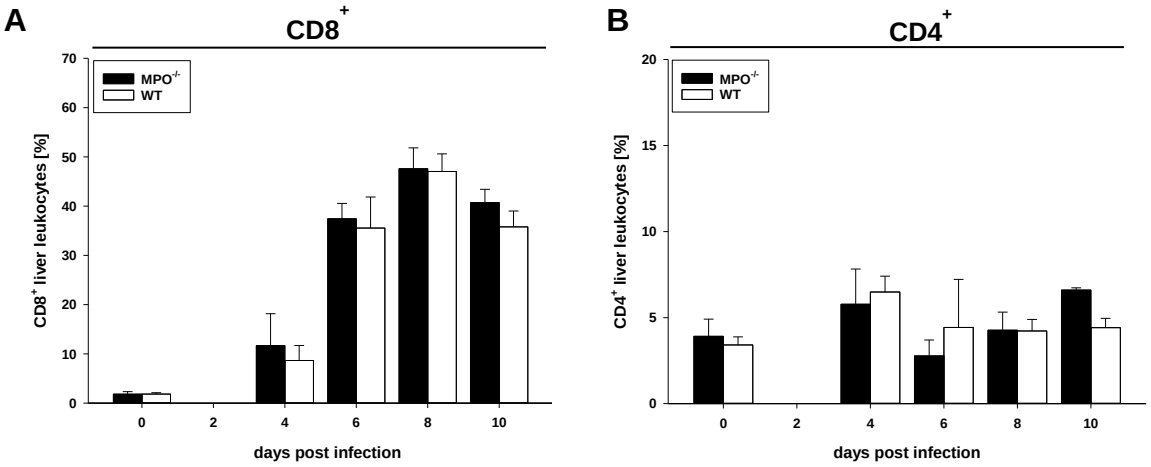

Fig. 11 Kinetics of hepatic $CD8^+$ and $CD4^+$ T cells during acute LCMV-induced hepatitis
Groups of $MPO^{-/-}$ and wt mice were infected by i.p. injection with 10^6 IU of LCMV, strain WE. In the perfused liver, percentages of (**A**) $CD8^+$ and (**B**) $CD4^+$ T cells among leukocytes were determined by flow cytometry. Shown are cumulative data as means ±SEM from 2 (day 0), 3 (day 4), 1 (days 6 and 10) and 4 (day 8) experiments with n = 4 (day 0), n = 5 (day 4) n = 2 (days 6 and 10) and n = 9 (day 8) $MPO^{-/-}$ mice and from 2 (day 0), 3 (day 4), 1 (days 6 and 10), 4 (day 8) experiments with n = 4 (day 0), n = 5 (day 4), n = 2 (days 6 and 10) and n = 10 (day 8) wt mice.

3.2.4 The impact of MPO on the cytotoxic activity of liver-infiltrating $CD8^+$ T cells

The LCMV-specific response of liver-infiltrating $CD8^+$ T cells from $MPO^{-/-}$ and wt mice was characterized by measuring the cytotoxic activity *ex vivo*.

In wt mice, serum transaminase levels peaked on day 8 p.i. and correlated with the course of the immune response of $CD8^+$ T cells. Serum AST activity in $MPO^{-/-}$ mice was already reduced on day 7 p.i.. Therefore, the cytotoxic activity of liver-infiltrating $CD8^+$ T cells was analyzed on days 7 and 8 p.i..

On day 7 p.i., enriched $CD8^+$ T cells from the liver of either $MPO^{-/-}$ or wt mice already exerted a strong LCMV-specific cytolysis of about 60 % at an effector:target ratio of 100:1 (**Fig. 12A**). On day 8 p.i., the cytotoxic activity of liver-infiltrating $CD8^+$ T cells was further enhanced to about 70 % at an effector:target ratio of 100:1 (**Fig. 12B**). Virus-specific $CD8^+$ T cells from $MPO^{-/-}$ and wt mice exerted similar specific lysis on days 7 and 8 p.i..

The frequencies of virus-specific $CD8^+$ T cells were analyzed by flow cytometry using dextramers loaded with either of the three H-$2D^b$-restricted immunodominant epitopes of LCMV. On day 7 p.i., about 30 % of liver-infiltrating $CD8^+$ T cells expressed TCR_{LCMV}^+ among the lymphatic cells in $MPO^{-/-}$ and wt mice (**Fig. 13**).

On day 8 p.i., about 34 % of liver-infiltrating $CD8^+$ T cells in $MPO^{-/-}$ mice and 28 % in wt mice expressed TCR_{LCMV}^+. This difference was not significant.

Activated CTLs produce IFNγ as long as TCR stimulation persists (reviewed in [89, 123]). Because of that, IFNγ accumulation in immunomagnetically enriched liver-infiltrating $CD8^+$ T cells was assessed by flow cytometry after 4 h *in vitro* stimulation with non-infected or LCMV-infected syngeneic fibroblasts on day 8 p.i. (**Fig.14**). After stimulation of liver-infiltrating $CD8^+$ T cells with non-infected fibroblasts, about 4 % expressed IFNγ in both $MPO^{-/-}$ and wt mice. After stimulation with LCMV-infected fibroblasts about 10 % of $CD8^+$ T cells responded with IFNγ production. In both, $MPO^{-/-}$ and wt mice, the frequencies of IFNγ-expressing liver-infiltrating $CD8^+$ T cells were similar.

In line with the results for splenic $CD8^+$ T cells, the cytotoxic activity and the frequencies of liver-infiltrating $CD8^+$ T cells expressing TCR_{LCMV}^+ were similar in

MPO$^{-/-}$ and wt mice. MPO did not alter the response of CD8^{+} T cells in the liver neither on day 7 p.i. nor on day 8 p.i..

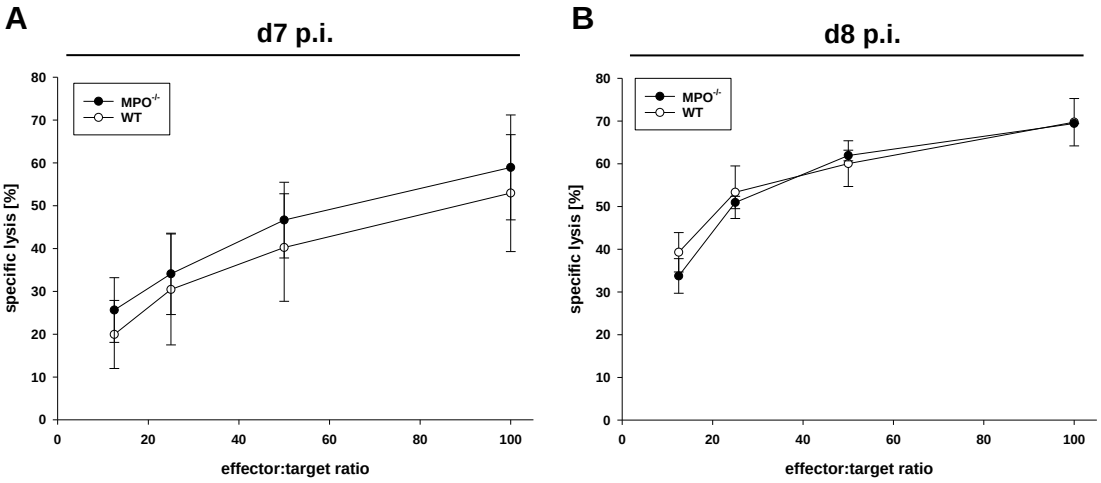

Fig. 12 Cytotoxic activity of liver-infiltrating CD8^{+} T cells on days 7 and 8 p.i.

Groups of MPO$^{-/-}$ and wt mice were infected by i.p. injection with 10^6 IU of LCMV, strain WE. At days (**A**) 7 and (**B**) 8 p.i. LCMV-specific cytotoxic activity of immunomagnetically enriched CD8^{+} effector cells from the liver (purity >95 %) against LCMV-infected syngeneic fibroblasts was determined by 4 h [51Cr]-release assays. Cytotoxic activity is shown as mean ±SEM from 1 experiment with n = 2 MPO$^{-/-}$ mice and n = 2 wt mice.

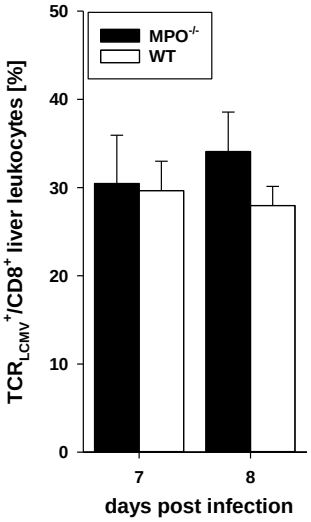

Fig. 13 Frequencies of liver-infiltrating, LCMV-specific CD8^{+} T cells on days 7 and 8 p.i.

-Legend continued on next page-

-Continued legend-

Fig. 13 Frequencies of liver-infiltrating, LCMV-specific CD8$^+$ T cells on days 7 and 8 p.i.
Groups of MPO$^{-/-}$ and wt mice were infected by i.p. injection with 10^6 IU of LCMV, strain WE. At days (**A**) 7 and (**B**) 8 p.i. percentages of LCMV-specific CD8$^+$ T cells were determined by flow cytometry with MHC dextramers loaded with LCMV-specific epitopes (MHC I alleles and epitopes: H-2D^b-restricted immunodominant epitopes GP_{33-41}, $GP_{276-286}$, and $NP_{396-404}$). From these data, the frequencies of LCMV-specific CD8$^+$ T cells were calculated as follows: % TCR_{LCMV}^+ CD8$^+$ cells / % CD8$^+$ liver cells x 100 %. Column diagrams show cumulative data of the frequencies of LCMV-specific CD8$^+$ leukocytes as means ±SEM from 1 (day 7) and 4 experiments (day 8) with n = 2 (day 7) and n = 10 (day 8) MPO$^{-/-}$ and wt mice.

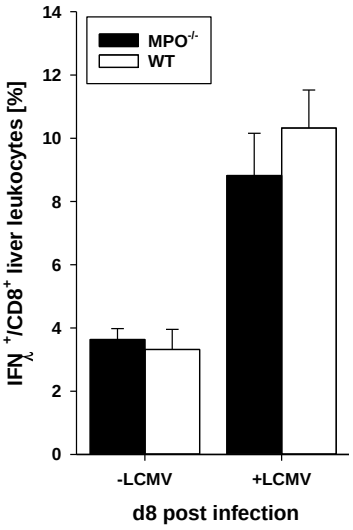

Fig. 14 IFNγ accumulation in liver-infiltrating CD8$^+$ T cells after stimulation with LCMV-infected fibroblasts
Groups of MPO$^{-/-}$ and wt mice were infected by i.p. injection with 10^6 IU of LCMV, strain WE. At day 8 p.i., accumulation of intracellular IFNγ by immunomagnetically enriched CD8$^+$ effector cells upon 4 h co-culture with non-infected or LCMV-infected syngeneic fibroblasts was determined by flow cytometry. Frequencies of IFNγ$^+$/CD8$^+$ T cells are shown as mean ±SEM from 1 experiment with n = 3 MPO$^{-/-}$ and n = 3 wt mice.

3.3 Myeloid cells and LCMV-induced acute hepatitis

Immunopathology during LCMV-induced hepatitis is largely mediated by $CD8^+$ T cells. However in $MPO^{-/-}$ mice, the immune response of $CD8^+$ T cells was not altered over the course of infection. Due to that, we wanted to elucidate, to what extent myeloid cells contribute to liver injury.

3.3.1 Myeloid cells in the liver during LCMV-induced acute hepatitis

The recruitment of myeloid cells to the liver was analyzed in naïve mice and on day 8 p.i. by flow cytometry (**Fig. 15, 16**).

In naïve $MPO^{-/-}$ and wt mice, frequencies of neutrophils ($CD11b^+/Ly6G^{hi}$) among leukocytes in the liver were below 3 % (**Fig. 15A, 16A**) [124]. On day 8 p.i., frequencies increased to about 9 % in $MPO^{-/-}$ mice. In wt mice, percentages of neutrophils were slightly, but significantly lower with about 7 %. Infiltrating monocytes as identified by $CD11b^+/Ly6C^{hi}$ expression reached about 4 % of leukocytes in naïve $MPO^{-/-}$ and wt mice (**Fig. 15B, 16B**) [125]. On day 8 p.i., about 18 % of liver leukocytes were infiltrating monocytes in both, $MPO^{-/-}$ and wt mice. Infiltrating macrophages can be distinguished from Kupffer cells (KCs), which are resident liver macrophages, by low expression of F4/80 ($CD11b^+/F4/80^{low}$), while KCs have high expression of F4/80 ($CD11b^+/F4/80^{hi}$) [126]. In naïve $MPO^{-/-}$ and wt mice, percentages of $CD11b^+/F4/80^{low}$ macrophages were about 0.5 % (**Fig. 15C, 16C**). The frequencies of infiltrating macrophages increased to about 10 % in $MPO^{-/-}$ mice and to about 8 % in wt mice on day 8 p.i.. This difference was not significant. In naïve $MPO^{-/-}$ and wt mice KCs were present in the range of 11-14 % (**Fig. 15D, 16D**). On day 8 p.i., frequencies of KCs were not altered with about 14 % in both $MPO^{-/-}$ and wt mice.

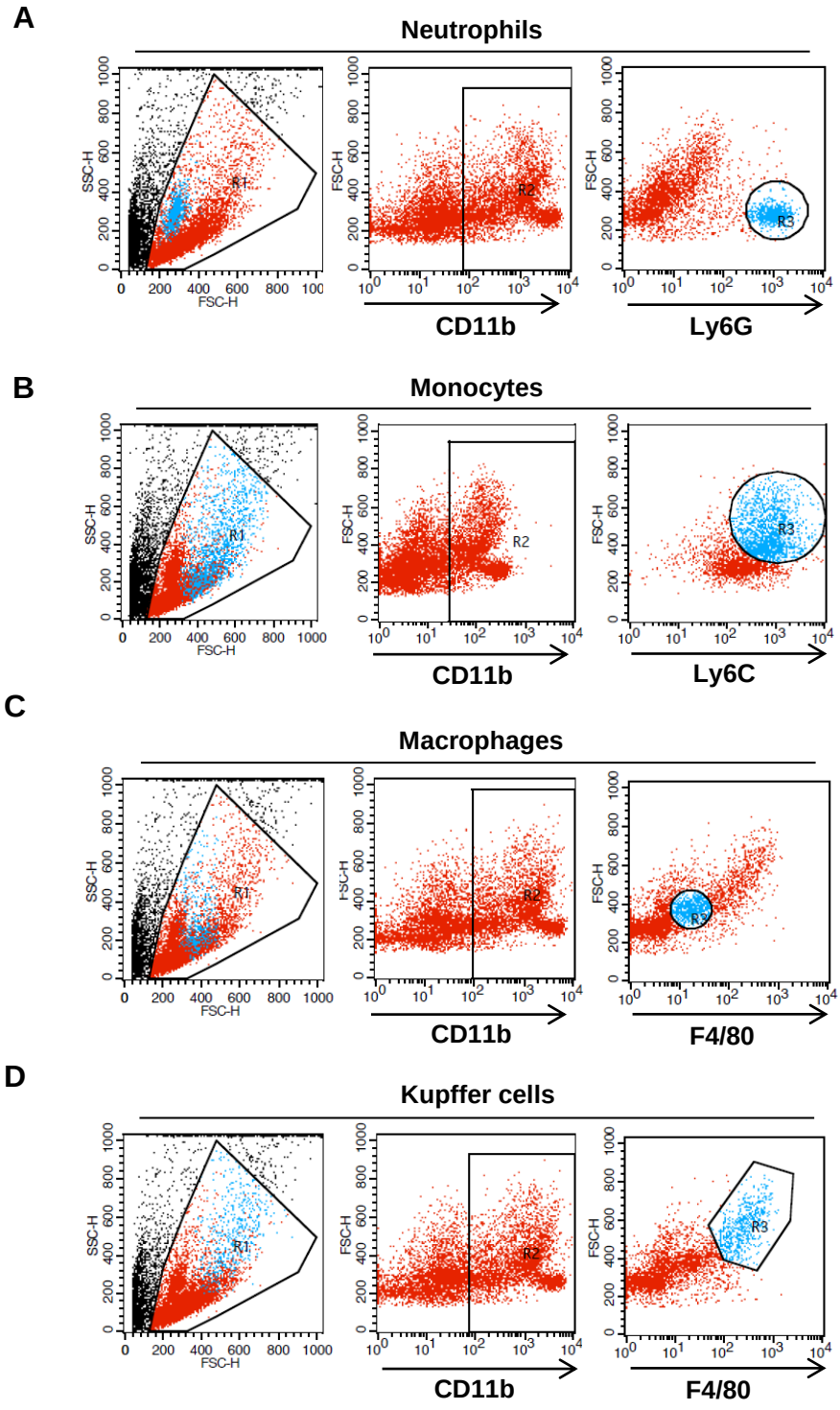

Fig. 15 FACS strategy for the identification of myeloid cells in the liver

Groups of MPO$^{-/-}$ and wt mice were infected by i.p. injection with 10^6 IU of LCMV, strain WE. Single cell suspensions of the perfused liver were prepared on the indicated days and percentages of (**A**) neutrophils (CD11b$^+$/Ly6G^{hi}), (**B**) monocytes (CD11b$^+$/Ly6C^{hi}), (**C**) macrophages (CD11b$^+$/F4/80$^+$) and (**D**) Kupffer cells (CD11b$^+$/F4/80^{hi}) among liver leukocytes were determined by flow cytometry. Shown are representative FACS Plots of wt mice from day 8 p.i..

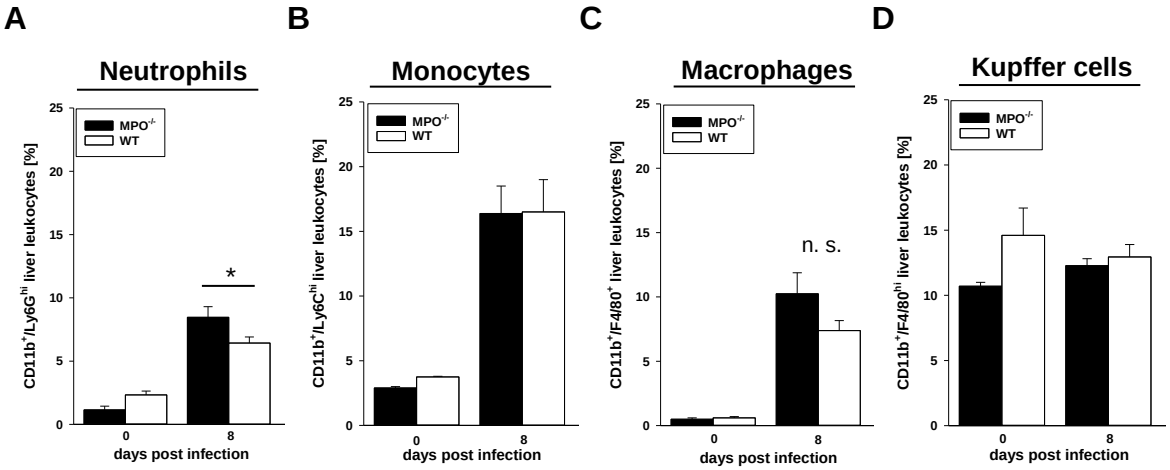

Fig. 16 Recruitment of myeloid cells to the liver during LCMV-induced hepatitis

Groups of MPO$^{-/-}$ and wt mice were infected by i.p. injection with 10^6 IU of LCMV, strain WE. Single cell suspensions of the perfused liver were prepared on the indicated days and percentages of (**A**) neutrophils (CD11b$^+$/Ly6G^{hi}), (**B**) monocytes (CD11b$^+$/Ly6C^{hi}), (**C**) macrophages (CD11b$^+$/F4/80$^+$) and (**D**) Kupffer cells (CD11b$^+$/F4/80^{hi}) among liver leukocytes were determined by flow cytometry. Shown are cumulative data as means ±SEM from 3 (day 0) and 5 (day 8) experiments with n = 5 (day 0) and n = 10 (day 8) MPO$^{-/-}$ and wt mice for neutrophils. 1 (day 0) and 2 (day 8) experiments with n = 2 (day 0) and n = 5 MPO$^{-/-}$ and wt mice for monocytes, macrophages and Kupffer cells. Statistical significance is indicated by * for p≤0.05.

3.3.2 Cell type-specific expression of MPO

MPO is predominantly located in primary granules of neutrophils [127]. In humans, MPO is expressed to a lesser extent by monocytes and macrophage subsets [128-130]. In rodents, little is known about MPO expression in myeloid cells, except for neutrophils [5].

MPO expression by neutrophils (CD11b$^+$/Ly6G^{hi}), monocytes (CD11b$^+$/Ly6C^{hi}), infiltrating macrophages (CD11b$^+$/F4/80$^{low/+}$) and KCs (CD11b$^+$/F4/80^{hi}) in the liver was assessed on day 8 p.i. according to FACS strategy in 3.3.1 (**Fig. 15**). Mean fluorescence intensity (MFI) of MPO expression was determined by substraction of cell type-specific autofluorescence from measurements of specifically stained samples (**Fig. 17**). In MPO$^{-/-}$ mice, MPO expression was absent in each neutrophils,

monocytes, macrophages or KCs. Among myeloid cells in the liver of wt mice, only neutrophils expressed high amounts of MPO (**Fig. 17A**). Monocytes and infiltrating macrophages contained very low levels of MPO (**Fig. 17 B, C**). MPO detection in monocytes and macrophages is not necessarily due to cell type-specific expression. Instead, phagocytosed contents of neutrophils may contain immunoreactive MPO during inflammation [131]. In KCs from wt mice MPO was not detectable (**Fig. 17D**). Taken together, these data indicate that among myeloid cells, neutrophils are the main source of MPO during LCMV-induced infection, in wt mice.

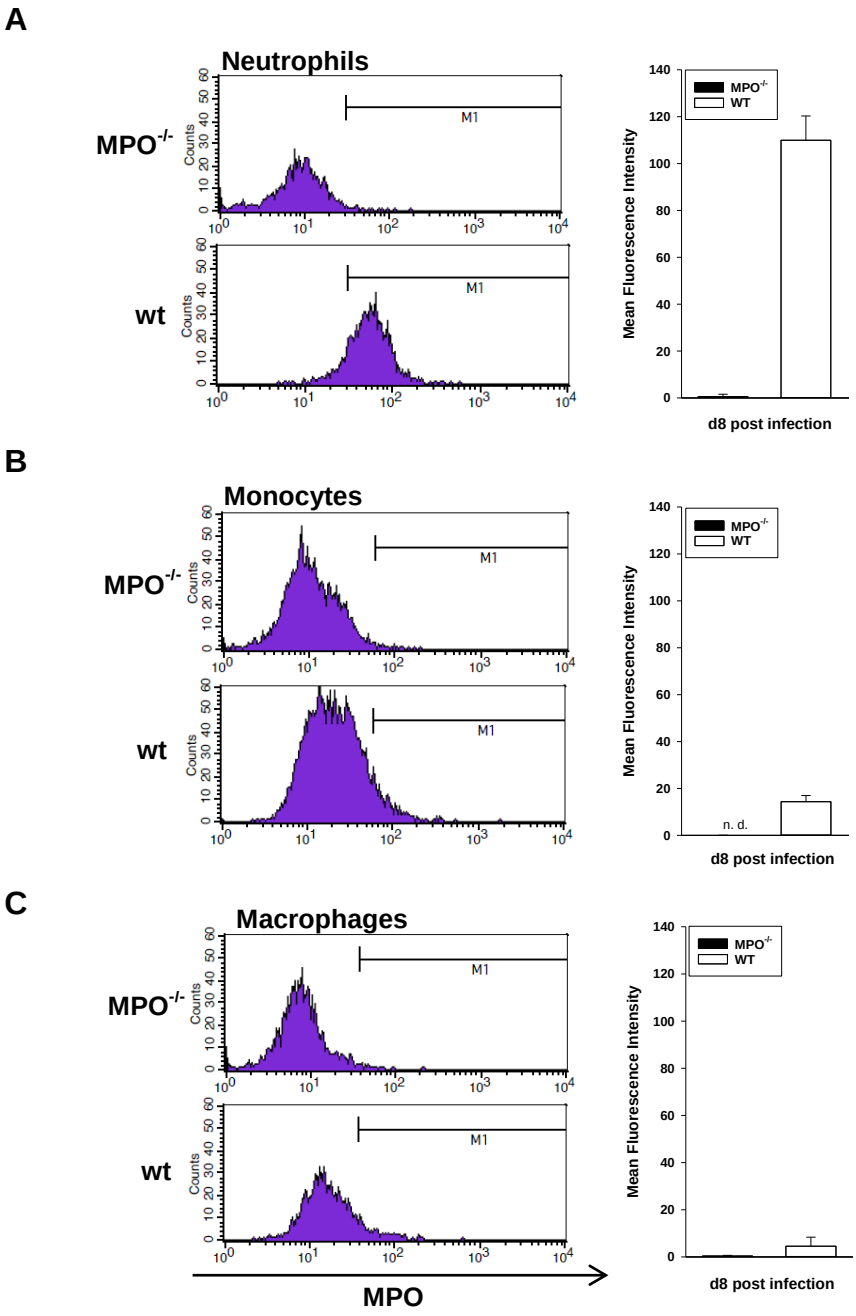

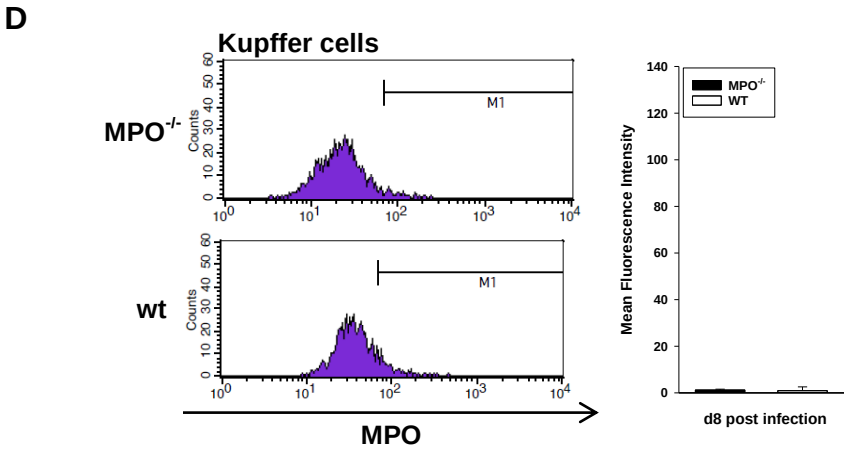

Fig. 17 Cell type-specific expression of MPO by myeloid cells in the liver

Groups of MPO$^{-/-}$ and wt mice were infected by i.p. injection with 10^6 IU of LCMV, strain WE. Single cell suspensions of the perfused liver were prepared on day 8 p.i. and gating strategy was assessed according to cell appearance in the FSC/SSC and surface marker staining according to FACS strategy in 3.3.1 Fig. 15. Expression of intracellular MPO by (**A**) neutrophils (CD11b$^+$/Ly6G^{hi}), (**B**) monocytes (CD11b$^+$/Ly6C$^+$), (**C**) macrophages (CD11b$^+$/F4/80$^+$) and (**D**) Kupffer cells (CD11b$^+$/F4/80^{hi}) was determined by flow cytometry. Intracellular expression of MPO is shown as means of mean fluorescence intensity (MFI) minus autofluorescence as ±SEM from 1 experiment with n = 2 MPO$^{-/-}$ mice and n = 2 wt mice.

3.3.3 Neutrophil recruitment to the liver over the course of LCMV infection

Neutrophils expressed the highest amounts of MPO in wt mice. Furthermore, frequencies of neutrophils were increased on day 8 p.i., in both MPO$^{-/-}$ and wt mice (**Fig. 16A**). Therefore, neutrophil infiltration in the liver over the whole course of infection was analyzed.

In naïve mice, as well as on days 2 and 4 p.i., less than 3 % among leukocytes in the liver amounted to neutrophils of both, MPO$^{-/-}$ and wt mice (**Fig. 18**). On day 6 p.i., frequencies increased to about 5-6 % in both genotypes. On day 8 p.i., about 8.5 % among leukocytes in the liver of MPO$^{-/-}$ mice were neutrophils. In wt mice, slightly, but significantly lower frequencies of about 6.5 % were detected. On day 10 p.i., percentages declined to about 5 % in MPO$^{-/-}$ and wt mice.

Together, these data show that neutrophil recruitment to the liver peaks on day 8 p.i. and declines afterwards. These kinetics correlate with the course of both, serum AST levels and infiltration of $CD8^+$ T cells in the liver. This is surprising, since neutrophils are known to be first-line defenders against invading pathogens, which are recruited shortly after infection [41]. However, here neutrophil infiltration in the liver parallels the course of the adaptive immune response against LCMV.

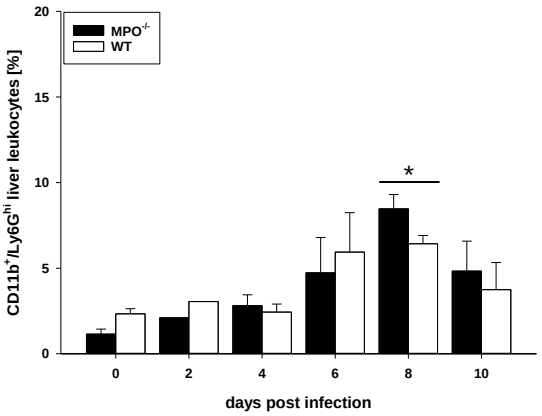

Fig. 18 Neutrophil recruitment to the liver over the course of LCMV infection

Groups of $MPO^{-/-}$ and wt mice were infected by i.p. injection with 10^6 IU of LCMV, strain WE. In the perfused liver, percentages of neutrophils ($CD11b^+/Ly6G^{hi}$) among leukocytes were determined by flow cytometry. Shown are cumulative data as means ±SEM from 3 (days 0 and 4), 1 (days 2 and 10), 5 (day 8) and 4 (day 8) experiments with n = 5 (days 0 and 4), n = 1 (day 2) n = 5 (day 4) and n = 3 (day 6), n = 10 (day8) and n = 2 (day 10) $MPO^{-/-}$ and wt mice. Statistical significance is indicated by * for $p \leq 0.05$.

3.3.4 LCMV-induced hepatitis in mice depleted of neutrophils

The kinetics of neutrophil recruitment to the liver correlated with the course of liver damage during LCMV-induced hepatitis. To assess the functional role of neutrophils in viral hepatitis, neutrophils were depleted in LCMV-infected wt mice with anti-Ly6G (clone 1A8) antibody at the day of infection and four days after infection. Neutrophils can be easily detected by Ly6G staining. However the depletion antibody is directed against Ly6G also. This means that false negative flow cytometry may be due to masking of the epitope Ly6G by the depletion antibody instead of successful elimination of neutrophils. Therefore, neutrophil depletion was assessed by flow cytometry of $CD11b^{+}/Gr\text{-}1^{hi}$ cells (**Fig. 19A**) [132].

To test whether antibody treatment itself causes liver damage, serum AST activity in naïve mice was measured one day after antibody injection (**Fig. 19B**). In comparison to untreated naïve mice, antibody treatment did not increase AST levels in serum of non-infected mice. Background AST activity was at about 90 U/L in both groups.

On days 7 and 8 p.i., AST activity was at about 1000 U/L in control mice, while in mice depleted of neutrophils, AST activity was highly significantly increased to about 3000 U/L on both days (**Fig. 19B**).

In comparison to control mice, viral loads in the liver and the spleen of neutrophil-depleted mice were slightly increased on days 1 and 2 p.i. (**Fig. 20**). However, on day 8 p.i., viral load in the liver and the spleen was significantly higher, in mice depleted of neutrophils.

This was surprising, since neutrophils are the main cell type expressing MPO. In our model, we could show that MPO is involved in aggravated tissue damage. Therefore, we hypothesized that neutrophil depletion would reduce liver damage in wt mice. However, a recent publication by Liang *et al*. revealed that the response of $CD8^{+}$ T cell is partially controlled by immunosuppressive neutrophils [133]. This means that neutrophils can be involved in minimizing tissue damage by suppressing a strong CTL response.

These data add up to a paradoxical constellation. On the one hand, neutrophils are involved in limiting LCMV-induced immunopathology. On the other hand, MPO largely expressed by neutrophils, contributes to LCMV-induced liver damage.

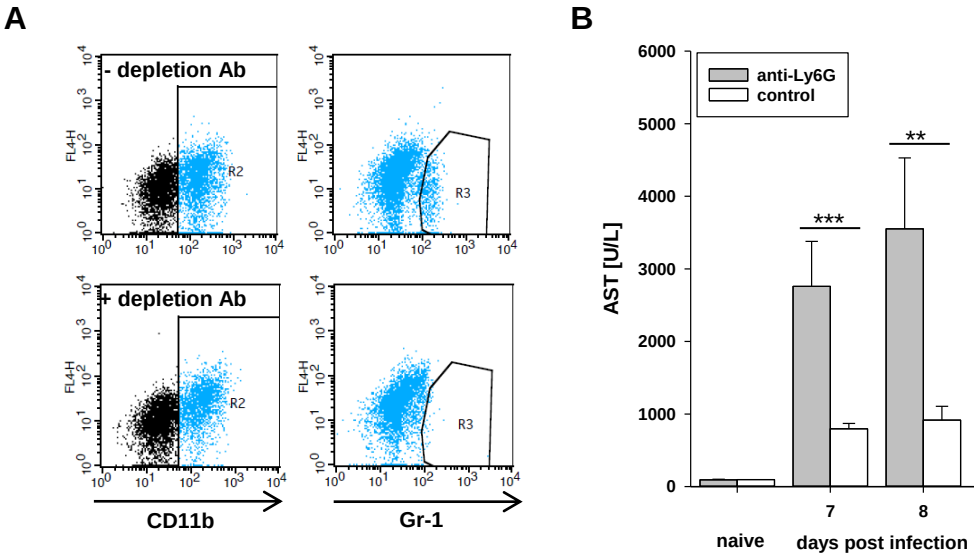

Fig. 19 Neutrophil depletion aggravates liver damage in mice infected with LCMV

Groups of Bl/6J wt mice were infected by i.p. injection of 10^6 IU of LCMV, strain WE. Neutrophils were depleted by i.p. injection of 400 µg anti-mouse Ly6G, clone 1A8. Control mice did not receive antibody treatment. (**A**) Neutrophil depletion in the liver was confirmed by CD11b and Gr-1 staining. Plots show representative examples of $CD11b^+/Gr\text{-}1^{hi}$ staining. (**B**) Activity of the serum transaminase AST was measured. Serum samples were prepared on the indicated days p.i.. Shown are cumulative data as means ±SEM from 1 (naïve) and 2 (days 7 and 8) experiments with n = 3 (naïve) and n = 7 (days 7 and 8) mice per group. Statistical significance was assessed by Student´s t-test and is indicated by ** for p≤0.01 and *** for p≤0.001.

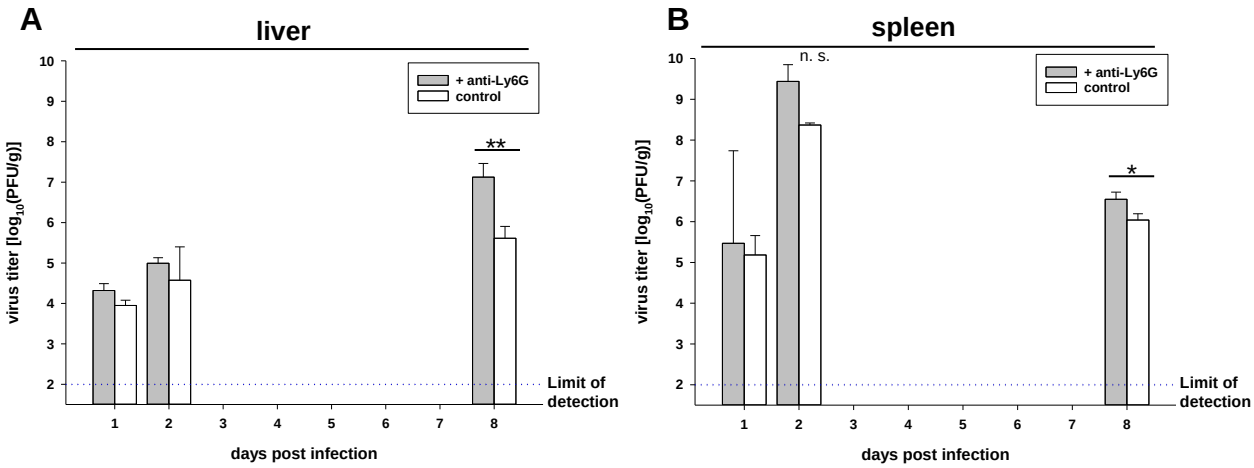

Fig. 20 Viral loads in the liver and the spleen after depletion of neutrophils

Groups of Bl/6J wt mice were infected by i.p. injection of 10^6 IU of LCMV, strain WE. Neutrophils were depleted by i.p. injection of 400 µg anti-mouse Ly6G, clone 1A8. Control mice did not receive antibody treatment. Viral loads in (**A**) liver and (**B**) spleen as [$\log_{10}$ (PFU/g)] were determined at the indicated days p.i.. Shown are cumulative data as means ±SEM from 1 (days 1 and 2) and 2 (day 8) experiments with n = 2 (days 1 and 2), n = 8 (day 8) mice per group. Statistical significance was assessed by Student´s t-test and is indicated by * for p≤0.05 and ** for p≤0.01.

3.4 The impact of MPO on neutrophil defense mechanisms in response to LCMV infection

Neutrophils are involved in the primary defense against infections by three major mechanisms, *i.e.* phagocytosis, degranulation and NETosis (reviewed in [41]). During these processes, pathogens are exposed to MPO-derived ROS.

We wanted to elucidate, whether MPO-induced immunopathology during acute LCMV infection can be attributed to these defense mechanisms.

3.4.1 The impact of intracellular MPO activity on LCMV-induced immunopathology

For the generation of hypohalous acids, MPO uses hydrogen peroxide produced by various ROS sources, *e.g.* NADPH oxidases (NOX) [10, 134, 135]. In neutrophils, intracellular ROS are predominantly produced by NOX2 [136]. Thus, particularly intracellular MPO activity, which contributes to microbial killing upon phagocytosis, is dependent on NOX2 [44].

Therefore, we studied mice with NOX2-deficiency in myeloid cells ($NOX2^{flox/flox}$ x LysM Cre^{pos}). In these mice, cells of the myeloid lineage *i.e.* granulocytes, monocytes and macrophages produce much lower amounts of ROS than wt cells [137, 138]. This potentially causes reduced intracellular levels of MPO-derived oxidants in neutrophils.

LCMV-induced liver damage was assessed by serum AST levels over the course of infection (**Fig. 21A**). On day 6 p.i., AST activity was at about 500 U/L in $NOX2^{flox/flox}$ x LysM Cre^{pos} and $NOX2^{flox/flox}$ x LysM Cre^{neg} mice. On days 7 and 8, AST activity increased to about 1500 U/L and declined to about 700 U/L by day 10 p.i. in both, $NOX2^{flox/flox}$ x LysM Cre^{pos} and $NOX2^{flox/flox}$ x LysM Cre^{neg} mice. Over the whole course of infection, AST activity was similar in $NOX2^{flox/flox}$ x LysM Cre^{pos} and $NOX2^{flox/flox}$ x LysM Cre^{neg} mice. Virus elimination from the liver and the spleen was also unaffected by NOX2-deficiency in myeloid cells (**Fig. 21B, C**)

These data show that LCMV-induced immunopathology is independent of NOX2 expression in myeloid cells. Since intracellular MPO requires hydrogen peroxide predominantly generated by NOX2, this suggests that immunopathology and virus elimination are largely independent on intracellular MPO activity in neutrophils.

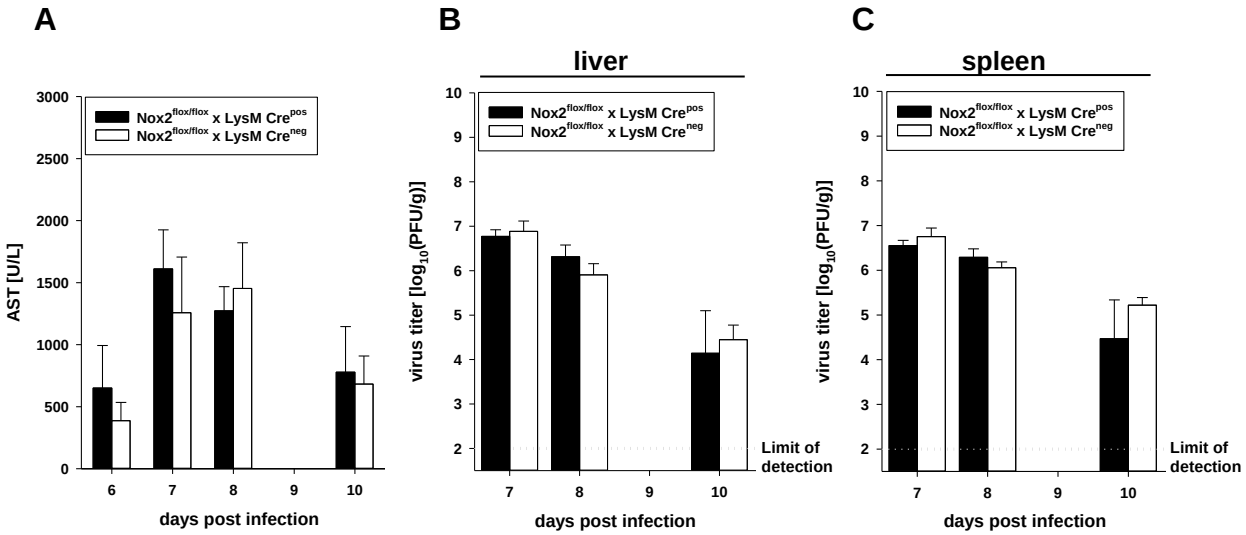

Fig. 21 Serum AST activity and viral loads in NOX2$^{flox/flox}$ x LysM Cre mice

Groups of NOX2$^{flox/flox}$ x LysM Cre^{pos} and NOX2$^{flox/flox}$ x LysM Cre^{neg} mice were infected by i.p. injection of 10^6 IU of LCMV, strain WE. (**A**) Activity of the transaminase AST was measured in serum samples, which were prepared on the indicated days p.i.. Shown are cumulative data as means ±SEM from 2 (days 6 and 10), 4 (days 7) and 5 (day 8) experiments with n = 8 (day 6), n = 15 (day 7), n = 13 (day 8), n = 10 (day 10) NOX2$^{flox/flox}$ x LysM Cre^{pos} and from 2 (day 6), 4 (day 7), 7 (day 8) and 3 (day 10) experiments with n = 6 (day 6), n = 12 (day 7), n = 15 (day 8), n = 7 (day 10) NOX2$^{flox/flox}$ x LysM Cre^{neg} mice. Viral load in (**B**) the liver and (**C**) the spleen as [log_{10} (PFU/g)] were determined at the indicated days p.i.. Shown are cumulative data as means ±SEM from 4 (days 7 and 8) and 1 experiment with n=15 (day 7) n=11 (day 8) and n=3 (day 10) NOX2$^{flox/flox}$ x LysM Cre^{pos} mice and n=12 (days 7 and 8) and n=3 (day 10) NOX2$^{flox/flox}$ x LysM Cre^{neg} mice.

3.4.2 Neutrophil extracellular trap formation by MPO$^{-/-}$ neutrophils

NETs are web-like chromatin structures, which are released by neutrophils in response to various stimuli (reviewed in [46]). NET-induced inactivation of various pathogens is, among other factors, dependent on MPO (reviewed in [42, 139, 140]). Besides pathogen clearance, excessive NET formation can aggravate tissue damage (reviewed in[46]). We wanted to investigate, if LCMV stimulates NET formation by neutrophils, which possibly may contribute to immunopathology.

To investigate NETosis in response to LCMV, neutrophils were enriched from the bone marrow of naïve $MPO^{-/-}$ and wt mice. NETosis was assessed after 4 h *in vitro* incubation with PMA or LCMV [141]. As a surrogate indicator of NETosis, extracellular DNA was stained with the plasma membrane-impermeable dye SYTOX Green and analyzed by flow cytometry (**Fig. 22**). Sytox $green^{pos}$ neutrophils after stimulation with 25 nM PMA are shown in representative FACS plots to introduce the gating strategy (**Fig. 22A**).

About 3.5 % of unstimulated neutrophils from $MPO^{-/-}$ mice and 2 % from wt mice released DNA spontaneously (**Fig. 22B**). When neutrophils were exposed to 25 nM PMA, about 12 % of cells were SYTOX $Green^{pos}$ from both $MPO^{-/-}$ and wt mice. Upon exposure to LCMV at either MOI 10 or MOI 100, about 10 % of neutrophils from $MPO^{-/-}$ mice and about 8 % from wt mice were SYTOX $Green^{pos}$. Under consideration of the level of spontaneous NETosis in both genotypes, this difference was not significant.

This *in vitro* study reveals that stimulation of neutrophils with high MOI of LCMV induces NETosis by murine neutrophils. However, this process is independent of MPO. With the observations from mice with NOX2-deficiency in cells of the myeloid lineage, these data suggest that immunopathology does not depend on the activity or presence of intracellular MPO. Even in the absence of the major source of intracellular hydrogen peroxide, NOX2, LCMV-induced immunopathology was unaltered and NETosis in response to LCMV was independent of MPO.

Together, these data imply that LCMV-induced immunopathology is independent of intracellular MPO activity. Instead, it may be caused by extracellular MPO, which retains its activity by consumption of ROS from various undefined sources.

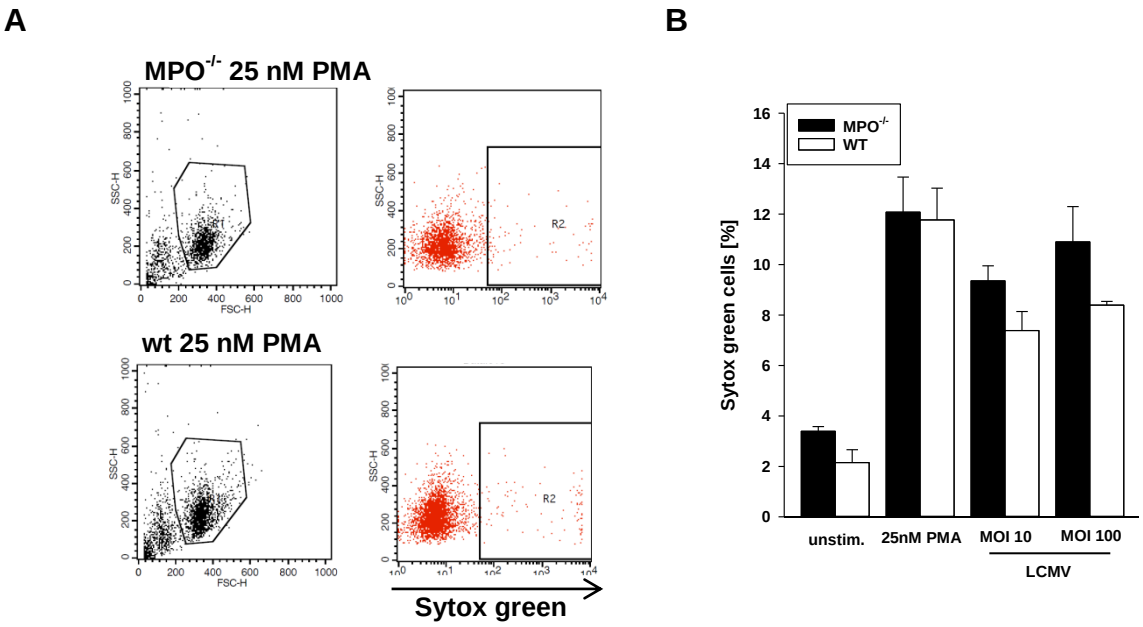

Fig. 22 NET formation by murine neutrophils in response to stimulation with LCMV
Neutrophils were negatively enriched from the bone marrow from groups of naïve MPO$^{-/-}$ and wt mice. Upon 4 h *in vitro* cultivation, extracellular DNA released by unstimulated cells or after incubation with 25 nM PMA, MOI 10 or MOI 100 LCMV was stained with plasma membrane-impermeable dye SYTOX green. (**A**) Shown are representative FACS plots of neutrophils stimulated with 25 nM PMA. (**B**) Shown are % SYTOX Green^{pos} cells as mean ±SEM from 1 experiment with n = 2 MPO$^{-/-}$ and wt mice.

3.5 Cytotoxic effects of MPO in the liver

By *in vivo* depletion of neutrophils, we observed that neutrophils seem to be involved in limiting immunopathology in the liver. In parallel, MPO is expressed exclusively by neutrophils and contributes to liver injury during LCMV-induced hepatitis. Extracellular MPO itself may directly contribute to tissue damage, especially under inflammatory conditions [44, 142]. In this context, we wanted to elucidate the cytotoxic effects of MPO on hepatocytes.

3.5.1 Cytotoxicity of MPO against hepatocytes

MPO concentrations in the plasma and in liver lysates of wt mice were determined over the course of LCMV infection.

Systemic levels of extracellular MPO in the plasma increased from background levels of about 15 ng/mL in naïve mice to about 60 ng/mL on day 2 p.i. (**Fig. 23A**). By day 4 p.i., MPO levels slightly declined to 30 ng/mL. Remarkably, on day 8 p.i., when liver damage peaks, MPO plasma levels were strongly increased to 150 ng/mL.

In liver lysates, total levels of MPO did not exceed background levels of about 20 pg/µg of total protein during the first four days after infection (**Fig 23B**). Similarly to systemic levels, the concentration of MPO in the liver increased to about 100 pg/µg by day 8 p.i..

To test the direct cytotoxicity of MPO, death of primary hepatocytes was quantified in the presence of MPO and the H_2O_2-donor glucose oxidase (GOX) *in vitro*. After 4 h incubation of freshly prepared hepatocytes from naïve wt mice with concentrations of 0.1 U/mL or 1.0 U/mL enzymatically active MPO, cell death was assessed by flow cytometry of Propidium iodide-positive (PI^{pos}) cells minus spontaneous cell death of untreated hepatocytes (**Fig. 24**). GOX generates H_2O_2, which is cytotoxic itself. About 9 % of hepatocytes were PI^{pos} after 4 h incubation with GOX alone. MPO without additional GOX was barely cytotoxic for hepatocytes. In the presence of GOX and 0.1 U/mL MPO, about 10 % among hepatocytes were PI^{pos}. GOX and 1.0 U/mL MPO induced cell death of about 17 % of hepatocytes after 4 h incubation.

Together, these data suggest that there is a correlation between MPO concentration and MPO-induced hepatocyte death *in vitro* and *in vivo*.

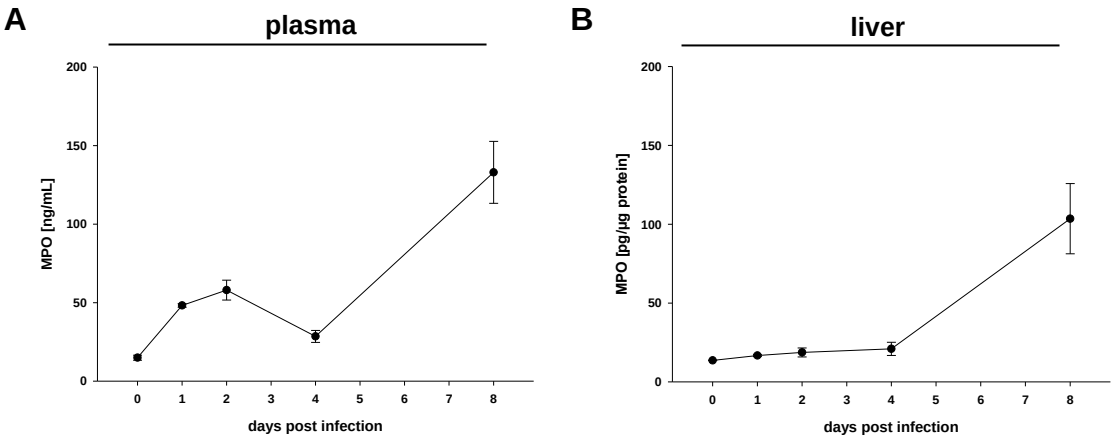

Fig. 23 MPO concentration in the plasma and in liver lysates over the course of LCMV infection

Groups of Bl/6J wt mice were infected by i.p. injection with 10^6 IU of LCMV, strain WE. Protein concentrations of extracellular MPO in the (**A**) plasma and total MPO in (**B**) liver lysates were determined by MPO-specific ELISA. Plasma and liver samples were prepared on the indicated days from naïve and infected mice. Shown are MPO concentrations as ±SEM from 1 experiment with n = 3 (days 0, 4 and 8), n = 2 (days 1 and 2) wt mice.

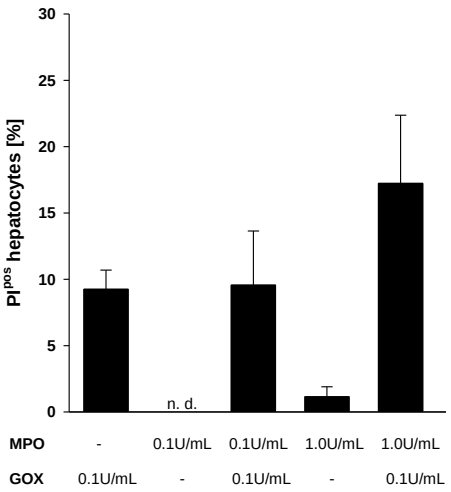

Fig. 24 MPO-induced hepatocyte death *in vitro*

Murine primary hepatocytes were incubated for 4 h with 0.1 U/mL GOX, 0.1 U/mL MPO or 1.0 U/mL MPO alone, or with combinations of GOX and MPO. Controls were left untreated. Cell death was quantified by flow cytometry of PI^{pos} hepatocytes. Shown are means of % PI^{pos} cells beyond spontaneous cell death. Means ±SEM of n=3 wt mice.

3.5.2 Co-localization of apoptotic hepatocytes with MPO *in vivo*

The abovementioned *in vitro* setup does not reflect physiological conditions. Therefore, we investigated, whether apoptotic hepatocytes co-localized with MPO or MPO-expressing cells *in vivo*. For that purpose, co-localization of apoptotic ($TUNEL^{pos}$) hepatocytes and MPO was analyzed by immunofluorescence microscopy of liver sections from naïve and LCMV-infected wt mice. In naïve wt mice, spontaneous cell death was almost absent. On the sections only very few cells were $TUNEL^{pos}$ (**Fig. 25A**). Additionally, none among $TUNEL^{pos}$ cells co-localized with MPO in naïve mice (**Fig. 25B, C**). On day 8 p.i., about 7 % of cells per visual field were $TUNEL^{pos}$ (**Fig. 25B**). Among MPO^{pos} events per visual field, about 27 % of cells were positively stained for TUNEL, on day 8 p.i. (**Fig. 25C**).

In conclusion, MPO concentration in the plasma and the liver coincide with the peak of liver damage and neutrophil infiltration on day 8 p.i.. In line with this, on day 8 p.i., apoptotic hepatocytes partially co-localize with MPO. Additionally, MPO induces hepatocyte death *in vitro* in a concentration-dependent manner. Together, these data suggest a correlation of liver damage with the total MPO concentration and neutrophil frequencies during LCMV-induced hepatitis.

A

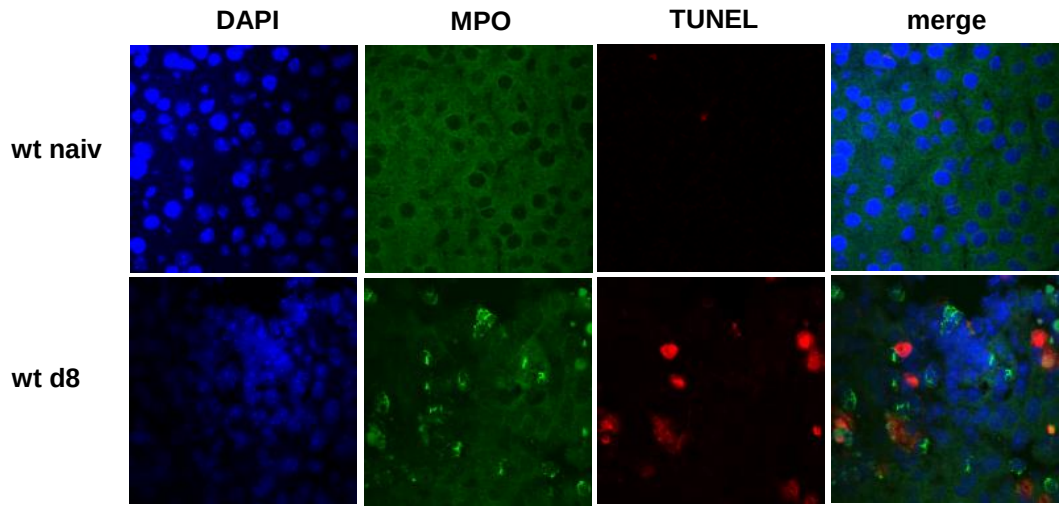

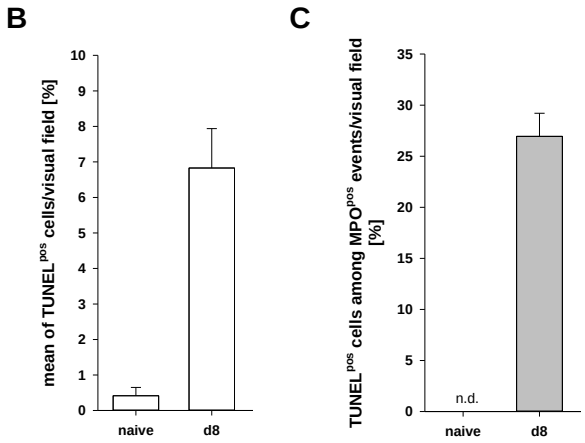

Fig. 25 Co-localization of apoptotic hepatocytes with MPO

Groups of Bl/6J wt mice were infected by i.p. injection with 10^6 IU of LCMV, strain WE. (**A**) Cryo sections (6 µm) of liver samples from naïve and infected mice were analyzed for DNA fragmentation via TUNEL staining and MPO expression using specific Ab by immunofluorescence microscopy. Representative micrographs are shown. (**B**) Total cell number in nine visual fields per sample was counted and the percentage of $TUNEL^{pos}$ cells in % among total cells was calculated. Shown are % of $TUNEL^{pos}$ cells as mean ±SEM of n=3 wt naïve and d8 p.i. mice. (**C**) Percentage of $TUNEL^{pos}$ cells among MPO^{pos} events was calculated. Shown are % of $TUNEL^{pos}/MPO^{pos}$ cells as mean ±SEM of n=3 wt naïve and d8 p.i. mice.

3.5.3 *In vivo* inhibition of extracellular MPO

Extracellularly added MPO in combination with a H_2O_2-donor induced hepatocyte death *in vitro*. Furthermore, histology revealed that apoptotic hepatocytes partially co-localize with MPO. In contrast, liver damage was not altered in NOX2 x LysM Cre^{pos} mice, which have reduced intracellular MPO activity. Based on these observations, mainly extracellular MPO is supposed to be involved in liver damage during LCMV-induced hepatitis. Therefore, we inhibited extracellular MPO in wt mice over the whole course of acute LCMV-infection.

The compound 4-Aminobenzoic acid hydrazide (4-ABAH) irreversibly inhibits MPO activity [143]. Upon *in vivo* application, largely extracellular MPO is inhibited due to poor cell membrane permeability of 4-ABAH [144, 145]. To assess the role of

extracellular MPO in LCMV-induced acute hepatitis, wt mice were treated every second day from day 1 p.i. with 4-ABAH over the course of infection.

On day 7 p.i., in mice treated with 4-ABAH, serum AST activity was at about 1100 U/L and at about 850 U/L in vehicle treated control mice (**Fig. 26**). Importantly, AST levels did not increase in 4-ABAH-treated mice by day 8 p.i.. Whereas in control mice significantly higher levels of about 2200 U/L were reached, 4-ABAH treated mice remained at levels of about 1100 U/L.

Previously, we observed that MPO-deficiency did not impair virus elimination. To test, whether 4-ABAH impacts virus elimination from the liver and the spleen, viral loads were quantified on days 7 and 8 p.i.. Indeed, the inhibitor had no influence on virus elimination, since viral loads in the liver and the spleen were similar in mice treated with 4-ABAH and in vehicle-treated mice (**Fig. 27**).

To further examine, whether 4-ABAH has an influence on immune cell recruitment to the liver, infiltration of $CD8^+$ T cells, $CD4^+$ T cells and $CD11b^+/Ly6G^{hi}$ neutrophils among leukocytes was assessed by flow cytometry. On day 7 p.i., the frequencies of infiltrating $CD8^+$ T cells in the liver reached about 35 % among leukocytes in both groups (**Fig. 28A**). On day 8 p.i., $CD8^+$ T cell frequencies similarly rose to about 40 % in both groups (**Fig. 28A**). To elucidate, if the generation of virus-specific $CD8^+$ T cells was manipulated by 4-ABAH, TCR_{LCMV}^+ T cells were analyzed by flow cytometry on day 8 p.i.. In both, 4-ABAH-treated and control mice, about 30 % among $CD8^+$ T cells expressed TCR_{LCMV}. On days 7 and 8 p.i., the frequencies of infiltrating $CD4^+$ T cells in the liver were at about 5 % among leukocytes in both groups (**Fig. 28B**).

On day 7 p.i., about 8 % were $CD11b^+/Ly6G^{hi}$ neutrophils in mice treated with 4-ABAH and in control mice (**Fig. 28C**). On day 8 p.i., in mice treated with 4-ABAH and in control mice, frequencies of neutrophils were similar at about 10 %.

Altogether, these data show that upon *in vivo* inhibition of extracellular MPO activity with 4-ABAH, LCMV-induced liver damage is significantly reduced on day 8 p.i.. Virus elimination and immune cell recruitment, as well as the generation of virus-specific $CD8^+$ T cells are not affected. Importantly, *in vivo* inhibition of extracellular MPO induces a similar phenotype observed in mice with constitutive knockout of MPO. This strengthens the conclusion that predominantly extracellular MPO contributes to immunopathology during LCMV-induced hepatitis.

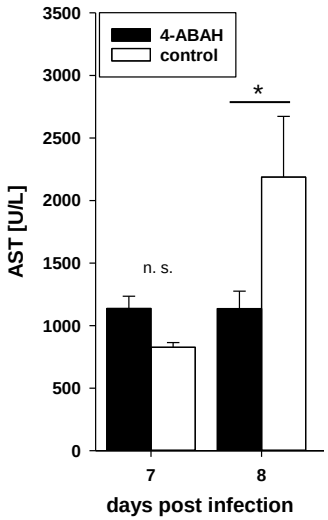

Fig. 26 Serum AST activity in wt mice upon inhibition of extracellular MPO with 4-ABAH

Groups of Bl/6J wt mice were infected by i.p. injection of 10^6 IU of LCMV, strain WE. Extracellular MPO was inhibited from day 1 p.i. by i.p. injection of 625 µg 4-ABAH every second day over the course of infection. Control mice were vehicle-treated with 15 % DMSO in PBS. Serum samples were prepared on the indicated days p.i. and activity of the transaminase AST was measured. Shown are cumulative data as means ±SEM from 1 (day 7) and 3 (day 8) experiments with n = 2 (day 7) and n = 15 mice per group. Statistical significance was assessed by Student´s t-test and is indicated by * for p≤0.05.

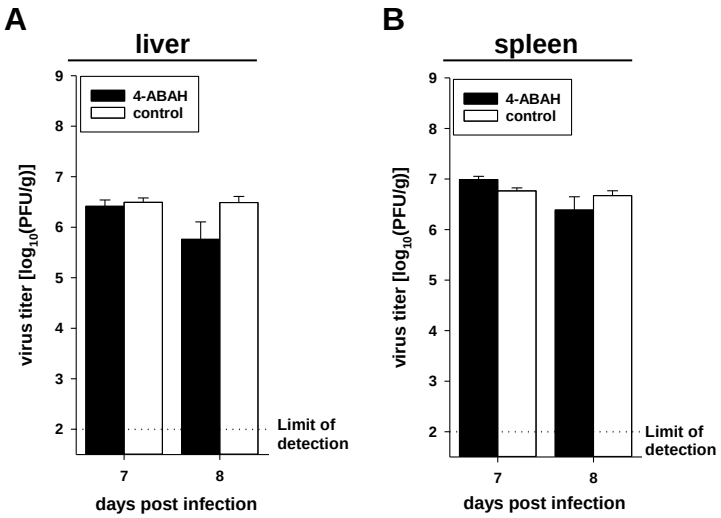

Fig. 27 Viral loads in the liver and the spleen upon inhibition of extracellular MPO

-Legend continued on next page-

-Continued legend-

Fig. 27 Viral loads in the liver and the spleen upon inhibition of extracellular MPO

Groups of Bl/6J wt mice were infected by i.p. injection of 10^6 IU of LCMV, strain WE. Extracellular MPO was inhibited by i.p. injection of 625 µg 4-ABAH every second day over the course of infection, from day 1 p.i. on. Control mice were vehicle-treated with 15 % DMSO in PBS. Viral loads in (**A**) liver and (**B**) spleen as [$\log_{10}$ (PFU/g)] were determined on the indicated days p.i.. Shown are cumulative data as means ±SEM 1 (day 7) and 2 (day 8) experiments with n = 3 (day 7), n = 8 (day 8) mice per group.

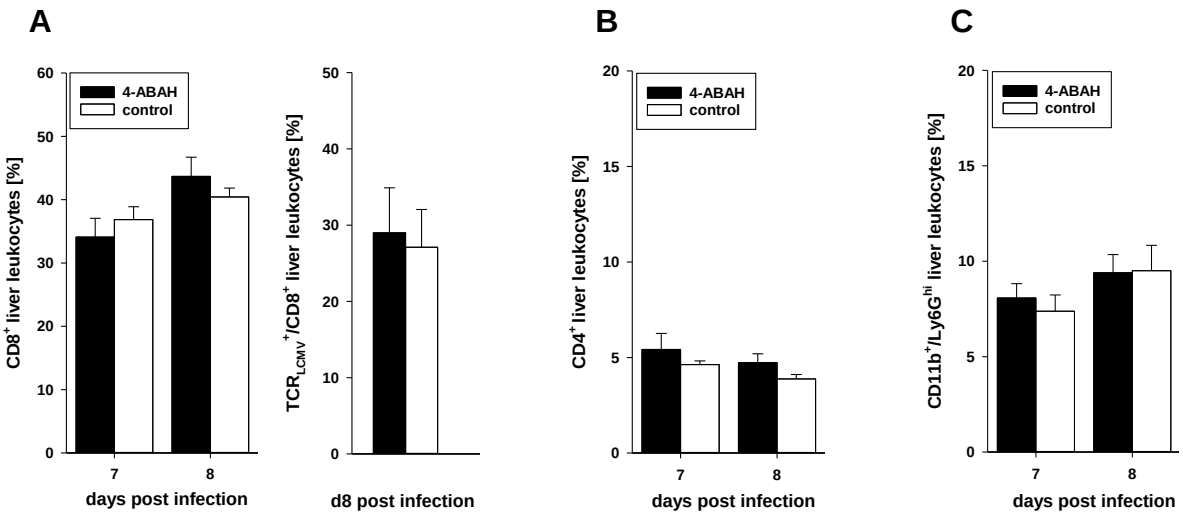

Fig. 28 Immune cell infiltration in the liver upon inhibition of extracellular MPO

Groups of Bl/6J wt mice were infected by i.p. injection of 10^6 IU of LCMV, strain WE. Extracellular MPO was inhibited by i.p. injection of 625 µg 4-ABAH every second day over the course of infection. Control mice were vehicle-treated with 15 % DMSO in PBS. In the perfused liver, percentages of (**A**) $CD8^+$ and $TCR_{LCMV}^+/CD8^+$ (**B**) $CD4^+$ and (**C**) $CD11b^+/Ly6G^{hi}$ cells among leukocytes were determined by flow cytometry. $TCR_{LCMV}^+/CD8^+$ cells were detected with MHC dextramers loaded with LCMV-specific epitopes (MHC I alleles and epitopes: H-$2D^b$-restricted immunodominant epitopes GP_{33-41}, $GP_{276-286}$, and $NP_{396-404}$). From these data, the frequencies of LCMV-specific $CD8^+$ T cells were calculated as follows: % TCR_{LCMV}^+ $CD8^+$ cells / % $CD8^+$ liver lymphocytes x 100 %. Column diagrams show cumulative data of the frequencies of $CD8^+$, $TCR_{LCMV}^+/CD8^+$, $CD4^+$ and $CD11b^+/Ly6G^{hi}$ liver cells as means ±SEM from 1 experiment (day 7) and 2 experiments (day 8) with n = 3 (day 7) and n = 6 (day 8) per group.

3.6 Mechanisms of MPO-induced hepatocyte death

Reactive oxidants generated by MPO can be cytotoxic for a variety of cell types *e.g.* endothelial cells, epithelial cells and fibroblasts (reviewed in [23]) [146-148]. Beyond that, MPO was also reported to be associated with the regulation of cellular processes, such as TGFβ signaling and growth arrest [30, 149]. We therefore wanted to elucidate, whether MPO has an influence on TGFβ-mediated processes or the cell cycle of hepatocytes during acute LCMV-induced hepatitis.

3.6.1 The role of MPO on the transcriptional regulation of NADPH oxidase 4

Upregulation of NOX4 can potentiate oxidative stress in hepatocytes [150]. One factor, which is involved in the transcriptional regulation of NOX4 is the transforming growth factor beta (TGFβ). TGFβ was reported to upregulate NOX4 expression, which correlated with pro-apoptotic activity in hepatocytes [151].

We wanted to investigate, whether MPO has an impact on the regulation of NOX4 during LCMV-induced hepatitis and if this may cause increased liver damage in wt mice. For that purpose, TGFβ and NOX4 expression in the liver of $MPO^{-/-}$ and wt mice were analyzed by qRT-PCR. On day 8 p.i., TGFβ expression in the liver did not differ in $MPO^{-/-}$ and wt mice (**Fig. 29A**). Additionally, NOX4 expression was similar in $MPO^{-/-}$ and wt mice on day 8 p.i. (**Fig. 29B**).

These data show that at the peak of LCMV-induced acute hepatitis on day 8 p.i., MPO has no influence on TGFβ and NOX4 expression. This indicates that exacerbated liver damage in wt mice is not due to a potentiation of oxidative stress by an increase in NOX4-generated ROS.

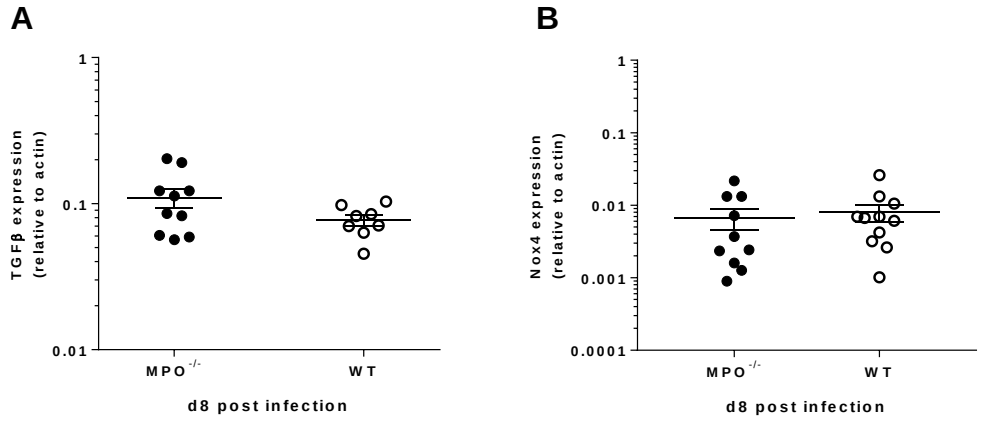

Fig. 29 Expression of TGFβ and NOX4 in the liver on day 8 p.i.

Groups of MPO$^{-/-}$ and wt mice were infected by i.p. injection of 10^6 IU of LCMV, strain WE. RNA was extracted from liver samples and qRT-PCR for expression of (**A**) TGFβ and (**B**) NOX4 was performed using DNA-binding dye SYBR green. Expression is shown relative to expression of β-actin as ±SEM of cumulative data from 3 experiments with n = 8 MPO$^{-/-}$ mice and n = 8 wt mice for TGFβ and from 3 experiments with n = 10 MPO and from 3 experiments with n = 10 MPO$^{-/-}$ mice and n = 11 wt mice.

3.6.2 Cell cycle progression of hepatocytes over the course of acute LCMV infection

To test, whether MPO influences the cell cycle of hepatocytes during LCMV-induced hepatitis the expression of the cell cycle-associated proteins p53 and p21 in the liver was analyzed by qRT-PCR on day 8 p.i. (**Fig. 30**). However both, MPO$^{-/-}$ and wt mice expressed p53 and p21 to a similar extent.

In 2015 a study by Beier *et al.*, infection of wt mice with LCMV, strain WE, resulted in impaired cell cycle progression of hepatocytes [152]. We wanted to investigate, if MPO has an impact on cell cycle progression of hepatocytes during infection of mice with LCMV. For this purpose, mitosis of primary hepatocytes from naïve and infected MPO$^{-/-}$ and wt mice was analyzed by flow cytometry via Propidium iodide (PI) staining. DNA staining with PI of fixed cells allows the quantification of DNA contents during mitosis, by which the interphases can be discriminated [153].

In naïve MPO$^{-/-}$ and wt mice, about 40 % of hepatocytes were in the G0/G1 phase of mitosis. In both, about 5 % of hepatocytes were in the S phase and 55 % had

entered the G2 phase (**Fig. 31A**). The frequencies of hepatocytes in G0/G1, S or G2 phase were similar in naïve MPO$^{-/-}$ and wt mice. Beier *et al.* observed an accumulation of hepatocytes arrested in the G0/G1 phase on day 4 p.i.. However, our analysis revealed that about 55 % of hepatocytes accumulated in the G0/G1 phase in both MPO$^{-/-}$ and wt mice on day 4 p.i. (**Fig. 31B**). About 5 % had entered the S phase, while about 40 % were in the G2 phase, indicating cell cycle progression. On day 8 p.i., about 25 % of hepatocytes were in the G0/G1 phase (**Fig. 31C**). 10 % had started DNA synthesis in the S phase and about 65 % had reached the G2 phase. Taken together, there was no difference between MPO$^{-/-}$ and wt mice at each time point of measurement.These data show that the regulation of the cell cycle associated genes p53 and p21 was independent of MPO. Additionally, infection of mice with LCMV, strain WE, indeed slightly altered cell cycle progression over the course of infection. However, MPO had no influence on this mechanism, since cell cycle progression was similar in MPO$^{-/-}$ and wt mice.

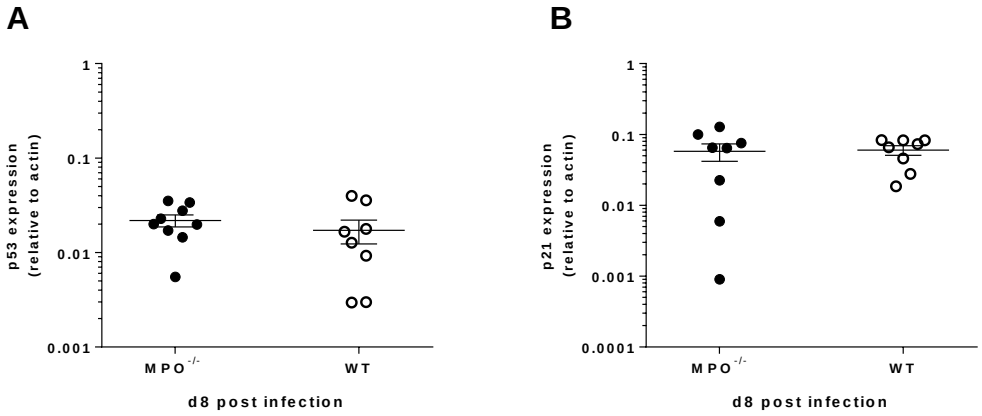

Fig. 30 Expression of cell cycle-associated genes p53 and p21 in the liver on day 8 p.i.
Groups of MPO$^{-/-}$ and wt mice were infected by i.p. injection of 10^6 IU of LCMV, strain WE. RNA was extracted from liver samples and qRT-PCR for expression of (**A**) p53 and (**B**) p21 was performed using DNA-binding dye SYBR green. Expression is shown relative to expression of β-actin as ±SEM of cumulative data from 3 experiments with n = 8 MPO$^{-/-}$ mice and n = 8 wt mice.

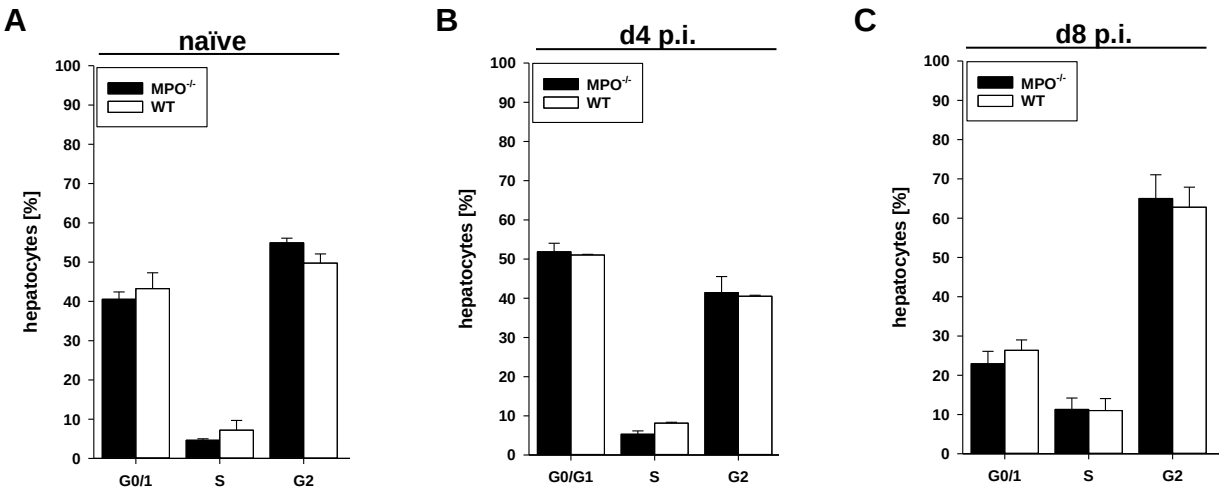

Fig. 31 Cell cycle progression of hepatocytes over the course of LCMV-induced acute hepatitis

Groups of MPO$^{-/-}$ and wt mice were infected by i.p. injection of 10^6 IU of LCMV, strain WE. Cell cycle analysis was performed in (**A**) naïve mice and on (**B**) day 4 or (**C**) day 8 p.i.. Single cell suspension of the liver was fixed and after RNase treatment, DNA was stained with Propidium iodide. Hepatocytes were gated by appearance in FSC and SSC. G0/G1, S and G2 phase were discriminated by DNA content. Shown are positively stained cells in % as ±SEM of cumulative data from 1 experiment (day 0), 1 experiment (day 4) and 2 experiments (day 8) with n = 2 (days 0 and 4) and n = 6 MPO$^{-/-}$ and wt mice.

Altogether these data indicate that MPO had no influence on the expression TGFβ or NOX4, which can also be involved in liver damage. Furthermore, MPO did not impact the expression of cell cycle associated genes or cell cycle progression.

4 Discussion

Neutrophils are recruited shortly after microbial invasion of the host as first responders to infections (reviewed in [41]). At the site of infection, they eliminate pathogens by several mechanisms, namely phagocytosis, degranulation, and the release of neutrophil extracellular traps (reviewed in [154]). Neutrophils express a variety of antimicrobial molecules, which are critically involved in the abovementioned processes. Besides the inactivation invading pathogens, these molecules may also induce host tissue damage (reviewed in [43]).

The most abundant of antimicrobial molecules of neutrophils is the heme enzyme myeloperoxidase (MPO), which generates highly reactive oxidants, *e.g.* hypochlorous acid (reviewed in [7]). The role of MPO in the defense of bacterial infections has been well characterized for decades (reviewed in [11, 12]). For viral infections, there are only few studies about the role of MPO (reviewed in [49, 50]).

ROS-induced oxidative stress may have a critical role in liver pathology in patients infected with hepatitis B virus (HBV) [155, 156]. In hepatitis C virus (HCV) infection, pathophysiology was also associated with increased levels of oxidative damage [157]. Another study about chronic HCV infection revealed that MPO levels in the plasma and liver tissue of patients correlated with liver aminotransferases AST and ALT, both important indicators of liver injury [53]. Worldwide, about 400 million people suffer from potentially life-threatening infections with hepatitis B and C, causing both acute and chronic disease (reviewed in [158, 159]). Therefore, it is of high clinical relevance to understand the basic biomedical mechanisms in order to therapeutically treat these diseases. However, the host range of the abovementioned hepatitis viruses is limited to humans and chimpanzees, small animal models are barely available [160].

The Lymphocytic Choriomeningitis Virus (LCMV) is a pathogen intensively used in murine models to reveal and characterize basic immune mechanisms. We used the murine LCMV model to explore the role of MPO in an anti-viral immune response. Acute LCMV infection induces a vigorous virus-specific immune response, which leads to rapid elimination of the virus. Importantly, depending on the route of virus inoculation, LCMV induces various immunopathological syndromes, including acute

hepatitis, choriomeningitis, or a delayed-type hypersensitivity (DTH) reaction (reviewed in [120]) [99].

Infection of mice with LCMV via i.p. inoculation causes a fulminant, but transient hepatitis [99]. Our experiments revealed that mice with MPO deficiency ($MPO^{-/-}$) had substantially decreased immunopathology during acute LCMV-induced hepatitis compared to wt animals. Additionally, $MPO^{-/-}$ mice had significantly lower transaminase activity in the serum. This was accompanied with a strong reduction in cleaved caspase 3 levels in the liver, which indicates reduced activation of apoptosis in these mice (reviewed in [161]) [162]. Thus, LCMV-induced liver pathology is partially dependent on MPO.

Regarding LCMV-induced meningitis, a study by McGavern *et al.* (2009) revealed that acute lethality after i.c. injection of LCMV depends on infiltrating neutrophils and monocytes causing vascular leakage in the brain [97]. Simultaneous depletion of both cell types extended survival by three days, while depletion of one cell type alone was not beneficial. When we intracerebrally infected $MPO^{-/-}$ mice with LCMV, the course of meningitis and acute lethality were similar to wt mice. Hence, mortality due to LCMV-induced meningitis appears to be mediated by other factors, but MPO.

The LCMV-induced DTH reaction is a T cell-dependent process. It is characterized by a transient, biphasic swelling reaction after s.c. inoculation into the hind footpad, sequentially mediated by $CD8^+$ and $CD4^+$ T cells [163, 164]. The potential impact of MPO on footpad swelling was compared in $MPO^{-/-}$ and wt mice over the course of infection. Our data demonstrate that the course of footpad swelling during LCMV-induced DTH reaction was independent of MPO

Altogether, the analysis of these three LCMV-induced immunopathological syndromes revealed that in acute infection of mice with LCMV, the involvement of MPO in immunopathology was solely restricted to the liver.

MPO-deficiency had an ameliorating effect on LCMV-induced immune-mediated hepatitis. Since LCMV is a non-cytopathic virus, tissue damage is largely mediated by the host´s immune response (reviewed in [81]) [82, 83]. To elucidate the impact of MPO on the virus-specific immune response, the course of acute hepatitis was characterized in $MPO^{-/-}$ mice over 10 to 14 days.

LCMV-induced immunopathology in the liver is induced consecutively by NK cells, $CD8^+$ T cells and $CD4^+$ T cells (reviewed in [84]) [165]. Clearance of the virus is

accomplished by $CD8^+$ T cells, which are necessary and sufficient for virus elimination within 10 to 14 days [86, 166]. Upon activation, virus-specific $CD8^+$ T cells expand up to 16.000-fold in the spleen and migrate to infected tissues [84]. In the periphery, the virus is eliminated by T cell-mediated, MHC class I-restricted induction of apoptosis of infected cells.

In intraperitoneally infected $MPO^{-/-}$ and wt mice, viral loads in the liver and the spleen were similar in both genotypes over the whole course of infection. This suggests that MPO is not involved in virus control during acute LCMV-induced hepatitis.

In this context, a recent publication of Lang and colleagues requires consideration. They observed a highly significant reduction in LCMV-induced liver immunopathology in mice with $p47^{phox}$-deficiency [167]. The $p47^{phox}$ subunit, *i.e.* the organizing subunit of the NADPH oxidase 2 (NOX2) complex, is indispensable for the assembly of the functional NOX2 complex (reviewed in [8]). Lang *et al.* observed lower ROS production in granulocytes of $p47^{phox}$-deficient mice accompanied by a more robust LCMV-specific immune response of $CD8^+$ T cells.

NOX2 and MPO are functionally connected, since MPO uses NOX2-derived ROS to produce highly reactive oxidants, *i.e.* hypochlorous acids. In our model, the expansion of $CD8^+$ and $CD4^+$ T cells was not affected by MPO and the generation of LCMV-specific $CD8^+$ T cells was similar in $MPO^{-/-}$ and wt mice. In addition, the recruitment of $CD8^+$ and $CD4^+$ T cells to the liver was independent of MPO. Beyond that, MPO had no impact on the LCMV-specific cytotoxic activity of splenic or hepatic $CD8^+$ T cells.

Taken together, unlike in mice with $p47^{phox}$-deficiency, MPO-deficiency has no effect on the generation of an LCMV-specific T cell response. NOX2 is the most widely distributed among the family of NOX isoforms (reviewed in [8]). Its expression is reported for various cell types and tissues [168]. In contrast, MPO expression is solely restricted to a few myeloid cells [169]. We suspect that deficiency in NOX2 may cause a more drastic reduction in ROS production, which might have distinct effects on the LCMV-specific T cell response, than deficiency in MPO.

In human blood up to 70 % among leukocytes are neutrophils [3]. The most abundantly expressed protein in neutrophils is MPO, which ranges from 2 - 5 % of total cellular protein. In mice, only 10-15 % of leukocytes are neutrophils and MPO levels per cell are about 10-times lower as compared to humans [170, 171]. Apart

from that, there is little information available, which cells beyond neutrophils actually express MPO in mice. One of the few studies about cell-specific MPO expression in rodents revealed that in the liver of rats, MPO expression was exclusively detected in neutrophils [5]. During LCMV-induced acute hepatitis, we identified neutrophils as the major cell type expressing MPO. Considerably lower amounts of MPO were detected in monocytes and macrophages. In humans, monocytes were reported to lose MPO activity upon tissue infiltration and differentiation into macrophages [172]. Furthermore, several independent groups demonstrated that the detection of MPO in these two cell types might be due to phagocytosis of apoptotic neutrophils or extracellular MPO (reviewed in [173]) [131, 174]. Thus, for the following investigations, we considered MPO in neutrophils to be predominantly involved in LCMV-induced immunopathology.

In bacterial infections, neutrophils are characterized as short-lived first line responders, which are recruited to the site of infection within 15 to 30 minutes (reviewed in [40, 41, 175, 176]). In contrast, during LCMV-induced hepatitis, the frequencies of liver-infiltrating neutrophils did not increase within the first few days after infection. Instead, the course of neutrophil recruitment to the liver paralleled the kinetics of the adaptive immune response of $CD8^+$ T cells. Recruitment of both, $CD8^+$ T cells and neutrophils peaked on day 8 p.i.. This correlated with maximum liver damage. Hence, neutrophils might contribute to LCMV-induced immunopathology several days after infection rather than in the first hours or days. Consequently, we hypothesized that *in vivo* depletion of neutrophils over the course of infection might ameliorate the symptoms of hepatitis.

On the first two days after infection viral loads in the liver and the spleen tended to barely differ in mice depleted of neutrophils and control mice. These data were collected from small mouse groups. However, this suggests that neutrophils seem to be dispensable for viral control early after LCMV infection.

On days 7 and 8 p.i., virus titers in the liver and the spleen, as well as serum transaminase levels were strongly increased after neutrophil depletion. At these time points, neutrophils appeared to be involved in limiting immunopathology especially at the peak of the $CD8^+$ T cell response on day 8 p.i.. Thus, the treatment of mice with a neutrophil-depleting antibody severely aggravated the course of hepatitis.

A recent publication revealed that neutrophils suppressed the $CD8^+$ T cell response at the immune contraction phase on day 14 p.i. after infection of mice with LCMV, strain clone 13 [133]. This observation suggests that after infection of mice with LCMV, strain WE, neutrophils might also be involved in controlling immunopathology. Nevertheless, the dynamics of the immune response may largely differ according to the LCMV strain. For instance, strains WE and Armstrong cause acute infections and induce a strong virus-specific immune response, which peaks between days 7 and 8 leading to rapid virus elimination [177]. In contrast, the acute immune response against LCMV, clone 13 peaks on day 6 p.i. [178]. However, instead of being eliminated, clone 13 establishes a persisting infection as a consequence of $CD8^+$ T cell exhaustion (reviewed in [84]) [179].

Based on the diverse courses of infection with various LCMV strains, the potential role of neutrophils in immunoregulation during the acute immune response against LCMV WE remains to be elucidated in detail. This requires extensive characterization of the heterogeneity of neutrophil phenotypes over the course of infection. In humans the $CD11b^{hi}/CD62L^{dim}$ subset was described to inhibit T cell proliferation *ex vivo* [180]. Furthermore, neutrophils can exert immunosuppression by ROS production (reviewed in [181]). By means of the abovementioned information, possible phenotypic alterations of neutrophils may be identified over the course of infection with LCMV WE.

Together, our findings support the view that neutrophils display an array of functions influencing both innate and adaptive immune responses [182].

The above described data revealed that neutrophils appear to be involved in immunoregulation during LCMV-induced hepatitis, but in a rather surprising way. The depletion of neutrophils over the course of infection severely aggravated immunopathology. Thus, neutrophils seem to be involved in dampening the disease. Contrarily, expression of MPO, which is predominantly restricted to neutrophils, promotes liver damage in wt mice. This suggests an involvement of MPO in immunopathology independent of the potential immunoregulatory functions of neutrophils.

In wt mice, MPO levels in the liver and the plasma were strongly increased by day 8 p.i.. We hypothesized that high tissue and plasma concentrations of MPO might potentiate LCMV-induced immunopathology. MPO was reported to contribute to

tissue damage in several ways (reviewed in [7]). MPO, which is released to the extracellular environment by degranulation of granulocytes can damage host cells and tissues (reviewed in [140]). Intracellularly, hypochlorous acid generated by MPO contributes to the inactivation of phagocytosed pathogens (reviewed in [12]). Additionally, intracellular MPO activity may mechanistically influence the cellular response of neutrophils themselves. Several studies revealed that hypochlorous acid could influence cellular processes *e.g.* by influencing the regulation of transcription factors, such as NFκB or p53 in various cell types (reviewed in [23]) [148, 183].

We aimed at analyzing to which extent intracellular MPO is involved in tissue damage during LCMV-induced hepatitis. Since it is not possible to exclusively inhibit intracellular MPO, we resorted to mice with NOX2-deficiency in myeloid cells (NOX2 x LysM Cre^{pos}) as an independent approach. In NOX2-deficient phagocytes intracellular ROS production is strongly reduced [137]. Intracellular MPO predominantly uses NOX2-derived ROS to generate hypochlorous acid (reviewed in [184]). Thus, due to low production of intracellular hydrogen peroxide, NOX2 x LysM Cre^{pos} mice should have strongly reduced intracellular MPO activity. In these mice, the course of hepatitis was not altered, suggesting that immunopathology is independent of intracellularly produced NOX2-derived ROS and hypochlorous acid in myeloid cells.

Extracellular MPO is rather linked to tissue damage than to host defense (reviewed in [7, 41, 185]). To elucidate its contribution to immunopathology, extracellular MPO was inhibited *in vivo*. The enzymatic activity of MPO can be irreversibly inactivated by the compound 4-ABAH, which is applicable *in vivo* [143]. MPO oxidizes 4-ABAH to a radical, which reduces MPO itself to an inactive intermediate. Upon *in vitro* or *in vivo* application, predominantly extracellular MPO is inhibited due to poor membrane permeability of 4-ABAH [144, 145].

On day 8 p.i., when the LCMV-specific immune response peaks, serum transaminase levels were significantly reduced after treatment of wt mice with 4-ABAH. This was not due to interference of 4-ABAH with the T cell response, since T cell recruitment to the liver, virus-specificity of CTLs and virus elimination were not affected in these mice.

These findings are in line with the *in vivo* data of $MPO^{-/-}$ mice. Here, the T cell response and virus elimination were not altered, while immunopathology was

ameliorated in the absence of MPO. This suggests that mainly extracellular MPO contributes to immunopathology during LCMV-induced acute hepatitis.

When MPO is released to the extracellular environment by NETosis, it can also contribute to host tissue damage (reviewed in [186]). In human neutrophils, NETosis was reported to be dependent on the presence of MPO according to the stimulus (reviewed in [139]) [187, 188]. Human $MPO^{-/-}$ neutrophils stimulated with PMA were less efficient in producing NETs, while treatment with *Pseudomonas aeruginosa*, *Staphylococcus aureus*, or *Escherichia coli* had no effect on NETosis.

Therefore, the relevance of MPO for the induction of NETosis in response to LCMV was investigated. The treatment of bone marrow-derived neutrophils from naïve $MPO^{-/-}$ mice with LCMV led to release of DNA *in vitro*. However, the frequency of NETosis was similar in $MPO^{-/-}$ and wt mice. This implies that NETosis in response to LCMV appears to be independent of MPO. In accordance with our findings, a study by Akong-Moore *et al.* revealed that MPO inhibition or knock-out did not impair NETosis in murine neutrophils stimulated with PMA [189].

The impact of extracellular MPO on the survival of hepatocytes was further elucidated. We and others observed that extracellularly added MPO caused hepatocyte death in the presence of hydrogen peroxide *in vitro* [30]. Moreover, the frequency of hepatocyte death was dependent on the MPO concentration. In parallel, our data indicate that hepatocyte death *in vivo* might also be related to systemic and tissue levels of MPO. For the most part, LCMV-induced immunopathology in the liver is mediated by virus-specific CTLs, which are sufficient to clear the infection [99]. Nevertheless in infected wt mice, we detected co-localization of MPO with apoptotic liver cells to a considerable degree.

Together, these data indicate that immunopathology was independent of intracellular MPO activity. Additionally, LCMV induced NETosis in neutrophils did not require MPO. Nevertheless, this mechanism might contribute to immunopathology in wt mice, since MPO is released to the extracellular environment as component of NETs (reviewed in [42]). Based on these observations, we assume that contact with extracellular MPO may contribute to hepatocyte death during LCMV-induced hepatitis.

The abovementioned data suggest that MPO may directly exert cytotoxicity most likely by causing oxidative damage and subsequent cell death via production of

highly reactive oxidants. This may involve induction of the apoptosis machinery. We wanted to reveal potential mechanisms leading to hepatocyte death depending on MPO activity, especially at the peak of immunopathology on day 8 p.i..

In this context, TGFβ was reported to be involved in several mechanisms promoting liver immunopathology induced by various stimuli (reviewed in [190]). The abovementioned publication by Pulli *et al*. revealed that in a model of non-alcoholic steatohepatitis (NASH), MPO-derived ROS induced TGFβ. This led to activation of hepatic stellate cells (HSCs), which contributed to fibrosis by increased production of collagen. In our model, MPO had no influence on TGFβ expression in the liver. Additionally in both $MPO^{-/-}$ and wt mice, liver fibrosis was absent on day 8 p.i.. Thus, MPO-mediated immunopathology in acute LCMV-induced hepatitis did not involve TGFβ [190].

Mechanistically, liver injury can also be due to potentiated oxidative stress by upregulation of NOX4 expression in hepatocytes [151, 191]. NOX4 is a constitutively active enzyme and the modulation of its activity is only achieved by transcriptional regulation (reviewed in [8]). This was reported to be regulated by TGFβ [151, 191]. Beyond TGFβ, NOX4 expression could potentially be regulated by other factors, such as MPO. We hypothesized that an MPO-dependent enhancement of NOX4 expression could aggravate liver damage in wt mice. However on day 8 p.i., NOX4 expression in the liver was similar in both $MPO^{-/-}$ and wt mice. This suggests that the milder course of immunopathology in $MPO^{-/-}$ mice was not due to MPO-mediated NOX4 regulation.

ROS can activate the transcription factor p53, which is involved in the induction of apoptosis by caspase activation in response to cellular stress (reviewed in [192, 193]), [194]. Moreover, p53 induces the cyclin-dependent kinase inhibitor p21, which is involved in the promotion of cell cycle arrest. Beier *et al*. reported in 2015 that acute infection of mice with LCMV WE caused cell cycle arrest of hepatocytes in the G1-phase of mitosis, which finally led to apoptosis [152].

In $MPO^{-/-}$ mice acutely infected with LCMV, the levels of cleaved caspase 3 were significantly lower, indicating reduced apoptosis in the liver of $MPO^{-/-}$ mice. We wanted to elucidate, whether hepatocyte death was due to differential regulation of p53 and p21, or cell cycle arrest in $MPO^{-/-}$ and wt mice. The expression of p53 and p21 was similar in both, $MPO^{-/-}$ and wt mice. Thus, during LCMV-induced hepatitis, both genes appear to be regulated independent of MPO-derived oxidants.

Acute infection of mice with LCMV influenced the distribution of hepatocytes in the cell cycle phases. Nevertheless, we could not detect the accumulation of hepatocytes in the G1, S or G2 phase, neither in $MPO^{-/-}$ mice nor in wt mice. Beyond that, the distribution of hepatocytes in the G0/1, S or G2 phase was similar in $MPO^{-/-}$ and wt mice over the course of infection. In contrast to Beier *et al*., we applied a more quantitative technique for the determination of cell cycle progression. In our experimental setup, DNA contents of single cell suspensions of the whole liver were stained with PI and quantitatively analyzed by flow cytometry. The authors used proliferating-cell-nuclear antigen (PCNA) staining of liver sections by immunohistochemistry. By this technique, the distinct mitosis states can be qualitatively determined according to intracellular PCNA distribution [195]. In comparison, flow cytometry allows a more quantitative analysis of the cell cycle.
Taken together in LCMV-induced acute hepatitis, it appears that MPO-mediated immunopathology does not involve the induction of p53- and p21-mediated apoptosis or cell cycle arrest in the G1, S or G2 phase of mitosis.

Altogether, we identified MPO as a so far unknown player in immunopathology during LCMV-induced hepatitis. The effects of MPO during acute infection of mice with LCMV were restricted to the liver. MPO-deficiency significantly ameliorated the course of acute hepatitis without affecting the virus-specific T cell response, or the elimination of the virus. In our model, neutrophils were the predominant cell type expressing MPO. Instead of being recruited early after infection, neutrophil infiltration to the liver and MPO levels paralleled the course of the adaptive immune response of $CD8^+$ T cells. Surprisingly, neutrophil depletion severely aggravated the course of hepatitis. The *in vivo* application of the MPO-inhibitor 4-ABAH revealed that inhibition of extracellular MPO significantly dampens LCMV-induced immunopathology, as does MPO-deficiency. In line with this, extracellularly added MPO induced hepatocyte death *in vitro.* Furthermore, immunofluorescence microscopy revealed that MPO partially co-localized with apoptotic hepatocytes.
These data suggest that MPO might be a potential target to therapeutically attenuate the clinical course of viral hepatitis. In this context one should consider that in humans, MPO levels are about ten-times higher than in mice, which might even enhance the health-promoting effect of MPO-inhibition in patients (reviewed in [7]). MPO-deficient individuals do not suffer from infections and are typically

asymptomatic (reviewed in [196-199]). Thus, adverse effects of blocking MPO activity are not obvious.

5 References

1. Agner, K., *Verdoperoxidase: a ferment isolated from leucocytes* Acta Chemica Scandinavica, 1941. **2**: p. 1-62.
2. Harrison, J.E., S. Pabalan, and J. Schultz, *The subunit structure of crystalline canine myeloperoxidase.* Biochim Biophys Acta, 1977. **493**(2): p. 247-59.
3. van der Veen, B.S., M.P. de Winther, and P. Heeringa, *Myeloperoxidase: molecular mechanisms of action and their relevance to human health and disease.* Antioxid Redox Signal, 2009. **11**(11): p. 2899-937.
4. Davies, M.J., et al., *Mammalian heme peroxidases: from molecular mechanisms to health implications.* Antioxid Redox Signal, 2008. **10**(7): p. 1199-234.
5. Amanzada, A., et al., *Myeloperoxidase and elastase are only expressed by neutrophils in normal and in inflamed liver.* Histochem Cell Biol, 2011. **135**(3): p. 305-15.
6. Kettle, A.J. and C.C. Winterbourn, *Myeloperoxidase: a key regulator of neutrophil oxidant production.* Redox Rep, 1997. **3**(1): p. 3-15.
7. Klebanoff, S.J., *Myeloperoxidase: friend and foe.* J Leukoc Biol, 2005. **77**(5): p. 598-625.
8. Bedard, K. and K.H. Krause, *The NOX family of ROS-generating NADPH oxidases: physiology and pathophysiology.* Physiol Rev, 2007. **87**(1): p. 245-313.
9. Murphy, M.P., *How mitochondria produce reactive oxygen species.* Biochem J, 2009. **417**(1): p. 1-13.
10. Harrison, J.E. and J. Schultz, *Studies on the chlorinating activity of myeloperoxidase.* J Biol Chem, 1976. **251**(5): p. 1371-4.
11. Klebanoff, S.J., et al., *Myeloperoxidase: a front-line defender against phagocytosed microorganisms.* J Leukoc Biol, 2013. **93**(2): p. 185-98.
12. Hampton, M.B., A.J. Kettle, and C.C. Winterbourn, *Inside the neutrophil phagosome: oxidants, myeloperoxidase, and bacterial killing.* Blood, 1998. **92**(9): p. 3007-17.

13. Winterbourn, C.C., et al., *Modeling the reactions of superoxide and myeloperoxidase in the neutrophil phagosome: implications for microbial killing.* J Biol Chem, 2006. **281**(52): p. 39860-9.
14. Cross, A.R. and A.W. Segal, *The NADPH oxidase of professional phagocytes--prototype of the NOX electron transport chain systems.* Biochim Biophys Acta, 2004. **1657**(1): p. 1-22.
15. Lacy, P., *Mechanisms of degranulation in neutrophils.* Allergy Asthma Clin Immunol, 2006. **2**(3): p. 98-108.
16. King, C.C., M.M. Jefferson, and E.L. Thomas, *Secretion and inactivation of myeloperoxidase by isolated neutrophils.* J Leukoc Biol, 1997. **61**(3): p. 293-302.
17. Schurmann, N., et al., *Myeloperoxidase targets oxidative host attacks to Salmonella and prevents collateral tissue damage.* Nat Microbiol, 2017. **2**: p. 16268.
18. Brinkmann, V., et al., *Neutrophil extracellular traps kill bacteria.* Science, 2004. **303**(5663): p. 1532-5.
19. Spickett, C.M., et al., *The reactions of hypochlorous acid, the reactive oxygen species produced by myeloperoxidase, with lipids.* Acta Biochim Pol, 2000. **47**(4): p. 889-99.
20. Albrich, J.M., et al., *Effects of the putative neutrophil-generated toxin, hypochlorous acid, on membrane permeability and transport systems of Escherichia coli.* J Clin Invest, 1986. **78**(1): p. 177-84.
21. McKenna, S.M. and K.J. Davies, *The inhibition of bacterial growth by hypochlorous acid. Possible role in the bactericidal activity of phagocytes.* Biochem J, 1988. **254**(3): p. 685-92.
22. Rosen, H., et al., *Loss of DNA-membrane interactions and cessation of DNA synthesis in myeloperoxidase-treated Escherichia coli.* Proc Natl Acad Sci U S A, 1990. **87**(24): p. 10048-52.
23. Pullar, J.M., M.C. Vissers, and C.C. Winterbourn, *Living with a killer: the effects of hypochlorous acid on mammalian cells.* IUBMB Life, 2000. **50**(4-5): p. 259-66.
24. Pattison, D.I. and M.J. Davies, *Reactions of myeloperoxidase-derived oxidants with biological substrates: gaining chemical insight into human inflammatory diseases.* Curr Med Chem, 2006. **13**(27): p. 3271-90.

25. Rayner, B.S., D.T. Love, and C.L. Hawkins, *Comparative reactivity of myeloperoxidase-derived oxidants with mammalian cells.* Free Radic Biol Med, 2014. **71**: p. 240-55.
26. Nicholls, S.J. and S.L. Hazen, *Myeloperoxidase and cardiovascular disease.* Arterioscler Thromb Vasc Biol, 2005. **25**(6): p. 1102-11.
27. Choi, D.K., et al., *Ablation of the inflammatory enzyme myeloperoxidase mitigates features of Parkinson's disease in mice.* J Neurosci, 2005. **25**(28): p. 6594-600.
28. Gray, E., et al., *Elevated myeloperoxidase activity in white matter in multiple sclerosis.* Neurosci Lett, 2008. **444**(2): p. 195-8.
29. Nusshold, C., et al., *Hypochlorite modification of sphingomyelin generates chlorinated lipid species that induce apoptosis and proteome alterations in dopaminergic PC12 neurons in vitro.* Free Radic Biol Med, 2010. **48**(12): p. 1588-600.
30. Pulli, B., et al., *Myeloperoxidase-Hepatocyte-Stellate Cell Cross Talk Promotes Hepatocyte Injury and Fibrosis in Experimental Nonalcoholic Steatohepatitis.* Antioxid Redox Signal, 2015. **23**(16): p. 1255-69.
31. Kampf, C. and G.M. Roomans, *Effects of hypochlorite on cultured respiratory epithelial cells.* Free Radic Res, 2001. **34**(5): p. 499-511.
32. Hidalgo, E., R. Bartolome, and C. Dominguez, *Cytotoxicity mechanisms of sodium hypochlorite in cultured human dermal fibroblasts and its bactericidal effectiveness.* Chem Biol Interact, 2002. **139**(3): p. 265-82.
33. Whiteman, M., et al., *Do mitochondriotropic antioxidants prevent chlorinative stress-induced mitochondrial and cellular injury?* Antioxid Redox Signal, 2008. **10**(3): p. 641-50.
34. Carr, A.C., J.J. van den Berg, and C.C. Winterbourn, *Chlorination of cholesterol in cell membranes by hypochlorous acid.* Arch Biochem Biophys, 1996. **332**(1): p. 63-9.
35. Schultz, J., et al., *Myeloperoxidase of the leucocyte of normal human blood. 3. Isolation of the peroxidase granule.* Arch Biochem Biophys, 1965. **111**(1): p. 73-9.
36. Khan, A.A., M.A. Alsahli, and A.H. Rahmani, *Myeloperoxidase as an Active Disease Biomarker: Recent Biochemical and Pathological Perspectives.* Med Sci (Basel), 2018. **6**(2).

37. Borregaard, N. and J.B. Cowland, *Granules of the human neutrophilic polymorphonuclear leukocyte.* Blood, 1997. **89**(10): p. 3503-21.
38. Faurschou, M. and N. Borregaard, *Neutrophil granules and secretory vesicles in inflammation.* Microbes Infect, 2003. **5**(14): p. 1317-27.
39. Lominadze, G., et al., *Proteomic analysis of human neutrophil granules.* Mol Cell Proteomics, 2005. **4**(10): p. 1503-21.
40. Amulic, B., et al., *Neutrophil function: from mechanisms to disease.* Annu Rev Immunol, 2012. **30**: p. 459-89.
41. Kolaczkowska, E. and P. Kubes, *Neutrophil recruitment and function in health and inflammation.* Nat Rev Immunol, 2013. **13**(3): p. 159-75.
42. Brinkmann, V. and A. Zychlinsky, *Neutrophil extracellular traps: is immunity the second function of chromatin?* J Cell Biol, 2012. **198**(5): p. 773-83.
43. Kruger, P., et al., *Neutrophils: Between host defence, immune modulation, and tissue injury.* PLoS Pathog, 2015. **11**(3): p. e1004651.
44. Bradley, P.P., R.D. Christensen, and G. Rothstein, *Cellular and extracellular myeloperoxidase in pyogenic inflammation.* Blood, 1982. **60**(3): p. 618-22.
45. Wadghiri, Y.Z., et al., *High-resolution Imaging of Myeloperoxidase Activity Sensors in Human Cerebrovascular Disease.* Scientific Reports, 2018. **8**(1): p. 7687.
46. Yipp, B.G. and P. Kubes, *NETosis: how vital is it?* Blood, 2013. **122**(16): p. 2784-94.
47. Urban, C.F., et al., *Neutrophil extracellular traps capture and kill Candida albicans yeast and hyphal forms.* Cell Microbiol, 2006. **8**(4): p. 668-76.
48. Saitoh, T., et al., *Neutrophil extracellular traps mediate a host defense response to human immunodeficiency virus-1.* Cell Host Microbe, 2012. **12**(1): p. 109-16.
49. Galani, I.E. and E. Andreakos, *Neutrophils in viral infections: Current concepts and caveats.* J Leukoc Biol, 2015. **98**(4): p. 557-64.
50. Drescher, B. and F. Bai, *Neutrophil in viral infections, friend or foe?* Virus Res, 2013. **171**(1): p. 1-7.
51. Tumpey, T.M., et al., *Pathogenicity of influenza viruses with genes from the 1918 pandemic virus: functional roles of alveolar macrophages and neutrophils in limiting virus replication and mortality in mice.* J Virol, 2005. **79**(23): p. 14933-44.

52. Tate, M.D., A.G. Brooks, and P.C. Reading, *The role of neutrophils in the upper and lower respiratory tract during influenza virus infection of mice.* Respir Res, 2008. **9**: p. 57.
53. Bekheet, I.W., et al., *The Role of Myeloperoxidase in Hepatitis C Virus Infection and Associated Liver Cirrhosis* The Open Tropical Medicine Journal, 2009. **2**: p. 1-7.
54. Zhang, J.Y., et al., *Hyper-activated pro-inflammatory CD16 monocytes correlate with the severity of liver injury and fibrosis in patients with chronic hepatitis B.* PLoS One, 2011. **6**(3): p. e17484.
55. Lumsden, L.L., *St. Louis encephalitis in 1933; observations on epidemiological features.* Public Health Rep, 1958. **73**(4): p. 340-53.
56. Barton, L.L., C.J. Peters, and T.G. Ksiazek, *Lymphocytic choriomeningitis virus: an unrecognized teratogenic pathogen.* Emerg Infect Dis, 1995. **1**(4): p. 152-3.
57. Biggar, R.J., et al., *Lymphocytic choriomeningitis outbreak associated with pet hamsters. Fifty-seven cases from New York State.* Jama, 1975. **232**(5): p. 494-500.
58. Bonthius, D.J., *Lymphocytic choriomeningitis virus: an underrecognized cause of neurologic disease in the fetus, child, and adult.* Semin Pediatr Neurol, 2012. **19**(3): p. 89-95.
59. Asnis, D.S., et al., *Lymphocytic choriomeningitis virus meningitis, New York, NY, USA, 2009.* Emerg Infect Dis, 2010. **16**(2): p. 328-30.
60. Childs, J.E., et al., *Human-rodent contact and infection with lymphocytic choriomeningitis and Seoul viruses in an inner-city population.* Am J Trop Med Hyg, 1991. **44**(2): p. 117-21.
61. Traub, E., *AN EPIDEMIC IN A MOUSE COLONY DUE TO THE VIRUS OF ACUTE LYMPHOCYTIC CHORIOMENINGITIS.* J Exp Med, 1936. **63**(4): p. 533-46.
62. Traub, E., *PERSISTENCE OF LYMPHOCYTIC CHORIOMENINGITIS VIRUS IN IMMUNE ANIMALS AND ITS RELATION TO IMMUNITY.* J Exp Med, 1936. **63**(6): p. 847-61.
63. Rivers, T.M. and T.F. Scott, *MENINGITIS IN MAN CAUSED BY A FILTERABLE VIRUS : II. IDENTIFICATION OF THE ETIOLOGICAL AGENT.* J Exp Med, 1936. **63**(3): p. 415-32.

64. Kaech, S.M., E.J. Wherry, and R. Ahmed, *Effector and memory T-cell differentiation: implications for vaccine development.* Nat Rev Immunol, 2002. **2**(4): p. 251-62.
65. Gilden, D.H., et al., *Immunopathogenesis of acute central nervous system disease produced by lymphocytic choriomeningitis virus. I. Cyclophosphamide-mediated induction by the virus-carrier state in adult mice.* J Exp Med, 1972. **135**(4): p. 860-73.
66. Gilden, D.H., G.A. Cole, and N. Nathanson, *Immunopathogenesis of acute central nervous system disease produced by lymphocytic choriomeningitis virus. II. Adoptive immunization of virus carriers.* J Exp Med, 1972. **135**(4): p. 874-89.
67. Cole, G.A., N. Nathanson, and R.A. Prendergast, *Requirement for theta-bearing cells in lymphocytic choriomeningitis virus-induced central nervous system disease.* Nature, 1972. **238**(5363): p. 335-7.
68. Zinkernagel, R.M. and P.C. Doherty, *Restriction of in vitro T cell-mediated cytotoxicity in lymphocytic choriomeningitis within a syngeneic or semiallogeneic system.* Nature, 1974. **248**(5450): p. 701-2.
69. Zinkernagel, R.M. and P.C. Doherty, *Immunological surveillance against altered self components by sensitised T lymphocytes in lymphocytic choriomeningitis.* Nature, 1974. **251**(5475): p. 547-8.
70. Zinkernagel, R.M. and P.C. Doherty, *H-2 compatability requirement for T-cell-mediated lysis of target cells infected with lymphocytic choriomeningitis virus. Different cytotoxic T-cell specificities are associated with structures coded for in H-2K or H-2D.* J Exp Med, 1975. **141**(6): p. 1427-36.
71. Moskophidis, D., et al., *Virus persistence in acutely infected immunocompetent mice by exhaustion of antiviral cytotoxic effector T cells.* Nature, 1993. **362**(6422): p. 758-61.
72. Lau, L.L., et al., *Cytotoxic T-cell memory without antigen.* Nature, 1994. **369**(6482): p. 648-52.
73. Zajac, A.J., et al., *Viral immune evasion due to persistence of activated T cells without effector function.* J Exp Med, 1998. **188**(12): p. 2205-13.
74. Murali-Krishna, K., et al., *Persistence of memory CD8 T cells in MHC class I-deficient mice.* Science, 1999. **286**(5443): p. 1377-81.

75. Blattman, J.N., et al., *Estimating the precursor frequency of naive antigen-specific CD8 T cells.* J Exp Med, 2002. **195**(5): p. 657-64.
76. Wherry, E.J., et al., *Lineage relationship and protective immunity of memory CD8 T cell subsets.* Nat Immunol, 2003. **4**(3): p. 225-34.
77. Wherry, E.J., et al., *Molecular signature of CD8+ T cell exhaustion during chronic viral infection.* Immunity, 2007. **27**(4): p. 670-84.
78. Mueller, S.N. and R. Ahmed, *High antigen levels are the cause of T cell exhaustion during chronic viral infection.* Proc Natl Acad Sci U S A, 2009. **106**(21): p. 8623-8.
79. Cao, W., et al., *Identification of alpha-dystroglycan as a receptor for lymphocytic choriomeningitis virus and Lassa fever virus.* Science, 1998. **282**(5396): p. 2079-81.
80. Durbeej, M., et al., *Distribution of dystroglycan in normal adult mouse tissues.* J Histochem Cytochem, 1998. **46**(4): p. 449-57.
81. Stitz, L., *Persistent virus infections in studies of the immune response.* Behring Inst Mitt, 1991(89): p. 231-7.
82. Moskophidis, D., et al., *Role of virus and host variables in virus persistence or immunopathological disease caused by a non-cytolytic virus.* J Gen Virol, 1995. **76 (Pt 2)**: p. 381-91.
83. Recher, M., et al., *Public, private and non-specific antibodies induced by non-cytopathic viral infections.* Curr Opin Microbiol, 2004. **7**(4): p. 426-33.
84. Zhou, X., et al., *Role of lymphocytic choriomeningitis virus (LCMV) in understanding viral immunology: past, present and future.* Viruses, 2012. **4**(11): p. 2650-69.
85. Welsh, R.M., Jr., *Cytotoxic cells induced during lymphocytic choriomeningitis virus infection of mice. I. Characterization of natural killer cell induction.* J Exp Med, 1978. **148**(1): p. 163-81.
86. Fung-Leung, W.P., et al., *Immune response against lymphocytic choriomeningitis virus infection in mice without CD8 expression.* J Exp Med, 1991. **174**(6): p. 1425-9.
87. Butz, E.A. and M.J. Bevan, *Massive expansion of antigen-specific CD8+ T cells during an acute virus infection.* Immunity, 1998. **8**(2): p. 167-75.
88. Lehmann-Grube, F., D. Moskophidis, and J. Lohler, *Recovery from acute virus infection. Role of cytotoxic T lymphocytes in the elimination of lymphocytic*

choriomeningitis virus from spleens of mice. Ann N Y Acad Sci, 1988. **532**: p. 238-56.

89. Berke, G., *The CTL's kiss of death.* Cell, 1995. **81**(1): p. 9-12.
90. Barry, M. and R.C. Bleackley, *Cytotoxic T lymphocytes: all roads lead to death.* Nat Rev Immunol, 2002. **2**(6): p. 401-9.
91. Kagi, D., et al., *Cytotoxicity mediated by T cells and natural killer cells is greatly impaired in perforin-deficient mice.* Nature, 1994. **369**(6475): p. 31-7.
92. Trapani, J.A. and M.J. Smyth, *Functional significance of the perforin/granzyme cell death pathway.* Nat Rev Immunol, 2002. **2**(10): p. 735-47.
93. Balkow, S., et al., *Concerted action of the FasL/Fas and perforin/granzyme A and B pathways is mandatory for the development of early viral hepatitis but not for recovery from viral infection.* J Virol, 2001. **75**(18): p. 8781-91.
94. Schroder, K., et al., *Interferon-gamma: an overview of signals, mechanisms and functions.* J Leukoc Biol, 2004. **75**(2): p. 163-89.
95. Van Herreweghe, F., et al., *Tumor necrosis factor-mediated cell death: to break or to burst, that's the question.* Cell Mol Life Sci, 2010. **67**(10): p. 1567-79.
96. Wohlleber, D., et al., *TNF-induced target cell killing by CTL activated through cross-presentation.* Cell Rep, 2012. **2**(3): p. 478-87.
97. Kim, J.V., et al., *Myelomonocytic cell recruitment causes fatal CNS vascular injury during acute viral meningitis.* Nature, 2009. **457**(7226): p. 191-5.
98. Moskophidis, D., et al., *Mechanism of recovery from acute virus infection. IX. Clearance of lymphocytic choriomeningitis (LCM) virus from the feet of mice undergoing LCM virus-specific delayed-type hypersensitivity reaction.* J Gen Virol, 1989. **70 (Pt 12)**: p. 3305-16.
99. Zinkernagel, R.M., et al., *T cell-mediated hepatitis in mice infected with lymphocytic choriomeningitis virus. Liver cell destruction by H-2 class I-restricted virus-specific cytotoxic T cells as a physiological correlate of the 51Cr-release assay?* J Exp Med, 1986. **164**(4): p. 1075-92.
100. Lehmann-Grube, F., *Lymphocytic Choriomeningitis Virus, in Lymphocytic Choriomeningitis Virus*, in *Springer Vienna*. 1971. p. 1-173.
101. Brennan, M.L., et al., *Increased atherosclerosis in myeloperoxidase-deficient mice.* J Clin Invest, 2001. **107**(4): p. 419-30.

102. Sag, C.M., et al., *Distinct Regulatory Effects of Myeloid Cell and Endothelial Cell NAPDH Oxidase 2 on Blood Pressure.* Circulation, 2017. **135**(22): p. 2163-2177.
103. Clausen, B.E., et al., *Conditional gene targeting in macrophages and granulocytes using LysMcre mice.* Transgenic Res, 1999. **8**(4): p. 265-77.
104. Lehmann-Grube, F. and J. Ambrassat, *A new method to detect lymphocytic choriomeningitis virus-specific antibody in human sera.* J Gen Virol, 1977. **37**(1): p. 85-92.
105. Offit, P.A. and Y.M. Svoboda, *Rotavirus-specific cytotoxic T lymphocyte response of mice after oral inoculation with candidate rotavirus vaccine strains RRV or WC3.* J Infect Dis, 1989. **160**(5): p. 783-8.
106. Lehmann-Grube, F., et al., *Mechanism of recovery from acute virus infection. I. Role of T lymphocytes in the clearance of lymphocytic choriomeningitis virus from spleens of mice.* J Immunol, 1985. **134**(1): p. 608-15.
107. Jarry, A., et al., *Mucosal IL-10 and TGF-beta play crucial roles in preventing LPS-driven, IFN-gamma-mediated epithelial damage in human colon explants.* The Journal of clinical investigation, 2008. **118**(3): p. 1132-42.
108. Schwartz, R.H., *T cell anergy.* Annual review of immunology, 2003. **21**: p. 305-34.
109. Ishak, K., et al., *Histological grading and staging of chronic hepatitis.* J Hepatol, 1995. **22**(6): p. 696-9.
110. Herz, J., et al., *Acid sphingomyelinase is a key regulator of cytotoxic granule secretion by primary T lymphocytes.* Nature immunology, 2009. **10**(7): p. 761-8.
111. Brunner, K.T., et al., *Quantitative assay of the lytic action of immune lymphoid cells on 51-Cr-labelled allogeneic target cells in vitro; inhibition by isoantibody and by drugs.* Immunology, 1968. **14**(2): p. 181-96.
112. Lehmann-Grube, F., et al., *Antiviral immune responses of lymphocytic choriomeningitis virus-infected mice lacking CD8+ T lymphocytes because of disruption of the beta 2-microglobulin gene.* J Virol, 1993. **67**(1): p. 332-9.
113. Li, T., et al., *Tumor suppression in the absence of p53-mediated cell-cycle arrest, apoptosis, and senescence.* Cell, 2012. **149**(6): p. 1269-83.
114. El-Far, Y., et al., *1. Antitumor effect of Chitosan and Silibinin and their combination in mice bearing Ehrlich ascites tumors: impact of p53 and p21.*

Yousra M. El-Far, Khaled H. Abd El Galil, Mahmoud M. Gaber, Laila A. Eissa, Mamdouh M. El-Shishtawy. Current Topics in Biochemical Research in press 2013. Current Topics in Biochemical Research in press 2013, 2013.

115. Balasubramanian, S., et al., *Orphan nuclear receptor Nur77 promotes acute kidney injury and renal epithelial apoptosis.* J Am Soc Nephrol, 2012. **23**(4): p. 674-86.
116. Zinkernagel, R.M. and H. Hengartner, *T-cell-mediated immunopathology versus direct cytolysis by virus: implications for HIV and AIDS.* Immunol Today, 1994. **15**(6): p. 262-8.
117. Trautmann, T., et al., *CD4+ T-cell help is required for effective CD8+ T cell-mediated resolution of acute viral hepatitis in mice.* PLoS One, 2014. **9**(1): p. e86348.
118. Kang, S.S. and D.B. McGavern, *Lymphocytic choriomeningitis infection of the central nervous system.* Front Biosci, 2008. **13**: p. 4529-43.
119. Moskophidis, D., et al., *Mechanism of recovery from acute virus infection: treatment of lymphocytic choriomeningitis virus-infected mice with monoclonal antibodies reveals that Lyt-2+ T lymphocytes mediate clearance of virus and regulate the antiviral antibody response.* J Virol, 1987. **61**(6): p. 1867-74.
120. Buchmeier, M.J., et al., *The virology and immunobiology of lymphocytic choriomeningitis virus infection.* Adv Immunol, 1980. **30**: p. 275-331.
121. Moskophidis, D., et al., *The immune response of the mouse to lymphocytic choriomeningitis virus. V. High numbers of cytolytic T lymphocytes are generated in the spleen during acute infection.* Eur J Immunol, 1987. **17**(7): p. 937-42.
122. Lang, P.A., et al., *Genes determining the course of virus persistence in the liver: lessons from murine infection with lymphocytic choriomeningitis virus.* Cell Physiol Biochem, 2010. **26**(3): p. 263-72.
123. Andersen, M.H., et al., *Cytotoxic T cells.* J Invest Dermatol, 2006. **126**(1): p. 32-41.
124. Juric, V., et al., *Monocytes promote liver carcinogenesis in an oncogene-specific manner.* J Hepatol, 2016. **64**(4): p. 881-90.
125. van de Garde, M.D., et al., *Liver Monocytes and Kupffer Cells Remain Transcriptionally Distinct during Chronic Viral Infection.* PLoS One, 2016. **11**(11): p. e0166094.

126. Holt, M.P., L. Cheng, and C. Ju, *Identification and characterization of infiltrating macrophages in acetaminophen-induced liver injury.* J Leukoc Biol, 2008. **84**(6): p. 1410-21.
127. Odobasic, D., A.R. Kitching, and S.R. Holdsworth, *Neutrophil-Mediated Regulation of Innate and Adaptive Immunity: The Role of Myeloperoxidase.* J Immunol Res, 2016. **2016**: p. 2349817.
128. Bos, A., R. Wever, and D. Roos, *Characterization and quantification of the peroxidase in human monocytes.* Biochim Biophys Acta, 1978. **525**(1): p. 37-44.
129. Brown, K.E., E.M. Brunt, and J.W. Heinecke, *Immunohistochemical detection of myeloperoxidase and its oxidation products in Kupffer cells of human liver.* Am J Pathol, 2001. **159**(6): p. 2081-8.
130. Rodrigues, M.R., et al., *Macrophage activation includes high intracellular myeloperoxidase activity.* Biochem Biophys Res Commun, 2002. **292**(4): p. 869-73.
131. Silva, M.T., *Macrophage phagocytosis of neutrophils at inflammatory/infectious foci: a cooperative mechanism in the control of infection and infectious inflammation.* J Leukoc Biol, 2011. **89**(5): p. 675-83.
132. Shi, C., et al., *Ly6G+ neutrophils are dispensable for defense against systemic Listeria monocytogenes infection.* J Immunol, 2011. **187**(10): p. 5293-8.
133. Liang, Y., et al., *IL-33 induces immunosuppressive neutrophils via a type 2 innate lymphoid cell/IL-13/STAT6 axis and protects the liver against injury in LCMV infection-induced viral hepatitis.* Cell Mol Immunol, 2018.
134. Albrich, J.M., C.A. McCarthy, and J.K. Hurst, *Biological reactivity of hypochlorous acid: implications for microbicidal mechanisms of leukocyte myeloperoxidase.* Proc Natl Acad Sci U S A, 1981. **78**(1): p. 210-4.
135. Weiss, S.J., et al., *Chlorination of taurine by human neutrophils. Evidence for hypochlorous acid generation.* J Clin Invest, 1982. **70**(3): p. 598-607.
136. Singel, K.L. and B.H. Segal, *NOX2-dependent regulation of inflammation.* Clin Sci (Lond), 2016. **130**(7): p. 479-90.
137. Herb, M., et al., *Mitochondrial reactive oxygen species enable proinflammatory signaling through disulfide linkage of NEMO.* 2019. **12**(568).

138. Mollers, B., et al., *The mouse M-lysozyme gene domain: identification of myeloid and differentiation specific DNasel hypersensitive sites and of a 3'-cis acting regulatory element.* Nucleic Acids Res, 1992. **20**(8): p. 1917-24.
139. Parker, H. and C.C. Winterbourn, *Reactive oxidants and myeloperoxidase and their involvement in neutrophil extracellular traps.* Front Immunol, 2012. **3**: p. 424.
140. Papayannopoulos, V., *Neutrophil extracellular traps in immunity and disease.* Nat Rev Immunol, 2018. **18**(2): p. 134-147.
141. Masuda, S., et al., *Measurement of NET formation in vitro and in vivo by flow cytometry.* Cytometry A, 2017. **91**(8): p. 822-829.
142. Aratani, Y., *Myeloperoxidase: Its role for host defense, inflammation, and neutrophil function.* Arch Biochem Biophys, 2018. **640**: p. 47-52.
143. Kettle, A.J., C.A. Gedye, and C.C. Winterbourn, *Mechanism of inactivation of myeloperoxidase by 4-aminobenzoic acid hydrazide.* Biochem J, 1997. **321 (Pt 2)**: p. 503-8.
144. Tseng, A., et al., *Myeloperoxidase Negatively Regulates Neutrophil-Endothelial Cell Interactions by Impairing alphaMbeta2 Integrin Function in Sterile Inflammation.* Front Med (Lausanne), 2018. **5**: p. 134.
145. Ullen, A., et al., *Myeloperoxidase-derived oxidants induce blood-brain barrier dysfunction in vitro and in vivo.* PLoS One, 2013. **8**(5): p. e64034.
146. Tatsumi, T. and H. Fliss, *Hypochlorous acid and chloramines increase endothelial permeability: possible involvement of cellular zinc.* Am J Physiol, 1994. **267**(4 Pt 2): p. H1597-607.
147. Venglarik, C.J., et al., *Hypochlorous acid alters bronchial epithelial cell membrane properties and prevention by extracellular glutathione.* J Appl Physiol (1985), 2003. **95**(6): p. 2444-52.
148. Vile, G.F., L.A. Rothwell, and A.J. Kettle, *Initiation of rapid, P53-dependent growth arrest in cultured human skin fibroblasts by reactive chlorine species.* Arch Biochem Biophys, 2000. **377**(1): p. 122-8.
149. Vissers, M.C., J.M. Pullar, and M.B. Hampton, *Hypochlorous acid causes caspase activation and apoptosis or growth arrest in human endothelial cells.* Biochem J, 1999. **344 Pt 2**: p. 443-9.

150. Bai, G., et al., *A far-upstream AP-1/Smad binding box regulates human NOX4 promoter activation by transforming growth factor-beta.* Gene, 2014. **540**(1): p. 62-7.
151. Carmona-Cuenca, I., et al., *Upregulation of the NADPH oxidase NOX4 by TGF-beta in hepatocytes is required for its pro-apoptotic activity.* J Hepatol, 2008. **49**(6): p. 965-76.
152. Beier, J.I., et al., *Novel mechanism of arenavirus-induced liver pathology.* PLoS One, 2015. **10**(3): p. e0122839.
153. Pozarowski, P. and Z. Darzynkiewicz, *Analysis of cell cycle by flow cytometry.* Methods Mol Biol, 2004. **281**: p. 301-11.
154. Mayadas, T.N., X. Cullere, and C.A. Lowell, *The multifaceted functions of neutrophils.* Annu Rev Pathol, 2014. **9**: p. 181-218.
155. Bolukbas, C., et al., *Increased oxidative stress associated with the severity of the liver disease in various forms of hepatitis B virus infection.* BMC Infectious Diseases, 2005. **5**(1): p. 95.
156. Alavian, S.M. and A. Showraki, *Hepatitis B and its Relationship With Oxidative Stress.* Hepat Mon, 2016. **16**(9): p. e37973.
157. Banasch, M., et al., *Longitudinal effects of hepatitis C virus treatment on hepatic mitochondrial dysfunction assessed by C-methionine breath test.* Aliment Pharmacol Ther, 2008. **28**(4): p. 443-9.
158. Seeger, C. and W.S. Mason, *Hepatitis B Virus Biology.* Microbiology and Molecular Biology Reviews, 2000. **64**(1): p. 51-68.
159. Millman, A.J., N.P. Nelson, and C. Vellozzi, *Hepatitis C: Review of the Epidemiology, Clinical Care, and Continued Challenges in the Direct Acting Antiviral Era.* Curr Epidemiol Rep, 2017. **4**(2): p. 174-185.
160. Iannacone, M. and L.G. Guidotti, *Mouse Models of Hepatitis B Virus Pathogenesis.* Cold Spring Harb Perspect Med, 2015. **5**(11).
161. Elmore, S., *Apoptosis: A Review of Programmed Cell Death.* Toxicologic Pathology, 2007. **35**(4): p. 495-516.
162. Deng, L., et al., *Hepatitis C Virus Infection Induces Apoptosis through a Bax-Triggered, Mitochondrion-Mediated, Caspase 3-Dependent Pathway.* Journal of Virology, 2008. **82**(21): p. 10375-10385.

163. Moskophidis, D. and F. Lehmann-Grube, *Virus-induced delayed-type hypersensitivity reaction is sequentially mediated by CD8+ and CD4+ T lymphocytes.* Proc Natl Acad Sci U S A, 1989. **86**(9): p. 3291-5.
164. Zinkernagel, R.M., *H-2 restriction of virus-specific T-cell-mediated effector functions in vivo. II. Adoptive transfer of delayed-type hypersensitivity to murine lymphocytic choriomeningits virus is restriced by the K and D region of H-2.* J Exp Med, 1976. **144**(3): p. 776-87.
165. De Boer, R.J., D. Homann, and A.S. Perelson, *Different dynamics of CD4+ and CD8+ T cell responses during and after acute lymphocytic choriomeningitis virus infection.* J Immunol, 2003. **171**(8): p. 3928-35.
166. Gossmann, J., et al., *Murine hepatitis caused by lymphocytic choriomeningitis virus. II. Cells involved in pathogenesis.* Lab Invest, 1995. **72**(5): p. 559-70.
167. Lang, P.A., et al., *Reactive oxygen species delay control of lymphocytic choriomeningitis virus.* Cell Death Differ, 2013. **20**(4): p. 649-58.
168. Cheng, G., et al., *Homologs of gp91phox: cloning and tissue expression of Nox3, Nox4, and Nox5.* Gene, 2001. **269**(1-2): p. 131-40.
169. Koeffler, H.P., J. Ranyard, and M. Pertcheck, *Myeloperoxidase: its structure and expression during myeloid differentiation.* Blood, 1985. **65**(2): p. 484-91.
170. Noguchi, N., et al., *Role of myeloperoxidase in the neutrophil-induced oxidation of low density lipoprotein as studied by myeloperoxidase-knockout mouse.* J Biochem, 2000. **127**(6): p. 971-6.
171. Rausch, P.G. and T.G. Moore, *Granule enzymes of polymorphonuclear neutrophils: A phylogenetic comparison.* Blood, 1975. **46**(6): p. 913-9.
172. Kumar, A.P., F.J. Piedrafita, and W.F. Reynolds, *Peroxisome proliferator-activated receptor gamma ligands regulate myeloperoxidase expression in macrophages by an estrogen-dependent mechanism involving the -463GA promoter polymorphism.* J Biol Chem, 2004. **279**(9): p. 8300-15.
173. Prame Kumar, K., A.J. Nicholls, and C.H.Y. Wong, *Partners in crime: neutrophils and monocytes/macrophages in inflammation and disease.* Cell Tissue Res, 2018. **371**(3): p. 551-565.
174. Savill, J.S., et al., *Macrophage phagocytosis of aging neutrophils in inflammation. Programmed cell death in the neutrophil leads to its recognition by macrophages.* J Clin Invest, 1989. **83**(3): p. 865-75.

175. Malech, H.L. and J.I. Gallin, *Current concepts: immunology. Neutrophils in human diseases.* N Engl J Med, 1987. **317**(11): p. 687-94.
176. Peiseler, M. and P. Kubes, *More friend than foe: the emerging role of neutrophils in tissue repair.* J Clin Invest, 2019. **129**(7): p. 2629-2639.
177. Althaus, C.L., V.V. Ganusov, and R.J. De Boer, *Dynamics of CD8+ T cell responses during acute and chronic lymphocytic choriomeningitis virus infection.* J Immunol, 2007. **179**(5): p. 2944-51.
178. Wherry, E.J., et al., *Viral persistence alters CD8 T-cell immunodominance and tissue distribution and results in distinct stages of functional impairment.* J Virol, 2003. **77**(8): p. 4911-27.
179. Barber, D.L., et al., *Restoring function in exhausted CD8 T cells during chronic viral infection.* Nature, 2006. **439**(7077): p. 682-7.
180. Pillay, J., et al., *A subset of neutrophils in human systemic inflammation inhibits T cell responses through Mac-1.* J Clin Invest, 2012. **122**(1): p. 327-36.
181. Silvestre-Roig, C., A. Hidalgo, and O. Soehnlein, *Neutrophil heterogeneity: implications for homeostasis and pathogenesis.* Blood, 2016. **127**(18): p. 2173-81.
182. Mantovani, A., et al., *Neutrophils in the activation and regulation of innate and adaptive immunity.* Nat Rev Immunol, 2011. **11**(8): p. 519-31.
183. Zhou, J., et al., *Hypochlorous acid via peroxynitrite activates protein kinase Ctheta and insulin resistance in adipocytes.* J Mol Endocrinol, 2015. **54**(1): p. 25-37.
184. Sirokmany, G. and M. Geiszt, *The Relationship of NADPH Oxidases and Heme Peroxidases: Fallin' in and Out.* Front Immunol, 2019. **10**: p. 394.
185. Zuo, L., et al., *Biological and physiological role of reactive oxygen species--the good, the bad and the ugly.* Acta Physiol (Oxf), 2015. **214**(3): p. 329-48.
186. Delgado-Rizo, V., et al., *Neutrophil Extracellular Traps and Its Implications in Inflammation: An Overview.* Front Immunol, 2017. **8**: p. 81.
187. Papayannopoulos, V., et al., *Neutrophil elastase and myeloperoxidase regulate the formation of neutrophil extracellular traps.* J Cell Biol, 2010. **191**(3): p. 677-91.
188. Metzler, K.D., et al., *Myeloperoxidase is required for neutrophil extracellular trap formation: implications for innate immunity.* Blood, 2011. **117**(3): p. 953-9.

189. Akong-Moore, K., et al., *Influences of chloride and hypochlorite on neutrophil extracellular trap formation.* PLoS One, 2012. **7**(8): p. e42984.
190. Fabregat, I., et al., *TGF-beta signalling and liver disease.* Febs j, 2016. **283**(12): p. 2219-32.
191. Carmona-Cuenca, I., et al., *EGF blocks NADPH oxidase activation by TGF-beta in fetal rat hepatocytes, impairing oxidative stress, and cell death.* J Cell Physiol, 2006. **207**(2): p. 322-30.
192. Shalini, S., et al., *Old, new and emerging functions of caspases.* Cell Death Differ, 2015. **22**(4): p. 526-39.
193. Liu, B., Y. Chen, and D.K. St Clair, *ROS and p53: a versatile partnership.* Free Radic Biol Med, 2008. **44**(8): p. 1529-35.
194. Schuler, M., et al., *p53 induces apoptosis by caspase activation through mitochondrial cytochrome c release.* J Biol Chem, 2000. **275**(10): p. 7337-42.
195. Schonenberger, F., et al., *Discrimination of cell cycle phases in PCNA-immunolabeled cells.* BMC Bioinformatics, 2015. **16**: p. 180.
196. Ren, R., *The Molecular Pathophysiology, Differential Diagnosis, and Treatment of MPO Deficiency.* Clinical & Experimental Pathology, 2012. **2**(3): p. 8.
197. Roos, D., *Chronic granulomatous disease.* Br Med Bull, 2016. **118**(1): p. 50-63.
198. Goldblatt, D. and A.J. Thrasher, *Chronic granulomatous disease.* Clin Exp Immunol, 2000. **122**(1): p. 1-9.
199. Pahwa, R. and I. Jialal, *Myeloperoxidase Deficiency*, in *StatPearls*. 2019, StatPearls Publishing

6 Summary

Myeloperoxidase (MPO)-derived ROS constitute an important part of the neutrophil-mediated antimicrobial activity. In bacterial and parasitic infections, MPO has been extensively studied as a major microbicidal molecule against such pathogens. The role of MPO in viral infections is less clear. Depending on the virus, MPO has been shown to contribute to viral clearance. However, excessive release of MPO over the course of viral infections was also associated with host tissue damage.
The Lymphocytic Choriomeningitis Virus (LCMV), strain WE, causes acute infections in mice. LCMV is a non-cytopathic virus, thus immunopathology is largely mediated by virus-specific $CD8^+$ T cells, which lyse infected host cells.
The question, to what extent MPO contributes to LCMV-induced immunopathology has not been addressed, yet. We report here that MPO-deficiency ($MPO^{-/-}$) specifically ameliorated the course of immunopathology during acute LCMV-induced hepatitis in mice. Depending on the route of virus inoculation, LCMV induces further immunopathological syndromes, *i.e.* lethal choriomeningitis or a delayed-type hypersensitivity (DTH) reaction. Interestingly, these two syndromes were not altered in $MPO^{-/-}$ mice, the ameliorating effect was only restricted to the liver. Remarkably, the strong virus-specific T cell response and virus control were independent of MPO. Instead, the kinetics of neutrophil recruitment to the liver and MPO plasma and tissue levels paralleled the course of hepatitis. Surprisingly, neutrophil depletion over the course of infection severely aggravated immunopathology, suggesting immunoregulatory functions beyond the effect of MPO. The *in vivo* inhibition of extracellular MPO during LCMV-induced hepatitis significantly attenuated the disease, while intracellular MPO activity was not involved in this process. In accordance with this, extracellularly added MPO caused hepatocyte death *in vitro* and apoptotic hepatocytes partially co-localized with MPO *in vivo*.

This study documents a physiological role of extracellular MPO in contributing to immunopathology in LCMV-induced acute hepatitis, without affecting the virus-specific T cell response or viral clearance.

6 Zusammenfassung

Von der Myeloperoxidase (MPO) generierte reaktive Sauerstoffspezies bilden einen wichtigen Teil der antimikrobiellen Aktivität von Neutrophilen. Aus einer Vielzahl von Studien ging hervor, dass die MPO in bakteriellen und parasitären Infektionen von großer Bedeutung für die Abwehr diverser Erreger ist. Die Rolle der MPO in viralen Infektionen hingegen ist weniger gut charakterisiert. Es wurde gezeigt, dass die MPO bei einigen Viren zu deren Eliminierung beitragen kann. Allerdings wurde die Aktivität der MPO auch mit der Schädigung von verschiedenen Geweben assoziiert.

Die akute Infektion der Maus mit dem Lymphozytäre Choriomeningitis Virus (LCMV), Stamm WE, ist ein anerkanntes Modell. Immunpathologie wird dabei hauptsächlich von Virus-spezifischen $CD8^+$ T Zellen vermittelt, da LCMV ein nicht-zytopathisches Virus ist.

Die Frage, ob die MPO zu der durch LCMV vermittelten Immunpathologie beiträgt, wurde bisher nicht untersucht. Diese Arbeit zeigt, dass MPO-Defizienz ($MPO^{-/-}$) die Immunpathologie über den Infektionsverlauf einer durch LCMV induzierten, akuten Hepatitis in Mäusen deutlich verringert. Abhängig von der Infektionsroute induziert LCMV weitere immunpathologische Syndrome, wie eine letale Choriomeningitis oder eine Hypersensitivitätsreaktion vom verzögerten Typ. Diese zwei Syndrome waren in $MPO^{-/-}$ Mäusen unverändert. Interessanterweise waren die starke Virus-spezifische T Zellantwort und die Viruskontrolle unabhängig von der MPO. Stattdessen verliefen die Kinetik der Rekrutierung von Neutrophilen in die Leber und der MPO Level im Plasma und Gewebe parallel zum Verlauf der Hepatitis. Die Depletion von Neutrophilen über den Infektionsverlauf steigerte die Immunpathologie überraschenderweise stark. Dies lässt eine immunregulatorische Funktion von Neutrophilen, unabhängig von der MPO vermuten. Die *in vivo* Inhibition der extrazellulären MPO während der durch LCMV induzierten Hepatitis hingegen, verbesserte die Symptome signifikant. Die intrazelluläre MPO war nicht in diesen Prozess involviert. In Übereinstimmung damit, induzierte die *in vitro* Behandlung von Hepatozyten mit der MPO, deren Zelluntergang. *In vivo* waren apoptotische Hepatozyten teilweise in Ko-lokalisation mit der MPO zu finden.

Diese Arbeit zeigt, dass die extrazelluläre MPO zur Immunpathologie während der durch LCMV induzierten Hepatitis beiträgt, ohne dabei die T Zellantwort oder Viruskontrolle zu beeinträchtigen.

7 Erklärung

Ich versichere, dass ich die von mir vorgelegte Dissertation selbstständig angefertigt, die benutzten Quellen und Hilfsmittel vollständig angegeben und die Stellen der Arbeit – einschließlich Tabellen, Karten und Abbildungen –, die anderen Werken im Wortlaut oder dem Sinn nach entnommen sind, in jedem Einzelfall als Entlehnung kenntlich gemacht habe; dass diese Dissertation noch keiner anderen Fakultät oder Universität zur Prüfung vorgelegen hat; dass sie – abgesehen von den in der Dissertation angegebenen Teilpublikationen – noch nicht veröffentlicht worden ist sowie, dass ich eine solche Veröffentlichung vor Abschluss des Promotionsverfahrens nicht vornehmen werde.
Ich versichere, dass ich alle Angaben wahrheitsgemäß nach bestem Wissen und Gewissen gemacht habe. Ich verpflichte mich, jedwede die obigen Angaben betreffenden Veränderung dem Dekanat unverzüglich mitzuteilen.
Aufgrund der Promotionsordnung (in der Fassung vom 02. Februar 2006 mit Änderungsordnungen vom 10.5.12, 16.01.13, 21.4.14) bitte ich um Zulassung zur Promotion.

Köln, 20. September 2019 _____
Arlette Paillard

Histopathologische Untersuchungen der Leber wurden in Kooperation mit Dr. Katharina Pütz, Institut für Pathologie, Universitätsklinikum Köln und Dr. Sonja Djudjaj, Institut für Pathologie, Universitätsklinikum RWTH Aachen, durchgeführt.

Cryoschnitte der Leber wurden von Gülsah Schwab, Herzzentrum, Universitätsklinikum Köln, angefertigt.

Danksagung

Jedem, der zu riesengroßen oder winzig kleinen Stücken, auf welcher Ebene auch immer, diesen Weg begleitet hat, gilt mein ganzer Dank.